[American Journal of Science, Vol. 313, October, 2013, P. 713–775, DOI 10.2475/08.2013.01]

American Journal of Science

OCTOBER 2013

THE MAJOR-ION COMPOSITION OF CENOZOIC SEAWATER: THE PAST 36 MILLION YEARS FROM FLUID INCLUSIONS IN MARINE HALITE

SEAN T. BRENNAN*,†, TIM K. LOWENSTEIN**, and DIONI I. CENDÓN***,§

ABSTRACT. **Fluid inclusions from ten Cenozoic (Eocene-Miocene) marine halites are used to quantify the major-ion composition (Mg^{2+}, Ca^{2+}, K^+, Na^+, SO_4^{2-}, and Cl^-) of seawater over the past 36 My. Criteria used to determine a seawater origin of the halites include: (1) stratigraphic, sedimentologic, and paleontologic observations; (2) Br^- in halite; (3) $\delta^{34}S$ of sulfate minerals; (4) $^{87}Sr/^{86}Sr$ of carbonates and sulfates; and (5) fluid inclusion brine compositions and evaporation paths, which must overlap from geographically separated basins of the same age to confirm a "global" seawater chemical signal.**

Changes in the major-ion chemistry of Cenozoic seawater record the end of a systematic, long term (>150 My) shift from the Ca^{2+}-rich, Mg^{2+}- and SO_4^{2-}-poor seawater of the Mesozoic ("$CaCl_2$ seas") to the "$MgSO_4$ seas" (with higher Mg^{2+} and $SO_4^{2-} > Ca^{2+}$) of the Cenozoic. The major ion composition of Cenozoic seawater is calculated for the Eocene-Oligocene (36-34 Ma), Serravallian-Tortonian (13.5-11.8 Ma) and the Messinian (6-5 Ma), assuming chlorinity (565 mmolal), salinity, and the K^+ concentration (11 mmolal) are constant and the same as in modern seawater. Fluid inclusions from Cenozoic marine halites show that the concentrations of Mg^{2+} and SO_4^{2-} have increased in seawater over the past 36 My and the concentration of Ca^{2+} has decreased. Mg^{2+} concentrations increased from 36 mmolal in Eocene-Oligocene seawater (36-34 Ma) to 55 mmolal in modern seawater. The Mg^{2+}/Ca^{2+} ratio of seawater has risen from ~2.3 at the end of the Eocene, to 3.4 and 4.0, respectively, at 13.5 to 11.8 Ma and 6 to 5 Ma, and to 5 in modern seawater.

Eocene-Oligocene seawater (36-34 Ma) has estimated ranges of SO_4^{2-} = 14–23 mmolal and Ca^{2+} = 11–20 mmolal. If the $(Ca^{2+})(SO_4^{2-})$ product is assumed to be the same as in modern seawater (~300 $mmolal^2$), Eocene-Oligocene seawater had Ca^{2+} ~16 mmolal and SO_4^{2-} ~19 mmolal. The same estimates of Ca^{2+} and SO_4^{2-} for Serravallian-Tortonian seawater (13.5-11.8 Ma) are SO_4^{2-} = 19–27 mmolal and Ca^{2+} = 8–16 mmolal and SO_4^{2-} ~24 mmolal and Ca^{2+} ~ 13 mmolal if the $(Ca^{2+})(SO_4^{2-})$ product is equal to that in modern seawater. Messinian seawater has an estimated range of SO_4^{2-} ~21–29 mmolal and Ca^{2+} ~7–15 mmolal with SO_4^{2-} ~26 mmolal and Ca^{2+} ~12 mmolal assuming the $(Ca^{2+})(SO_4^{2-})$ product is equal to that in modern seawater. Regardless of the estimation procedure, SO_4^{2-} shows progressively increasing concentrations from 36 Ma to the present values, which are the highest of the Cenozoic.

* United States Geological Survey, MS 956, National Center, 12201 Sunrise Valley Drive, Reston, Virginia 20192

** Department of Geological Sciences and Environmental Studies, State University of New York at Binghamton, Binghamton, New York 13902

*** Australian Nuclear Science and Technology Organisation, Kirrawee DC, NSW 2232, Australia

§ School of Biological, Earth and Environmental Sciences, University of New South Wales (UNSW), NSW 2052, Australia

† Corresponding author: sbrennan@usgs.gov

Key words: Seawater chemistry, fluid inclusions, Cenozoic, paleo-seawater, secular variation, evaporites, major-ion composition

INTRODUCTION

Recent studies of fluid inclusions in marine halites have shown that the major-ion composition of seawater varied during the Phanerozoic (Kovalevich and others, 1998, 2002, 2006; Zimmermann, 2000; Timofeeff and others, 2001, 2006; Lowenstein and others, 2001, 2003, 2005; Horita and others, 2002; Brennan and Lowenstein, 2002; Brennan and others, 2004; Petrychenko and Peryt, 2004; Petrychenko and others, 2005; Satterfield and others, 2005a, 2005b). However, there is some disagreement about the processes that controlled these chemical changes. Hardie (1996) and Lowenstein and others (2001) concluded that changes in seawater Mg^{2+}, SO_4^{2-}, and Ca^{2+} during the Phanerozoic were compatible with changes in mid-ocean ridge ("MOR") crust production and associated hydrothermal brine production that was controlled by global tectonism and volcanism. Holland (2005) suggested that increases in Mg^{2+} and SO_4^{2-} in Cenozoic seawater ~37, ~34, ~14 and ~5 Ma were linked to a progressive decrease in seawater-driven dolomitization of limestones, which left more Mg^{2+} and SO_4^{2-} to accumulate in the ocean. The major ion chemistry of Cenozoic seawater records the tail end of a systematic, long term >150 My shift from the relatively Ca^{2+}-rich, Mg^{2+}- and SO_4^{2-}-poor seawater of the Mesozoic ("$CaCl_2$ seas") to the "$MgSO_4$ seas" (with higher Mg^{2+} and SO_4^{2-}>Ca^{2+}) of the Cenozoic (Timofeeff and others, 2006). The crossover point at which the molality of SO_4^{2-} in seawater became greater than Ca^{2+} occurred sometime between 93.5 Ma and 36 Ma (Timofeeff and others, 2006).

This paper quantifies the evolution of the major-ion composition of seawater over the past 36 My from fluid inclusions in marine halites. We use a large data set of new and previously published analyses of inclusions to constrain possible causes of the variations in Cenozoic seawater chemistry: (1) variations in MOR brine production (Hardie, 1996; Lowenstein and others, 2001), (2) global, seawater-driven dolomitization (Holland, 2005), or (3) other factors.

A total of 583 fluid inclusion analyses are available to address these issues. We report 122 new fluid inclusion analyses (table 1) that are complemented by 395 fluid inclusion analyses from Cendón (ms, 1999) and Cendón and others (1998, 2003, 2004, 2008) and 66 fluid inclusion analyses from the earlier compilation of Zimmermann (2000) (table 1). However, not all of the fluid inclusions analyzed contain evaporated seawater because of possible non-marine inflows and recycling processes whereby evaporite deposits, either syndepositional or ancient, are dissolved and contribute solutes to surface brines (Taberner and others, 2000; Zimmermann, 2000; Ayora and others, 2001; Cendón and others, 2003, 2004, 2008). Therefore, the first step is to distinguish those halites formed from evaporation of seawater from those modified by non-marine inflow waters and recycling processes.

Zimmermann (2000) geochemically screened the Cenozoic fluid inclusion data (Ayora and others, 1994a, 1994b; García-Veigas and others, 1995; Galamay and Karoli, 1997; Galamay and others, 1997; Kovalevich and Petrichenko, 1997; Kovalevich and others, 1997; Lazar and Holland, 1999) using a Degree of Evaporation ("DE") approach to eliminate evolved fluid inclusion brines from which late-stage salts precipitated (such as polyhalite, hexahydrite, kieserite, sylvite, carnallite, [table 2]). Such evolved brines have different Mg^{2+}/K^+ ratios than the original parent water due to precipitation and/or dissolution of Mg- and K-bearing salts, which violates the conservative behavior of Mg^{2+} and K^+ needed to use the fluid inclusion analyses to determine the original seawater composition (Zimmermann, 2000; Brennan and Lowenstein, 2002).

TABLE 1

Basins discussed in this paper (numbers correspond to locations on fig. 1), their country (or region) of origin, approximate ages, the number fluid inclusions analyzed and sources of data

Cenozoic Basins		Age	This study	Cendón (1999); Cendón and others (1998, 2003, 2004, 2008)	Compiled in Zimmermann (2000)
Late Eocene-Early Oligocene					
(1) Ebro Basin (Spain)	Navarra sub-basin	~36 Ma	-	57	4 (Average values taken from 27 individual analyses from Ayora and others, 1994b)
	Catalan sub-basin	~36 Ma	-	101	-
(2) Bresse Basin (France)		~36 Ma	31	-	-
(3) Southern Rhine Graben (France)		~34 Ma	23	99	2 (Canals and others, 1993). Not used for this compilation.
Middle to Late Miocene					
(4) Carpathian Basins	Carpathian Foredeep Basin (Poland)	~13.5-12.5 Ma	30	42	19 (Galamay and others, 1997) 5 (Kovalevich and Petrichenko, 1997)
	East Slovakian Basin (Slovakia)	~13.5-12.5 Ma	-	-	14 (Galamay and Karoli, 1997) 2 (Kovalevich and Petrichenko, 1997)
(5) Gulf of Suez (Egypt)		~11.8 Ma	30	-	-
Late Miocene					
(6) Lorca Basin (Spain)		~ 7.6 Ma	-	70	2 (Ayora and others, 1994a). Not used for this compilation.
(7) Caltanissetta Basin (Sicily)		5.6-6 Ma	8	27	7 (García-Veigas and others, 1995) 2 (Zimmermann, 2000)
(8) Red Sea (Middle East)		~5-6 Ma	-	-	5 (Kovalevich and others, 1997) 4 (Lazar and Holland, 1999)
Analyses used in this compilation (583)			122	395	66

García-Veigas and others (1995), Taberner and others (2000), and Cendón and others (2003, 2004, 2008) used an integrated approach involving stratigraphic, sedimentologic, and petrographic observations coupled with $^{87}Sr/^{86}Sr$, $\delta^{34}S$, $\delta^{18}O$, Br^- in halite, and major ion chemistry of fluid inclusions in halite, to determine the origin of evaporites (and fluid inclusions) from the Eocene age South Pyrenean Basin and Miocene age Lorca Basin of Spain, the Eocene age Bresse Basin and Oligocene age Rhine Graben of France, the Miocene age Carpathian Basins of Poland and Slovakia, and the Miocene age Caltanissetta Basin of Sicily (table 1, fig. 1). This paper follows the same approach and combines the sedimentological and geochemical criteria of Taberner and others (2000), Zimmermann (2000), and Cendón and others (2003, 2004, 2008) with new

TABLE 2

Minerals discussed in the paper and their respective formulae

Mineral	Formula
Calcite	$CaCO_3$
Gypsum	$CaSO_4 \cdot 2H_2O$
Anhydrite	$CaSO_4$
Halite	NaCl
Sylvite	KCl
Carnallite	$KMgCl_3 \cdot 6H_2O$
Tachyhydrite	$CaMg_2Cl_6 \cdot 12H_2O$
Bischofite	$MgCl_2 \cdot 6H_2O$
Polyhalite	$K_2Ca_2Mg(SO_4)_4 \cdot 2H_2O$
Epsomite	$MgSO_4 \cdot 7H_2O$
Hexahydrite	$MgSO_4 \cdot 6H_2O$
Kieserite	$MgSO_4 \cdot H_2O$
Kainite	$KMgSO_4Cl \cdot 3H_2O$
Langbeinite	$K_2Mg_2(SO_4)_3$

inclusion analyses (table 1) to further determine the origin of the parent water for each basin studied here. Specifically, criteria used to determine a seawater origin of the evaporites include: (1) stratigraphic, sedimentologic, and paleontologic observations and interpretations; (2) Br^- in halite; (3) $\delta^{34}S$ of sulfate minerals in the evaporite sequence; (4) $^{87}Sr/^{86}Sr$ analyses of carbonates and sulfates in the evaporite succession; and (5) fluid inclusion brine compositions and evaporation paths, which must overlap from geographically separated basins of the same age to confirm a "global" seawater chemical signal (table 3). Once halites of marine origin are identified, the fluid inclusions can be used to determine the composition of the parent seawater using the methods of Brennan and Lowenstein (2002), Horita and others (2002), Brennan and others (2004), and Lowenstein and others (2005).

OVERVIEW OF HALITE SOURCE AND ORIGIN

Criteria Used to Assess Marine versus Non-marine Origin

Where biochemical and preservational conditions permit, marine deposits and fossils should underlie, overlie, or occur interbedded with evaporites that are marine in origin. Non-marine deposits or fossils conformably underlying or interbedded with evaporites suggest a non-marine origin. Halite interbedded with late-stage salts may contain fluid inclusion brines with Mg^{2+}/K^+ ratios that are different than the parent seawater due to the precipitation and/or partial dissolution of the Mg^{2+}- and K^+-bearing salts.

Analyses of Br^- in halite, $\delta^{34}S$ of sulfates, and $^{87}Sr/^{86}Sr$ of sulfates and carbonates are helpful for interpreting evaporites as marine or non-marine. However, to avoid false seawater or non-marine signals, detailed petrographic observations are needed to show that only primary minerals with no evidence of diagenetic alteration were analyzed.

Bromide is present in seawater and all marine halites contain bromide. A continuous increase in the Br^- concentration of halite at progressively higher strati-

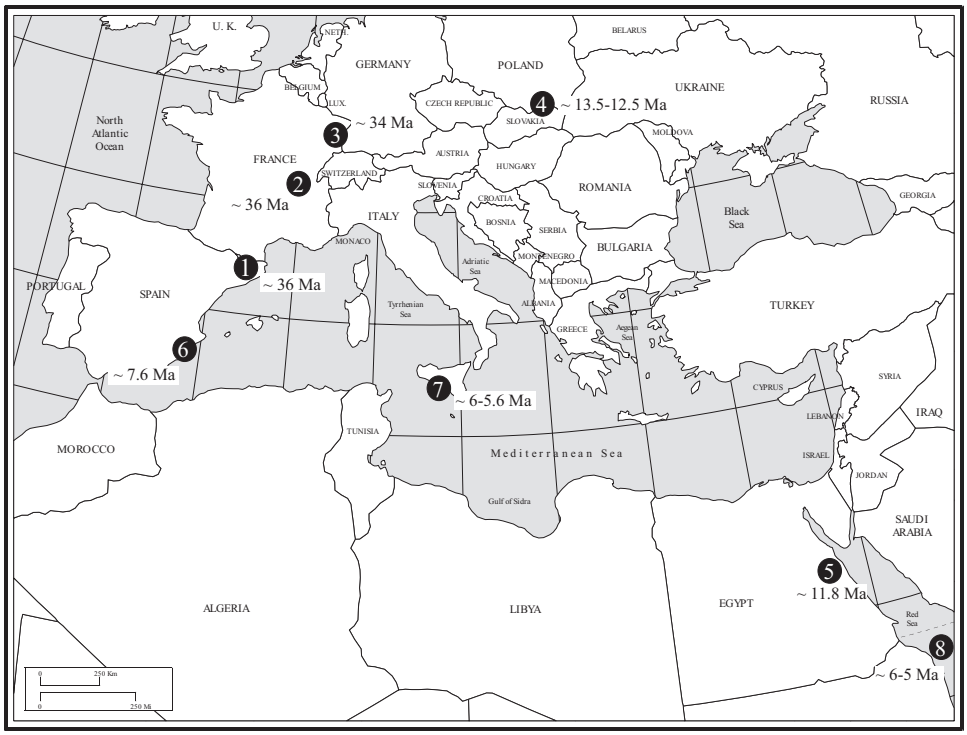

Fig. 1. Location map of the evaporite deposits discussed in this study with approximate ages shown. (1) South Pyrenean Basin, location of the Navarra and Catalan sub-basins (Late Eocene, ~36 Ma), (2) Bresse Graben (Late Eocene ~36 Ma), (3) Southern Rhine Graben (Early Oligocene, ~34 Ma), (4) Carpathian Basins (Middle Miocene, ~13.5-12.5 Ma), (5) Gulf of Suez (Late Miocene, ~11.8 Ma), (6) Lorca Basin (Late Miocene, ~7.6 Ma), (7) Caltanissetta Basin (Late Miocene, ~6-5.6 Ma), (8) Red Sea (Late Miocene, ~6-5 Ma).

graphic levels indicates rising bromide concentrations of the parent waters due to evaporation. These "bromide profiles" suggest that the halites formed from the evaporation and likely drawdown of a large, isolated, perennial body of water that is highly saline (Holser, 1966). Erratic changes in the bromide concentration of halite upsection indicate that (1) a new type of water entered the basin, (2) evaporites were recycled, or (3) the halite was altered or recrystallized during burial diagenesis (Holser, 1966).

The theoretical concentration of Br^- in marine "first halites," that is halites precipitated as evaporating seawater first reaches halite saturation, is ~65 to 75 ppm (Braitsch and Herrmann, 1963). However, modern marine first halites from Baja California, Mexico, have Br^- values of ~50 ppm (Holser, 1966), and first halites experimentally produced from Mediterranean seawater have Br^- concentrations as low as 38 ppm (Bloch and Scherb, 1953). Therefore, the first halites formed from the evaporation of modern seawater should have Br^- concentrations of at least 40 ppm. Halites formed from seawater from 36 Ma through the present should also contain Br^- above 40 ppm, because Br-residence time in the oceans is about 100 My (Holland, 1984) However, halite with Br^- concentrations of less than 40 ppm do not preclude a seawater parent. If seawater dissolved and "recycled" halite as it flowed into a basin, then first halite precipitation would occur at a lower concentration factor, which would reduce the amount of bromide in the halite. Halites formed by these types of parent

TABLE 3

Criteria for marine vs. non-marine samples

Criteria		Marine	Non-marine
Deposits and Fossils		Marine deposits and fossils below, interbedded with, or above evaporites	Continental deposits or fossils below or interbedded with evaporites suggest non-marine parent
Br^- concentration of halite		Halite with Br^->40 ppm. Halite Br^- concentrations should increase upsection	Halite with low Br^- cannot form from simple seawater evaporation. Br^- concentrations that decrease upsection indicate seawater recycling or non-marine waters entered basin.
$\delta^{34}S$ of sulfate mineral		Sulfates interbedded with halite must have marine $\delta^{34}S$ values: +20 to +23‰ for Cenozoic	Sulfates with $\delta^{34}S$ concentrations <+20 or >+23‰ are not derived from pristine seawater.
$^{87}Sr/^{86}Sr$ of sulfates and carbonates		Sulfates and carbonates must have Cenozoic seawater $^{87}Sr/^{86}Sr$ values (from ~40 Ma to present range from 0.7077 to 0.7091).	Sulfates or carbonates with radiogenic $^{87}Sr/^{86}Sr$ values (> marine) are not pristine seawater.
Fluid inclusions	Brines	Basins must have consistent fluid inclusion brine compositions (i.e. Na-Mg-K-Cl-SO_4 or Na-Mg-K-Ca-Cl type)	Different brine types from coeval inclusions indicate that the parent water was from a mixed source, i.e. non-marine
	Evaporation paths	Fluid inclusion brine compositions from a basin must follow evaporation paths on concentration crossplots	Scatter on concentration crossplots indicates mixed source brine
	Overlapping evaporation paths	Fluid inclusion brines from contemporaneous, geographically separated basins must have overlapping evaporation paths	Paths that do not overlap indicate different parent waters in the basins, i.e. some or all are non-marine.

waters should still exhibit increasing bromide concentrations upsection. As the dissolution of halite only affects the Na^+ and Cl^- concentrations of the parent water, fluid inclusions in these low Br^- halite samples may still be used to determine seawater compositions.

Some non-marine halites, such as the Eocene Green River Formation of Colorado and Wyoming (Dyni and others, 1970) have high concentrations of Br^-. Therefore, although all marine halites must contain Br^-, high Br^- concentrations are not a unique indicator of a seawater parent (Hardie, 1984).

The $\delta^{34}S$ of seawater has been ~+20 to +23 permil for the past ~36 My (Claypool and others, 1980; Paytan and others, 1998; Strauss, 1999). Therefore, Cenozoic marine evaporites will have values in this range, and sulfate minerals that do not fall in this range cannot have had a pristine seawater parentage. Seawater $^{87}Sr/^{86}Sr$ composition

has risen from 0.7077 to 0.7091 over the past ~40 My (DePaolo and Ingram, 1985; McArthur and others, 2001). Strontium replaces calcium in both CaCO3 and $CaSO_4$, and there is no partitioning of Sr isotopes in the crystal structure. Therefore, Cenozoic marine evaporites less than 40 My old will have values in this range. If the $^{87}Sr/^{86}Sr$ ratio of unaltered carbonates or sulfates is different than the contemporaneous seawater, then the parent could not have been pure seawater. It should be noted that in a study by Denison and others (1998), Permian sulfates from the Salado and Rustler Formations have Permian seawater $\delta^{34}S$ values, but the $^{87}Sr/^{86}Sr$ ratio of the sulfates indicated non-marine input. Therefore, marine sulfates with $\delta^{34}S$ values of contemporary seawater are a necessary, but not complete, indicator of a pure seawater parentage.

Late Eocene-Early Oligocene Basins (Priabonian-Rupelian, ~36 to 34 Ma)

In the Paleocene, a compressional event caused by the collision of the Iberian and European plates created the South Pyrenean Basin (Puigdefàbregas and Souquet, 1986; Zoetemeijer and others, 1990), a foreland basin to the south of the Pyrenees (fig. 1). The inception of the Western European rift system to the northeast was synchronous with the creation of the South Pyrenean foredeep forming a series of north-south elongate basins (Rouchy, 1997) including the Bresse and Rhine Grabens (fig. 1).

South Pyrenean Basin.—The South Pyrenean Basin was an east-west trending foreland basin with Late Paleocene through Miocene deposits (Santanach, 1997). During the Late Eocene (Priabonian, ~36 Ma), there were two separate evaporite depocenters (~700 km^2), the Navarra sub-basin to the west and the Catalan sub-basin to the east (Ayora and others, 1994b; Cendón and others, 1998, 2003; Taberner and others, 2000). The basal deposits in both sub-basins are deep-water marine marls (fig. 2). The marls of the Navarra sub-basin contain deep water, marine fauna and the Catalan sub-basin is rimmed by Late Eocene carbonate reefs (Rosell and Pueyo, 1997). The marine marls are overlain by an anhydrite unit, a halite unit, and a potash unit, with sylvite and carnallite, in both sub-basins (fig. 2) (Rosell and Pueyo, 1997). The halite is referred to as the "lower halite unit" (~78 m thick in the Catalan sub-basin and ~20 m thick in the Navarra sub-basin) and is composed of cumulate halite crystals with anhydrite and polyhalite along crystal boundaries (Ayora and others, 1994b; Cendón and others, 2003). Between the lower halite unit and the potash unit of the Catalan sub-basin is a layer composed of halite, polyhalite, and red clays, referred to as the "upper part of the lower halite unit" (Cendón and others, 2003). The overlying potash unit contains interbedded halite, sylvite, and carnallite (Ayora and others, 1994b; Cendón and others, 2003). $MgSO_4$-type salts other than polyhalite are not found in either sub-basin.

The Navarra sub-basin potash unit is overlain by halite (fig. 2). This "upper halite unit" is composed of centimeter-thick layers of halite, anhydrite, and clay; the clay content increases upwards in this unit, suggesting continental sediment influx (Ayora and others, 1994b). The Catalan sub-basin potash unit is overlain by a thin upper halite unit followed by anhydrite, sandstone, and a sylvite-rich potash unit (fig. 2). The succession in the Catalan sub-basin is capped by red beds with nodular anhydrite that have been interpreted as continental in origin (Cendón and others, 2003).

The Navarra sub-basin halites (lower halite unit) have initial Br^- concentrations of 50 ppm; halite Br^- concentrations increase upsection to ~150 ppm (Ayora and others, 1994b) (fig. 2, table 4). The Catalan sub-basin halites have initial Br concentrations of 11 ppm; halite Br concentrations increase upsection to 220 ppm (Cendón and others, 2003) (fig. 2). The $\delta^{34}S$ values of sulfates interbedded with the Navarra sub-basin halites are ~+20 permil (Ayora and others, 1995) and the $\delta^{34}S$ values of sulfates interbedded with the Catalan sub-basin halites (lower halite unit) range from +20.86 to +22.09 permil (table 4) (Cendón and others, 2003). Therefore, the Br concentrations, bromide profiles, and $\delta^{34}S$ values of South Pyrenean Basin evaporites

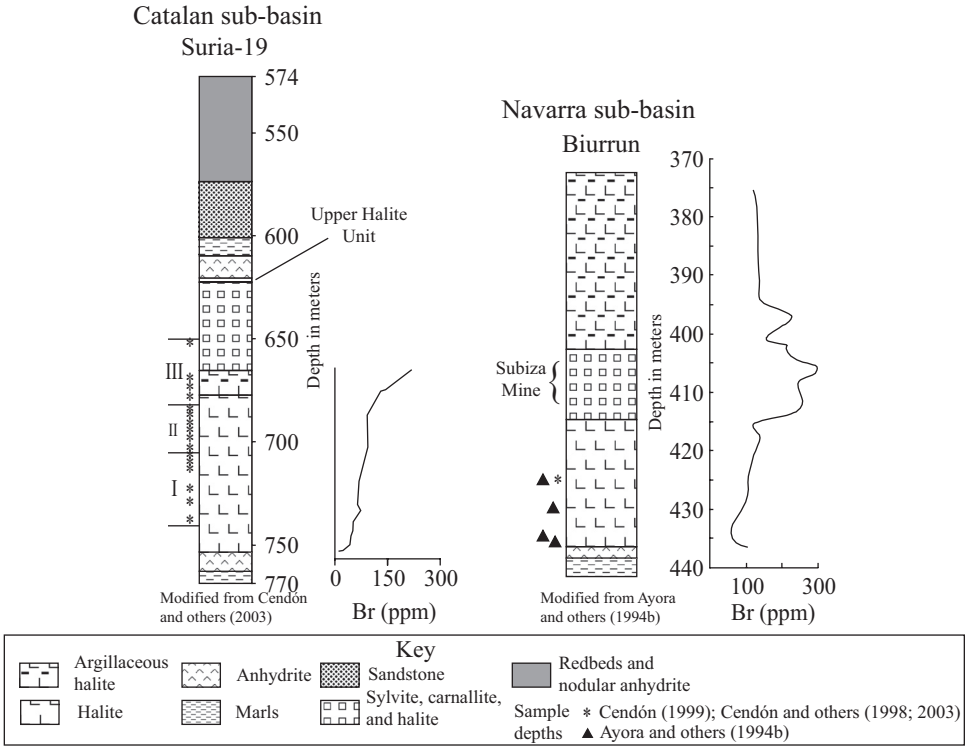

Fig. 2. Stratigraphy and bromide profile of the Late Eocene (~36 Ma) Navarra (Biurrun Core) and Catalan (Suria-19 core) sub-basins (Ayora and others, 1994b; Cendón, ms, 1999; Cendón and others, 1998, 2003). Samples analyzed by Cendón (ms, 1999), Cendón and others (1998, 2003) and Ayora and others (1994b) used in this study are indicated by asterisks and triangles respectively. Stratigraphic position of the Subiza Mine section analyzed by Cendón and others (1998) is indicated on Navarra succession. Criteria for separating Catalan samples into groups I, II, and III are discussed in the text.

are consistent with a seawater parent (table 4). There are no reported $^{87}Sr/^{86}Sr$ analyses from the South Pyrenean Basin.

Cendón (ms, 1999) and Cendón and others (2003) report fluid inclusion chemistries from the Navarra (Biurrun core and Subiza mine) and Catalan (Súria-19 core) sub-basins (table 1; Appendix table A2). Ayora and others (1994b) report fluid inclusion chemistries from the Navarra sub-basin (Biurrun core); only the data screened by Zimmermann (2000) are reported here (table 1; Appendix table A3). The stratigraphic positions of the samples are shown on figure 2.

Bresse Graben.—The Bresse Graben, France, (fig. 1) is a north-south trending, elongate tectonic depression (30-60 km wide by ~200 km long) formed by continental rifting in western Europe (Rouchy, 1997) between the mid-Eocene and the Miocene (Curial and Moretto, 1997). Most of the evaporites (~800 m thick) deposited in the Bresse Graben during the Late Eocene through the Early Oligocene have been interpreted as continental in origin because there is no paleontological or sedimentological evidence of marine conditions during that time period (Moretto, 1987; Curial and Moretto, 1997). The initial deposits in the basin are glauconitic sandstones, which are overlain by the E6 unit, an anhydrite-rich shale (fig. 3). Curial and Moretto (1997) determined that the glauconitic sandstones were sourced from the erosion of adjacent Mesozoic units and do not indicate marine conditions. The E6 unit is overlain by five

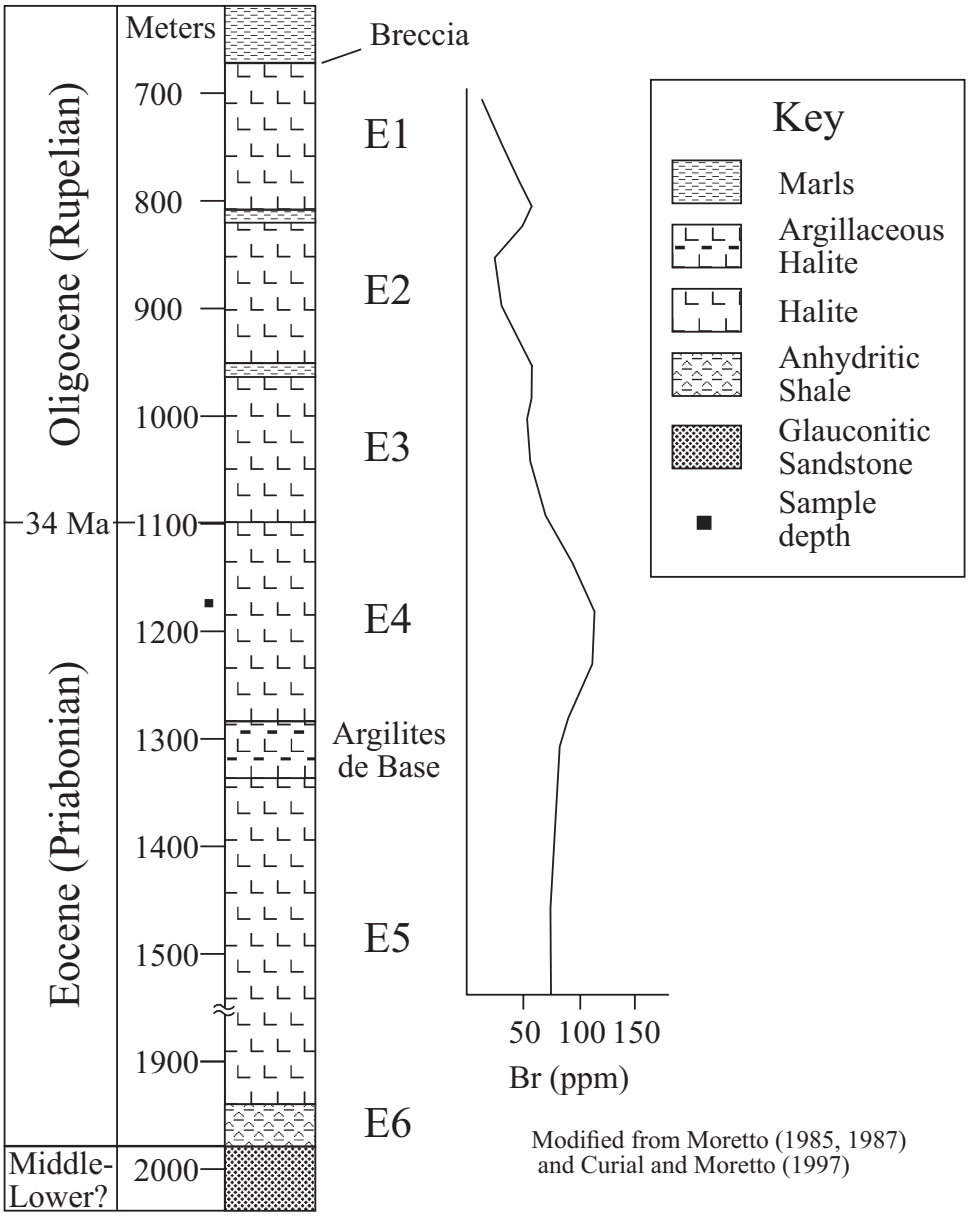

Fig. 3. Stratigraphy and bromide profile of Bresse Basin, modified from Curial and Moretto (1997). Depths are from Moretto (1987) and halite unit thicknesses are from Moretto (1985). The Late Eocene E4 salt (~36 Ma), sampled for this study, is indicated by a square.

separate evaporites, E5 through E1 (fig. 3), defined by marker beds and well log data (Curial and Moretto, 1997). Only the E4 (Priabonian, ~36 Ma) and E3 (Rupelian ~34 Ma) units contain bedded chevron-rich halite; all other halite has recrystallized (Curial and Moretto, 1997). The E1 salt is overlain by a breccia composed of carbonate, sulfate, and clay-rich clasts that likely formed by the dissolution of the underlying salt (Curial and Moretto, 1997). The breccia is overlain by carbonate-rich marls that have been

altered by pedogenesis (Curial and Moretto, 1997), which indicates chemical weathering during subaerial exposure.

Bromide concentrations of the Bresse Basin halites range from ~10 to ~150 ppm (Moretto, 1987) (fig. 3). The halites of the E4 unit have Br concentrations that increase upsection from ~100 to ~150 ppm. The E3 through E1 unit halites have Br concentrations that decrease upsection from ~80 to ~10 ppm, which suggests that bromide-poor waters entered the basin. Therefore, only the halites of the E4 Unit have Br concentrations and a bromide profile consistent with a seawater parent. There are no reported analyses of $\delta^{34}S$ or $^{87}Sr/^{86}Sr$ analyses from the Bresse basin evaporites. Fluid inclusions in halite analyzed for this study come from the E4 unit (table 1), whose stratigraphic position is shown on figure 3.

Southern Rhine Graben.—The Rhine Graben (fig. 1) is a north-south trending, elongate tectonic depression (10 to 25 km wide by 150 km long) (Lowenstein and Spencer, 1990) that was also formed during the western European rifting (Rouchy, 1997). The Rhine Graben contains over 2500 m of evaporites and marls deposited in the Late Eocene through the Early Oligocene; evaporitic deposits account for ~1600 m of the section (Blanc-Valleron and Schuler, 1997) (fig. 4). The samples from this study are from the Early Rupelian (~34 Ma) Salt IV unit (~210 m thick), which is underlain by the "Fossiliferous Zone" (~80 m). The upper ~20 m of the Fossiliferous Zone is the Marnes à Hydrobies (Blanc-Valleron and Schuler, 1997), which contains marine nannoplankton, shallow water benthic foraminifera, and dinokyste assemblages (Rauscher and Schuler, 1988). The Salt IV unit contains a series of interbedded anhydritic marl, halite, and potash units (predominantly sylvite, with minor carnallite) (Blanc-Valleron and Schuler, 1997). Salt IV is overlain by the Salt V unit and a series of marly units.

Cendón and others (2008) describe the lowermost section of the Salt IV unit (fig. 4). The Marnes à Hydrobies is overlain by the anhydrite-rich marls of the S2 unit, which is overlain by the halites of the S1 unit. The S1 unit is overlain by the anhydrite-rich marls of the S unit, which is overlain by the Mi and Ci units. The Mi unit contains halite, and the Ci unit is composed primarily of interbedded anhydrite, halite, and sylvite. The abundant cumulate and chevron halite crystals and the relatively flat and undisturbed layers of the S1, Mi, and Ci units have been interpreted as original sedimentary features and primary mineralogies (Lowenstein and Spencer, 1990).

The halites of the S unit of Salt IV have initial Br concentrations of 31 ppm; halite Br concentrations increase upsection to 300 ppm (Lutz, ms, 1975; Cendón and others, 2008) (fig. 4). The $\delta^{34}S$ values of sulfates range from ~+12.4 to +23 permil (Cendón and others, 2008): the $\delta^{34}S$ values of sulfates from the S2 and lowest S1 units (~677.5 to 673.5 m) range from ~+19.5 to +23 permil; the $\delta^{34}S$ values from the upper S1 through Ci units (~665 to 647 m) range from ~+12.4 to +18 permil. Therefore, the Br^- values, bromide profile, and the $\delta^{34}S$ values of the S2 and lower S1 unit evaporites (677 to 670 m) are consistent with a seawater parent. The $\delta^{34}S$ values of sulfates interbedded with halites from the upper S1, Mi, and Ci units (670 to 643 m) are below marine values, which indicate that these evaporites did not have a pristine seawater parent.

Reported $^{87}Sr/^{86}Sr$ values from the Salt IV succession range from 0.70907 to 0.70962 (Cendón and others, 2008); these are greater than the $^{87}Sr/^{86}Sr$ values for Early Oligocene seawater (0.70805, Elderfield, 1986). Cendon and others (2008) suggest that a small volume of inflow water, similar in composition to modern thermal waters from the Alsace region with radiogenic Sr, could explain the elevated $^{87}Sr/^{86}Sr$ values of the Salt IV evaporites. These Sr isotope values indicate that the parent waters for the Salt IV evaporites were not pristine seawater, and that a source of non-marine radiogenic Sr is required.

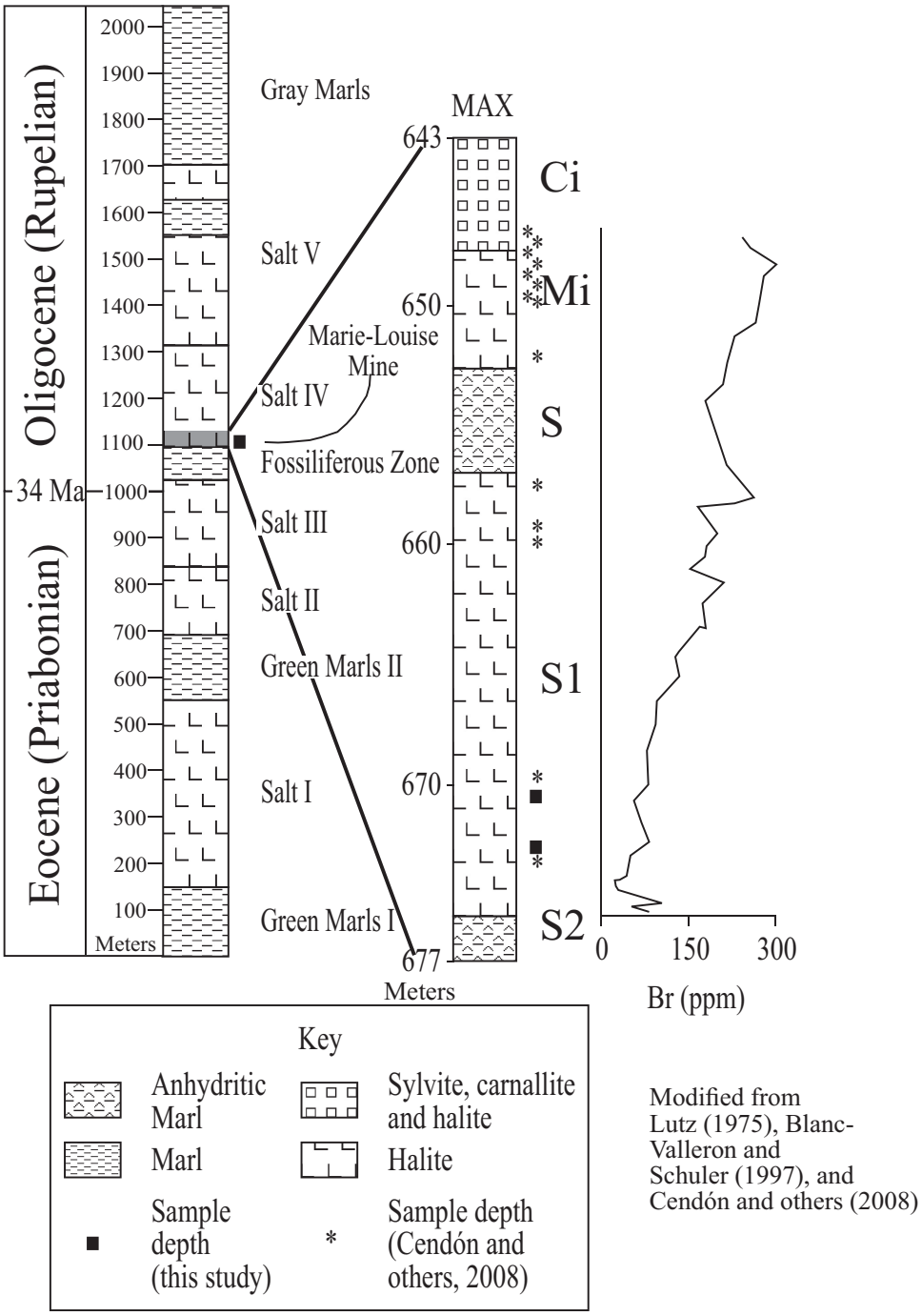

Fig. 4. Stratigraphy of the Rhine Graben with the detailed succession and bromide profile of the lowest portion of the Early Oligocene Salt IV (~34 Ma). The general stratigraphy of the Rhine graben is from Blanc-Valleron and Schuler (1997). The thicknesses in meters next to the general stratigraphic column are average thicknesses of units (Cendón and others, 2008), and are not associated with any particular core. Detailed stratigraphy and bromide profile of lowest ~34 m of Salt IV are from the MAX core as described by Cendón and others (2008) and Lutz (ms, 1975). Core depths of samples analyzed in this study and by Cendón and others (2008) are indicated by squares and asterisks respectively. The sample analyzed in this study from the Marie-Louise Mine, 21 m below the Ci unit, is indicated on the Rhine Graben succession on the left.

Samples analyzed for this study (table 1) were from the S1 unit. Cendón and others (2008) reports analyses (table 1) from the S1, Mi, and Ci Units. The stratigraphic positions of the samples are shown on figure 4. Two analyses from the non-pristine seawater Mi Unit (Canals and others, 1992), reported in Zimmermann (2000), were not used in this study.

Middle–Late Miocene (Serravallian-Tortonian, ~13.5 to ~11.8 Ma)

Carpathian Basins.—The Carpathian Basins (fig. 1) were formed by Late Oligocene through Late Miocene tectonism associated with the suturing of the European and African plates (Kovalevich and Petrichenko, 1997; Krzywiec, 2001). The Carpathian Foredeep Basin (CFB) formed by flexural folding due to thrust sheet loading associated with tectonic activity in the Carpathian Mountains (Krzywiec, 2001). The formation of the East Slovakian Basin (ESB), a back-arc extensional basin, was roughly synchronous with the CFB (Karoli and others, 1997; Krzywiec, 2001). The CFB and ESB occupied the northernmost portion of the Paratethys sea (Krzywiec, 2001).

The initial deposits in both basins were primarily turbidites and deltaic siliciclastics (Bukowski, 1997), which contain marine nannoplankton that place the onset of evaporite deposition at ~13.5 to 12.5 Ma (Early Serravallian) (Krzywiec, 2001). These siliciclastics are overlain by the Zbudza Formation in the ESB and the Wieliczka Formation in the CFB. The Zbudza Formation is composed of clay-rich siltstones, overlain by chevron-rich halites, which are capped by a clay-rich siltstone (Galamay and Karoli, 1997). The basal Wieliczka Formation deposits (fig. 5) are recrystallized halites of the "Oldest Salts," which are overlain by the claystones, sandstones, and conglomerates of the Undersalt Sandstone (Galamay and others, 1997). These siliciclastics are overlain by chevron halites and interbedded clays of the Stratiform Green Salts followed by the Shaft and Spiza Salts (fig. 5) (Garlicki and Wiewiórka, 1981; Galamay and others, 1997). The Spiza Salts are divided into the Lower and Upper Spiza Salts by a clay-rich terrigenous deposit that is several meters thick (Garlicki and Wiewiórka, 1981).

Halites of the CFB and the ESB have initial bromide concentrations of 13 ppm; halite Br concentrations increase upsection to 89 ppm (Garlicki and Wiewiórka, 1981; Garlicki and Wali, 1981; Galamay and Karoli, 1997; Cendón and others, 2004) (fig. 5). Most halite from the CFB and ESB has Br^- concentrations between 30 and 50 ppm. Though halites have Br concentrations below 40 ppm, the normal lower limit of halite formed from seawater, Br^- concentrations do increase upsection. The $\delta^{34}S$ values of sulfates in the Wojnicz borehole are 22.61 ± 0.34 permil (Cendón and others, 2004); $\delta^{34}S$ from sulfate minerals in the Cieszanów-1 core average 22.74± 0.4 permil (Cendón and others, 2004). $\delta^{34}S$ values in laterally adjacent gypsum deposits are 22.7 ± 0.4 permil (Peryt and others, 1997). Therefore, the Br^- profiles and $\delta^{34}S$ values of the evaporites are consistent with a seawater parent, but Br^- in halite is below typical seawater values probably due to syndepositional recycling of NaCl (see below and Cendón and others, 2004). No $^{87}Sr/^{86}Sr$ analyses are reported from the CFB or the ESB.

Samples analyzed for this study (table 1) are from the CFB (Wieliczka Mine, Poland). Cendón and others (2004) reports analyses (table 1) from the CFB (IG-4 core, Wojnicz, Poland).

Galamay and others (1997) and Kovalevich and Petrichenko (1997) report analyses from the CFB and Galamay and Karoli (1997) and Kovalevich and Petrichenko (1997) report analyses from the ESB; only the data screened by Zimmermann (2000) are reported here (table 1). The stratigraphic positions of the samples from the Wieliczka Mine are shown on figure 5.

Gulf of Suez.—The Gulf of Suez (fig. 1) is a roughly northwest-southeast trending, elongate tectonic depression (400 km long by 60 to 80 km wide). The timing of the

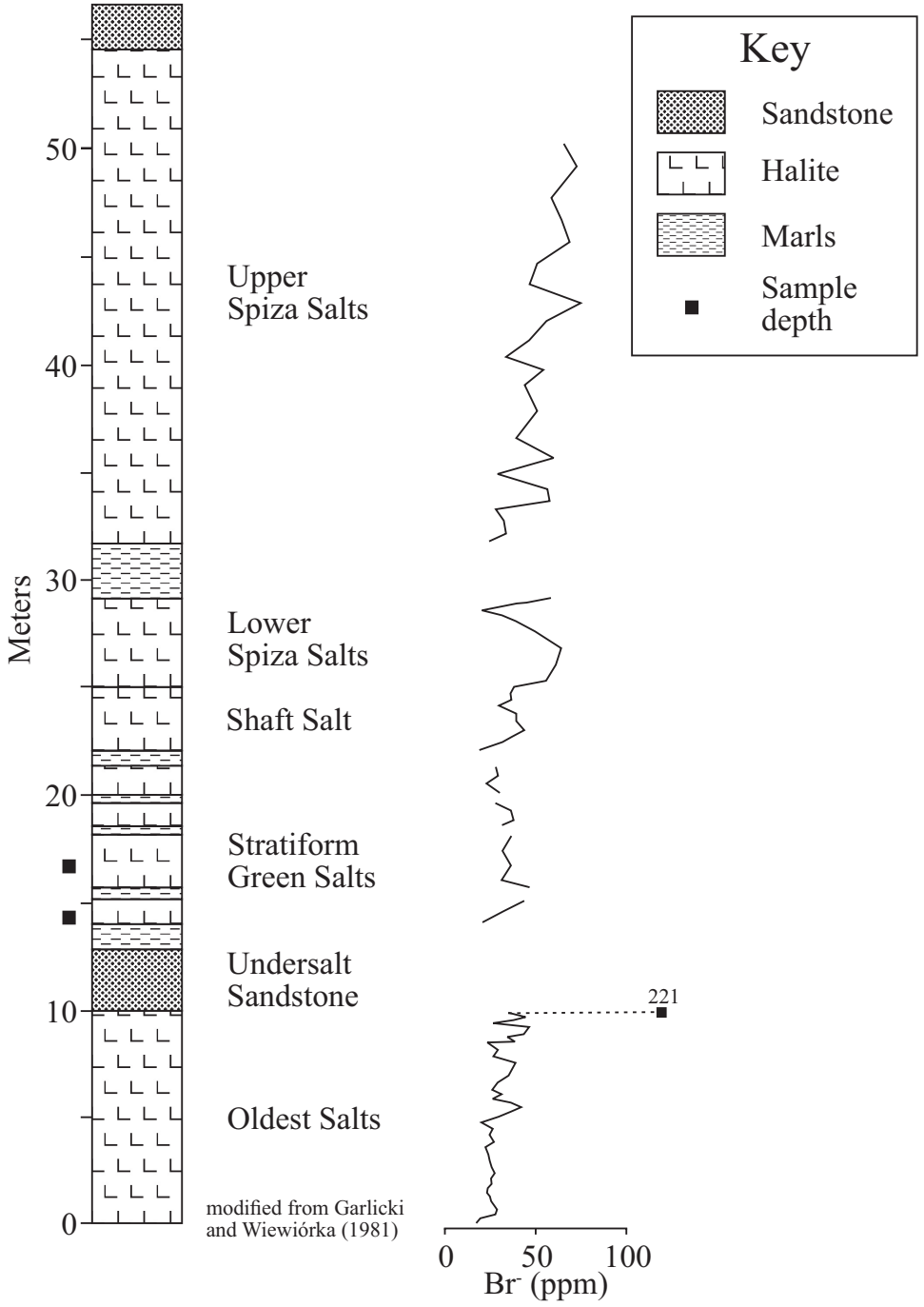

Fig. 5. Stratigraphy and bromide profile of the Wieliczka salt mine, Carpathian Foredeep Basin, Poland (Garlicki and Wiewiórka, 1981). One anomalous Br^- value of 221 ppm is identified by a dashed line. The salt deposits in the Wieliczka salt mine are Serravallian in age (~13.5-12.5 Ma). The depths of the samples analyzed in this study are marked by squares.

inception of the Gulf of Suez Rift is poorly constrained, but the best estimates place the initial rifting at the end of the Oligocene (~25 Ma) with extensional tectonism most active during the Burdigalian through the early Serravallian (~20 through ~14 Ma) (Patton and others, 1994). Active extension of the rift apparently ended in the Middle Miocene and the contemporaneous deposits indicate restricted conditions (Patton and others, 1994). The initial post-rift deposit was the Belayim Formation, a 75 to 150 m thick unit composed of evaporites (primarily anhydrite) and shales interbedded with limestones and sandstones (fig. 6). Fossils in the Belayim Formation and the underlying rift deposits are Mediterranean (Patton and others, 1994). The Belayim Formation is overlain by the Tortonian South Gharib Formation (~300-1200 m thick), which is composed of chevron-rich halite layers with disseminated polyhalite interbedded with shales (Schütz, 1994) that lack fossils (Ouda and others, 2000). The South Gharib Formation is overlain by the Late Tortonian marine Geisum Formation (~60 m thick), a marl unit that contains abundant Indian Ocean fossils (Ouda and others, 2000). The fossils from the Belayim and Geisum Formations bracket the age of the South Gharib Formation to between 11.8 and 8.3 Ma (Ouda and others, 2000). The Geisum Formation is overlain by the Messinian Zeit Formation (45-1000 m thick), which is composed primarily of anhydrite (Griffin, 1999).

Sulfates from the Belayim Formation have reported $\delta^{34}S$ values that range from +21.7 to +23.6 permil (Attia and others, 1995), which are consistent with a seawater parent (Claypool and others, 1980). There are no reported bromide or $^{87}Sr/^{86}Sr$ analyses from the South Gharib Formation.

Samples analyzed for this study (table 1) are from the South Gharib Formation (D-23R core, Hurghada, Egypt) (fig. 6). Samples were recovered from the bottom of the core (fig. 6), which was drilled near the base of the South Gharib Formation. Therefore, the age of the halite samples analyzed is slightly younger than ~11.8 Ma (Ouda and others, 2000), and close in age to the samples from the Carpathian Basins (~13.5-12.5 Ma).

Late Miocene (Tortonian-Messinian, ~7.6 to ~5 Ma)

Lorca Basin.—The Lorca Basin, Spain (fig. 1) is a small basin (~200 km^2) that formed in the early Tortonian (Krijgsman and others, 2000) and was marginal to the Mediterranean Sea during the Late Miocene (Rouchy and others, 1998). The basal deposits in the basin are marine marls of the Hondo Formation (fig. 7), which contain Tortonian nannofossils and planktonic foraminifera (Rouchy and others, 1998; Krijgsman and others, 2000). The Hondo Formation is overlain by the Late Tortonian Serrata Formation (Krijgsman and others, 2000) [also called the Tripoli Unit by Rouchy and others (1998)], composed of a diatomaceous lower member and a silty upper member. The diatoms in the upper portion of the Serrata Formation are non-marine (Servant-Vildary and others, 1990), which indicates inflow of continental waters (Benali and others, 1995). In outcrops, the Serrata Formation is overlain by the "Main Gypsum Unit" (Geel, 1976), composed of clastic, that is remobilized, gypsum, bottom growth gypsum, and nodular anhydrite layers (Taberner and others, 2000). The Main Gypsum Unit is overlain by continental red beds (Rouchy and others, 1998; Taberner and others, 2000).

The stratigraphic position of the "Halite Unit" is not well constrained. The Halite Unit (~250 m thick) in the Lorca Basin is only found in two cores (Lorca-4 and Lorca-5). The Halite Unit (fig. 7) is underlain by a silty, clay-rich unit, similar to the upper Serrata Formation (Upper Tripoli Unit) and is overlain by gypsum, similar to the Main Gypsum Unit. There is a dissolutional unconformity between the Halite Unit and overlying gypsum (Rouchy and others, 1998; Taberner and others, 2000). Therefore, the Halite Unit likely post-dates the Serrata Formation and pre-dates the Main Gypsum Unit placing its age at ~7.6 Ma (Krijgsman and others, 2000).

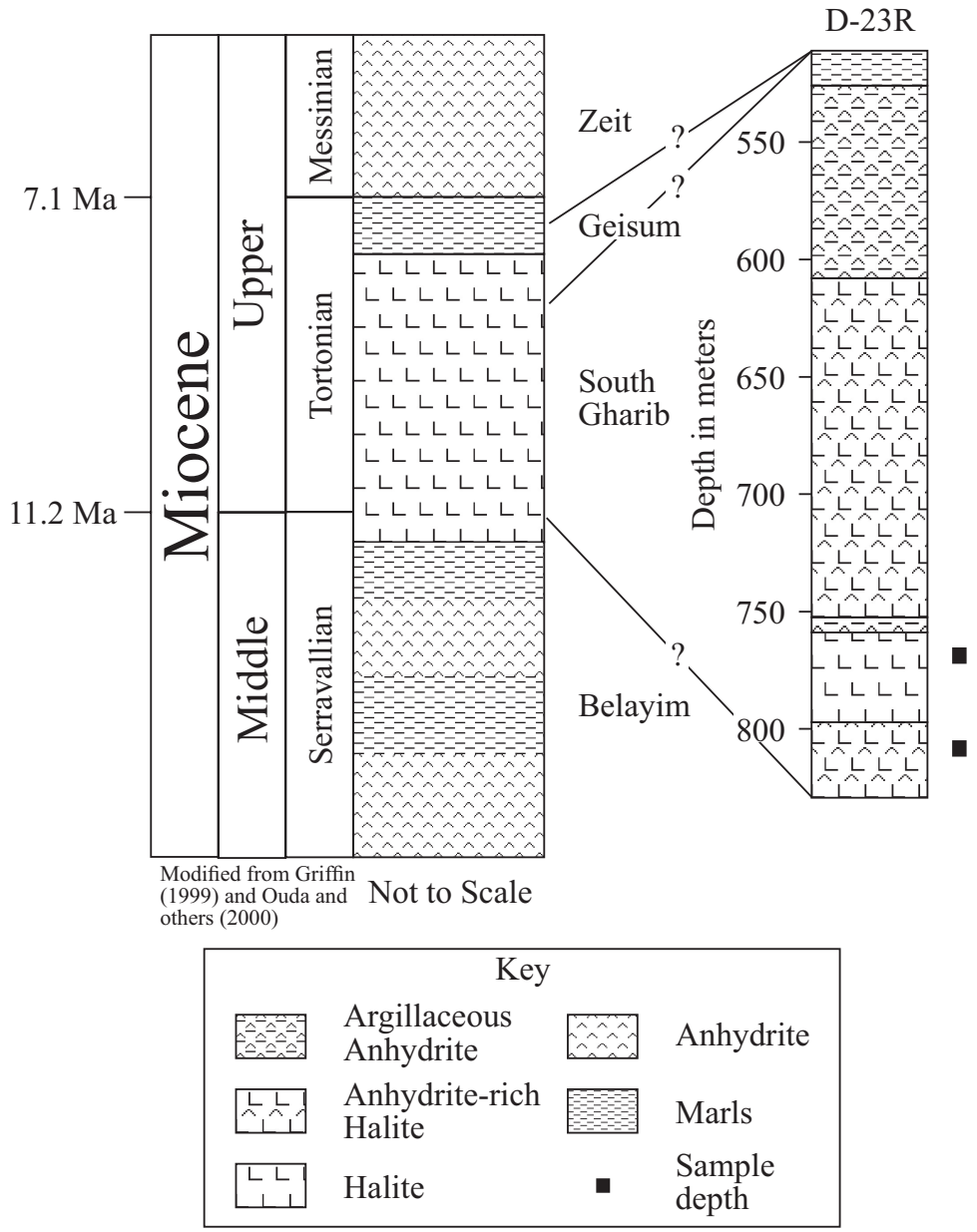

Fig. 6. Stratigraphic column of the Middle and Late Miocene of the Red Sea rift basin, with detailed stratigraphy of the South Gharib Formation. Stratigraphic column of Middle and Upper Miocene deposits of the Red Sea Rift is modified from Griffin (1999). Stratigraphic column of the South Gharib Formation is from a description of core DH-23R provided by BHP minerals (personal communication). Depths of samples analyzed in this study are indicated by squares. Question marks on the lines that connect regional stratigraphy and the core units show tentative correlations. Shales at the top of the core may be the Geisum Formation, or part of the South Gharib Formation.

The Halite Unit (fig. 7) is composed of bedded halite and massive halite (Ayora and others, 1994a; García-Veigas and others, 1994; Taberner and others, 2000). The bedded halite contains bottom growth chevrons with sulfate-rich clay partings (Tab-

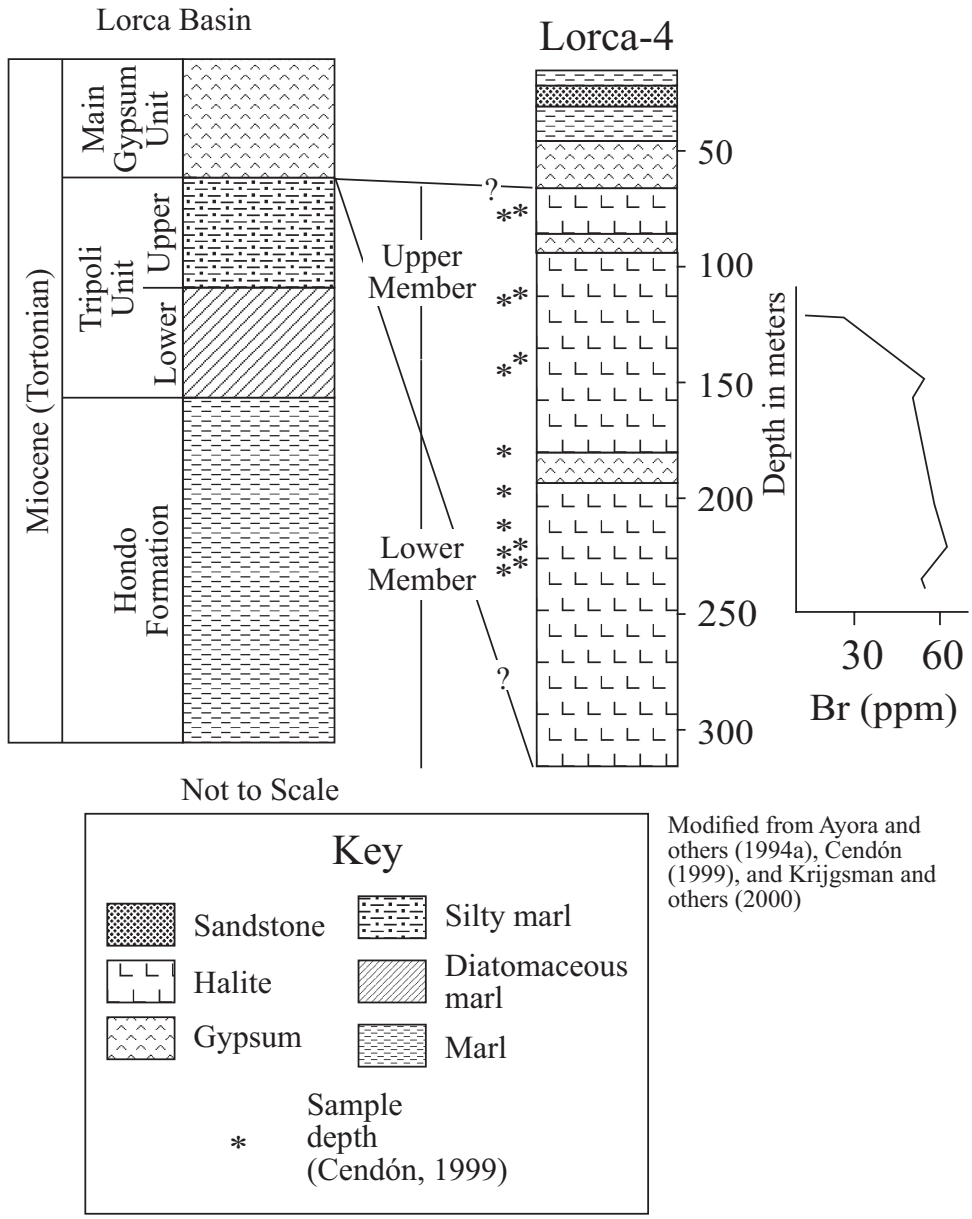

Fig. 7. Regional stratigraphy of the Lorca Basin (~7.6 Ma) based on Krijgsman and others (2000). Stratigraphic column and bromide profile are from the Lorca-4 core (Ayora and others, 1994a; Cendón, ms, 1999). Depths of samples analyzed by Cendón (ms, 1999) are indicated by asterisks. The base of the Main Gypsum Unit is at ~65 m; there is a dissolutional contact between the underlying Halite Unit and the Main Gypsum Unit. The upper and lower members of the Halite Unit are marked on the Lorca-4 core. Question marks on lines that connect the basin stratigraphy to the cores reflect the uncertainty regarding the stratigraphic position of the Halite Unit.

erner and others, 2000). The massive halite is composed of diagenetic halite formed displacively within a clay matrix (Taberner and others, 2000). Anhydrite and polyhalite occur in halite layers and are most abundant in the lower portion of the succession (Ayora and others, 1994a).

The halites of the Lorca Basin have basal bromide concentrations of ~45 ppm; Br concentrations increase upsection to ~60 ppm at ~140 m; however, from ~140 to ~75 m, halite Br^- concentrations decrease from 30 ppm to below detection limits (<10 ppm) (Ayora and others, 1994a; García-Veigas and others, 1995) (fig. 7). Ayora and others (1994a) use this change in the bromide concentration of halite at ~140 m to divide the Halite Unit into the Lower and Upper Members (fig. 7). The $\delta^{34}S$ of the sulfates interbedded with the Lower Halite Member range from +21.37 to +22.86 permil and those interbedded with the Upper Halite Member range from+20.83 to +22.15 permil (Taberner and others, 2000). Therefore, the evaporites of Lower Halite Member have Br^- concentrations, a bromide profile, and $\delta^{34}S$ values consistent with a seawater parent. The evaporites of the Upper Member have a Br^- profile consistent with the introduction of bromide-poor inflow to the basin, which indicates that they did not form by evaporation of pristine seawater. There are no reported $^{87}Sr/^{86}Sr$ analyses from the Lorca Basin.

Cendón (ms, 1999) reports 70 analyses from the halites of the Lorca Basin (Lorca 4 samples), 57 of which are recalculated from Ayora and others (1994a) (table 1).

Caltanissetta Basin.—The Caltanissetta Basin (fig. 1) is a northeast-southwest trending basin (roughly 100 km by 100 km), formed in the Late Miocene by compressive tectonics (Butler and Lickorish, 1997). The initial deposits of the Caltanissetta Basin are Tortonian marine marls overlain by the Messinian Gessoso-Solfifera Formation (fig. 8), which contains diatomites, carbonates, and evaporites (Decima and Wezel, 1971). The diatomaceous unit is the marine Tripoli Member, which is overlain by the Calcare di Base Member (García-Veigas and others, 1995), an inorganic carbonate interpreted to have formed under evaporative conditions (Decima and others, 1988). The Calcare di Base Member grades basinward into the Cattolica Gypsum Member, which grades into the Halite Member (García-Veigas and others, 1995). These deposits are overlain by the Pasquasia Gypsum Member followed by the continental Arenazzolo Member (García-Veigas and others, 1995). The Arenazzolo Member is unconformably overlain by the Early Pliocene marine Trubi Chalk (Decima and Wezel, 1971).

The Halite Member is composed of halite and potash salts (García-Veigas and others, 1995) and has been separated into Units A through D (Decima and Wezel, 1971) (fig. 8). Unit A is composed of laminated gray halite that grades upwards into massive layers of cumulate halite crystals (Lugli and others, 1999). The overlying Unit B, separated from Unit A by a thin dark gray mudstone, contains massive layers of gray cumulate halite crystals interbedded with six separate kainite (table 2) layers in the Realmonte Mine (Lugli and others, 1999). However, in other locations in Sicily, Unit B contains carnallite, bischofite, sylvite, kieserite, and langbeinite (table 2) in the same stratigraphic position as the kainite (Decima and Wezel, 1971; Lugli and others, 1999). The top of Unit B is marked by large salt polygons, interpreted to have formed by desiccation (Lugli and others, 1999). The overlying Unit C is composed of cumulate and chevron-rich halites and clay-rich partings; Unit C is overlain by Unit D, composed of anhydrite and halite (Lugli and others, 1999).

Clay layers from Units A and B contain marine foraminifera but no nannofossils (Bertini and others, 1998). Clay layers from Units C and D exhibit a rich and diverse assemblage of Messinian (5.6-6.0 Ma) foraminifera and nannofossils that indicates that the basin was first desiccated and then flooded by seawater (Bertini and others, 1998).

Bromide concentrations in the halite of the Halite Member range from below detection (<13 ppm) to 400 ppm, but vary greatly between the high values obtained by Decima (1978) and the lower values of García-Veigas and others (1995). Halites of Unit C from the Realmonte Salt Mine, from which fluid inclusions were analyzed for major ion composition in this study [Cendón (ms, 1999) and García-Veigas and others

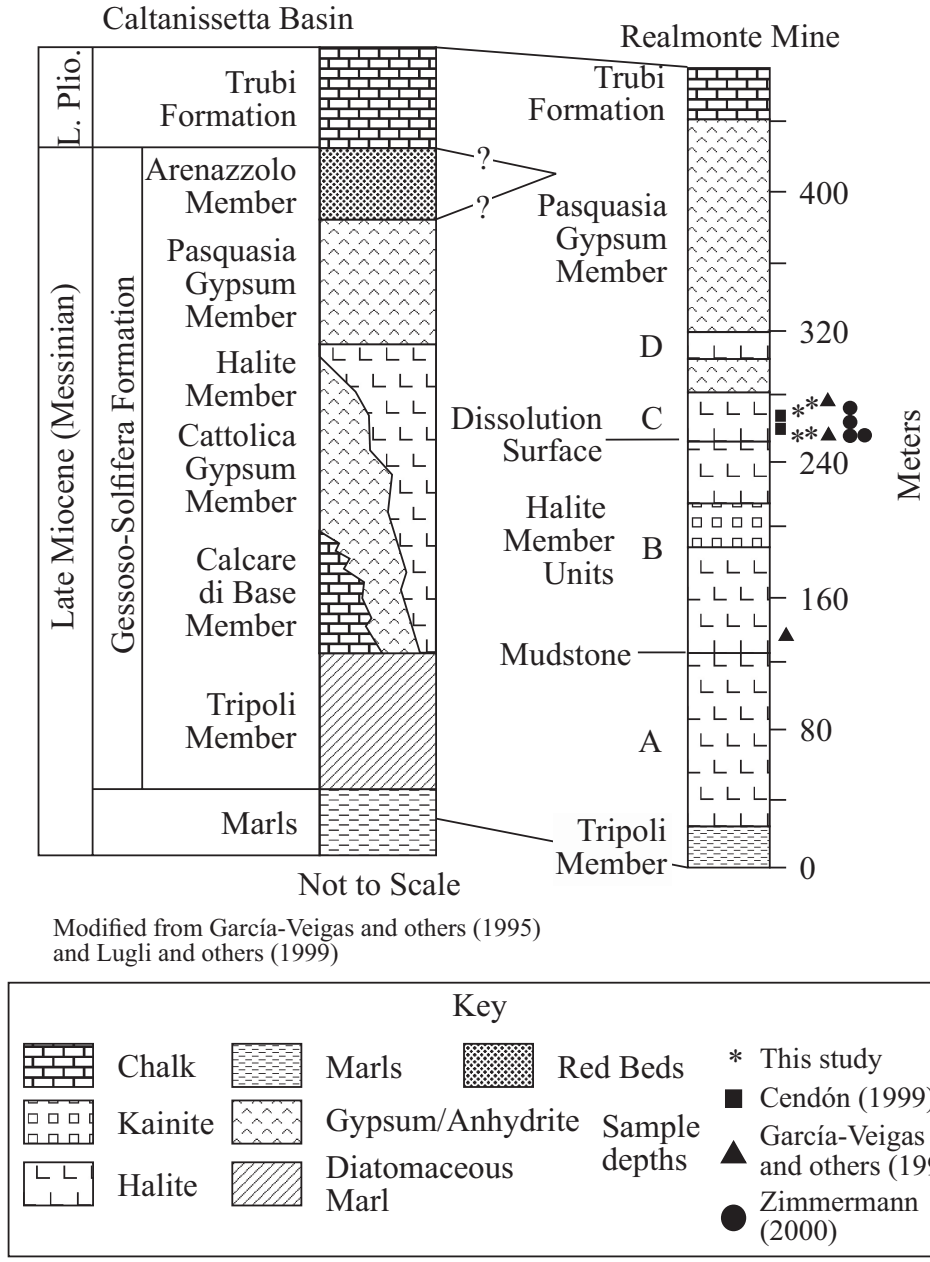

Fig. 8. Regional stratigraphy of the Caltanissetta Basin based on García-Veigas and others (1995). The Calcare di Base grades basinward into the Cattolica Gypsum, which grades into the Salt Member. Stratigraphic section is from the Realmonte Mine (García-Veigas and others, 1995; Lugli and others, 1999). Depths of samples analyzed in this study and by Cendón (ms, 1999), García-Veigas and others (1995), and compiled by Zimmermann (2000) from the Realmonte Mine are shown with separate symbols next to the stratigraphic column. Question marks on the lines indicating the pinching out of the Arenazzolo Member are due to the lack of information about this deposit in the Realmonte Mine.

(1995)] have bromide concentrations of <20 ppm (2 measurements by García-Veigas and others, 1995). The $\delta^{34}S$ values of sulfates within the Halite Member range from +21.2 to +24.3 permil (García-Veigas and others, 1995). The $^{87}Sr/^{86}Sr$ analyses of the sulfates from the Cattolica Gypsum Member average 0.70890 ± 0.00003 and from the Halite Member average 0.70888± 0.00002 (Zimmermann, 2000). Therefore, the evaporites of the Halite Member have marine fossils and $\delta^{34}S$ and $^{87}Sr/^{86}Sr$ values consistent with a seawater parent (Müller and Mueller, 1991). However, the low Br^- concentrations of Unit C halites were interpreted by García-Veigas and others (1995) to be have been produced by syndepositional recycling of halite.

Samples analyzed in this study (table 1) were from the Realmonte Mine (Unit C). Cendón (ms, 1999) also reports analyses (table 1) from the Realmonte Mine (Unit C). García-Veigas and others (1995) report analyses from Units A, B, and C (Realmonte Mine; Cattolica-5; Siculiana-1; and Porto-Empedocle-38). Two analyses from Unit C of the Realmonte Mine, compiled by Zimmermann (2000), are also used in this paper (table 1). The stratigraphic position of the Realmonte Mine samples is shown in figure 8.

Red Sea.—The Red Sea (fig. 1) is an elongate basin, ~2000 km long and between 180 and 360 km wide. This basin was connected to the Mediterranean Sea prior to ~8.3 Ma (Ouda and others, 2000) and is currently connected to the Indian Ocean. Late Miocene evaporites, primarily composed of anhydrite and halite, were recovered from the Red Sea at Sites 225 and 227 of Leg 23 of the Deep Sea Drilling Project (Witmarsh and others, 1974a, 1974b). The evaporites are from the deepest cores; deposits below the evaporites were not penetrated at Sites 225 or 227 and therefore remain speculative at this location (Stoffers and Ross, 1974). However, the halite and anhydrite layers are interbedded with marine black shales, which contain Late Messinian (~5 Ma) marine benthic foraminifera and nannofossils (Stoffers and Ross, 1974). The evaporites are overlain by a marine dolomitic claystone, which contains Early Pliocene benthonic and planktonic foraminifera and nannofossils (Stoffers and Ross, 1974).

The halites from Sites 225 and 227 have initial bromide concentrations of 48 ppm; halite Br^- concentrations increase upsection to 228 ppm (Stoffers and Kühn, 1974). The $\delta^{34}S$ analyses of sulfates interbedded with the halite range from +22.8 to +23.3 permil (Shanks and others, 1974). Therefore, the Br^- concentration, bromide profile, and the $\delta^{34}S$ values of the evaporites are consistent with a seawater parent. There are no reported $^{87}Sr/^{86}Sr$ analyses of carbonates or sulfates from the Messinian of the Red Sea.

Kovalevich and others (1997) report analyses from Sites 225 and 227; Lazar and Holland (1999) report analyses from Site 227. Only the data geochemically screened by Zimmermann (2000) are presented here (table 1).

METHODS

Fluid Inclusion Analysis Technique

A total of 583 fluid inclusions were incorporated for this study, with 122 not previously reported fluid inclusion analyses. Fluid inclusion analyses were collected from halites with chevron petrographic textures that are diagnostic of precipitation at the bottom of a brine body and indicate that the halite precipitated from surface brines and not from ground waters or subsurface diagenetic brines (Lowenstein and Hardie, 1985). Chevrons are bands of primary fluid inclusions parallel to crystal growth faces, which form by the entrapment of parent waters during halite precipitation (Lowenstein and Hardie, 1985). Samples with obvious secondary fluid inclusions along healed fractures or with large, solitary fluid inclusions (ambiguous origin) were not analyzed.

The new data presented in this study (Appendix table A1) were gathered using the cryoenvironmental scanning electron microscope ("ESEM") technique (Timofeeff

and others, 2000, 2001). Halite samples were broken into cleavage chips approximately $10 \times 6 \times 2$ mm in size. Fluid inclusions in these chips and aqueous standard solutions were simultaneously flash-frozen to a homogeneous glass by dipping them into a slush of solid and liquid nitrogen. A sample holder containing the halite chip and frozen aqueous standards was placed in a cryogenic vacuum chamber attached to an ESEM (model: Electroscan 2020) where the halite was cut with a manipulator knife to expose frozen inclusions. The sample holder was moved from the cryo-chamber into the ESEM where the fluid inclusions and standards were analyzed by an attached electron dispersive spectrometer ("EDS"). The detection limit for this instrument is 0.5 wt.% for Na^+ and 0.1 wt.% for Mg^{2+}, Ca^{2+}, K^+, SO_4^{2-}, and Cl^-, with typical precisions between 2 and 7 percent and accuracies less than 7 percent (Timofeeff and others, 2000).

The ESEM operates under a low-pressure N_2 environment, which causes slight scattering of incident beam electrons. This phenomenon, referred to as the "skirt-effect," produces a halo of electrons, some of which impact the host halite. The signal from the halite matrix caused by stray electrons produces elevated Na^+ and Cl^- values. Other major-ion concentrations are not affected by the skirt effect. The Na^+ and Cl^- concentrations must therefore be adjusted using the Harvie-Møller-Weare ("HMW") (Harvie and others, 1984) equilibrium thermodynamic model for brines, assuming halite saturation at 25 °C and the measured concentrations of all other ions in solution (K^+, Ca^{2+}, Mg^{2+}, and SO_4^{2-}) (Timofeeff and others, 2001).

The data of Cendón (ms, 1999), listed in Appendix table A2, were gathered using the cryo-scanning electron microscope ("SEM") technique outlined in Ayora and Fontarnau (1990) and Ayora and others (1994a). The cryo-SEM technique is very similar to the cryo-ESEM technique. The major difference is that the SEM samples must have a conductive coating and no coating is necessary for the ESEM method. The data compiled by Zimmermann (2000) also includes some fluid inclusion analyses that followed a microdrilling and pipette sampling technique coupled with wet chemical methods (Petrichenko, 1973).

The concentrations of Na^+ and Cl^- reported by Cendón (ms, 1999) and Zimmermann (2000) were recalculated in a charge-balanced, halite-saturated brine at 25 °C using the HMW computer model. The original data reported by Cendón (ms, 1999) are shown in Appendix table A2, along with the recalculated brine chemistries. The data used by Zimmermann (2000), along with recalculated brine chemistries, are shown in Appendix table A3.

The major-ion compositions of fluid inclusions in marine halite of the same age, when plotted on concentration crossplots, should display compositional trends produced by evaporative concentration and precipitation of salts. These "evaporation paths" indicate the evolution of a single brine, unaffected by late-stage salt recycling or the influence of different inflow waters (for example, continental or hydrothermal). Poorly defined evaporation paths, that is scattered data on concentration crossplots, indicate a "mixed source" parent (Hardie, 1984), which by definition cannot be pure seawater. Therefore, marine halites of the same age must exhibit a global chemical signal with brine inclusion compositions that outline distinctive evaporation paths. Most important is that the evaporation paths from geographically-separated, and broadly syndepositional marine basins must overlap on concentration crossplots.

RESULTS

The major-ion chemistries of fluid inclusions from Cenozoic halites are listed in Appendix tables A1, A2, and A3 and plotted on figures 9, 10, 11, and 12. The bulk of the inclusions contain Na-MgK-Cl-SO_4 brines. Only the Bresse Basin and a small number of Catalan sub-basin halites contain fluid inclusions with Na-Mg-K-Ca-Cl brines. The low concentration of calcium and relatively high concentration of sulfate in most Cenozoic brine inclusions indicate that the parent waters contained molar

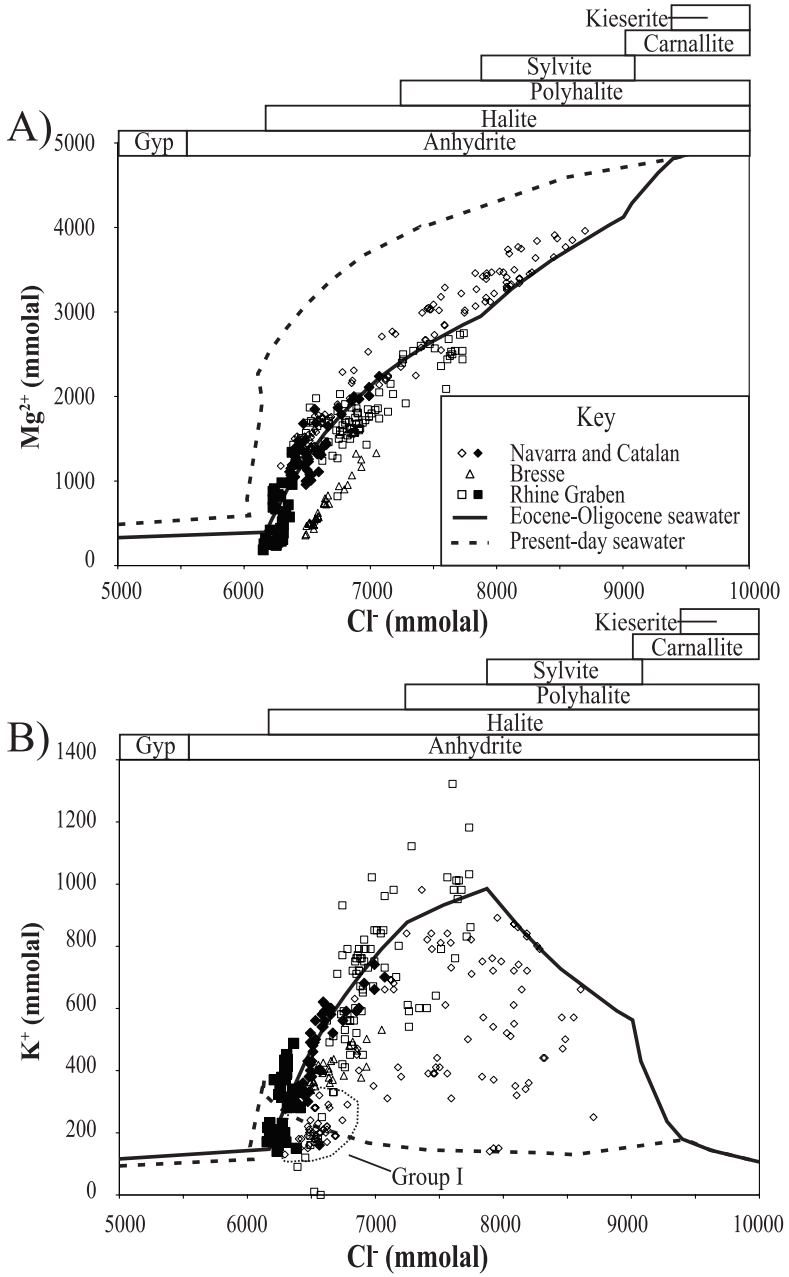

Fig. 9. Plots of the major ion chemistry of Late Eocene-Early Oligocene (36-34 Ma) fluid inclusions. Closed symbols represent fluid inclusions interpreted to be composed of evaporated seawater. Open symbols represent fluid inclusions from non-marine or questionable samples. See text for details. Solid lines are the evaporation pathways simulated by the HMW computer program using the calculated composition of Eocene-Oligocene seawater (table 8). Minerals predicted to precipitate during the evaporation of Eocene-Oligocene seawater are shown above each plot. Dashed lines represent the evaporation pathways generated by the HMW computer program for modern seawater (table 8). Evaporation paths are graphical representations of brine evolution, which is controlled by evaporative concentration and precipitation of salts. Changes in the slopes of evaporation paths are caused by salt precipitation.

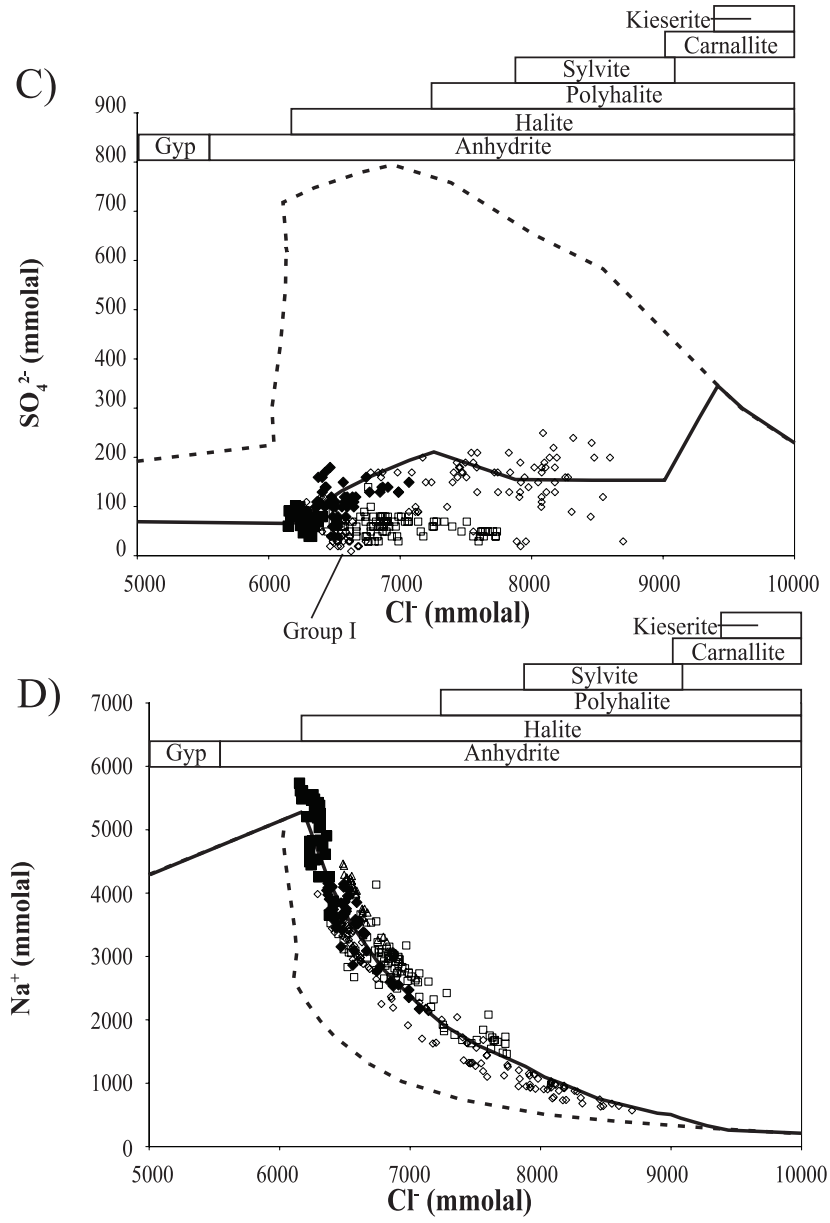

Fig. 9 (continued).

$SO_4^{2-} > Ca^{2+} - 1/2HCO_3^-$, which, following evaporation and precipitation of calcite and gypsum, produced a SO_4^{2-}-rich, Ca^{2+}-depleted brine at halite saturation. That pathway, with waters falling on the SO_4^{2-}-rich side of the Ca^{2+}-SO_4^{2-} chemical divide (Hardie and Eugster, 1970), is similar to the evaporation of modern seawater. The Ca^{2+}-rich, SO_4^{2-}-depleted brines in the Bresse Basin and in some of the Catalan sub-basin inclusions indicate that the parent waters of these halites were different from other Late Eocene marine halites.

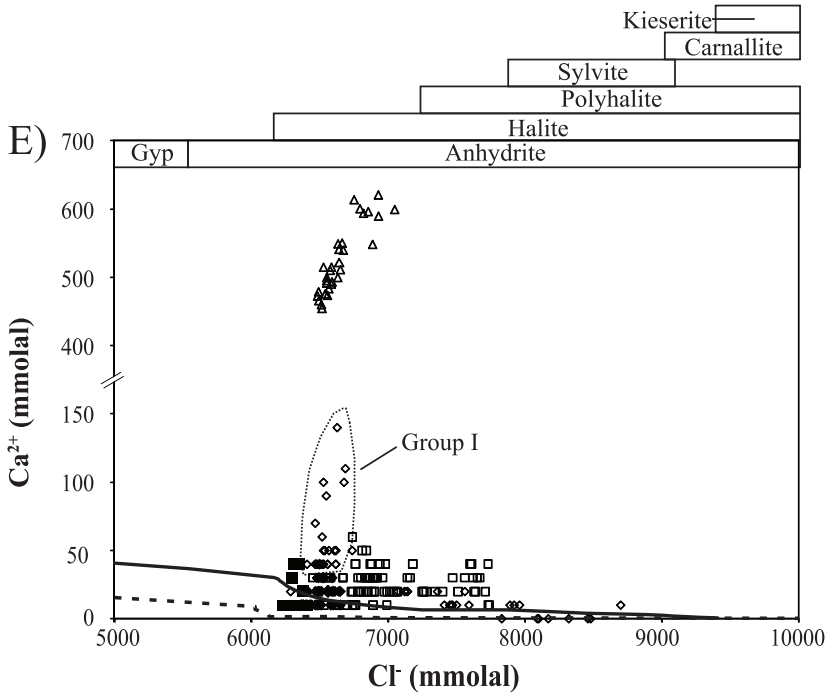

Fig. 9 (continued).

Before interpretations are made about changes in Cenozoic seawater from fluid inclusion compositions, samples formed from pristine seawater must be distinguished from those formed from non-marine or mixed marine-non-marine waters using the sedimentological and geochemical evidence outlined above. However, even though the evidence may indicate that the halite is marine in origin, the fluid inclusion data may indicate a mixed origin. Therefore, the fluid inclusion chemistries themselves can serve as a check on their seawater origin.

The sedimentological and geochemical evidence for the Late Eocene-Early Oligocene basins (36-34 Ma) is summarized in table 4. Some of the halites clearly did not have a pristine seawater parent, including: (1) The Subiza Mine samples from the Navarra sub-basin, which are from layers interbedded with potash salts; and (2) Rhine Graben samples from 670 to 643 m of the MAX core, which had evaporites with non-marine $\delta^{34}S$ and $^{87}Sr/^{86}Sr$ values. Some samples have questionable origins. The lowest halite from the Catalan sub-basin (Group I, figs. 2 and 9), for example, has inclusions with both Ca^{2+}-rich and SO_4^{2-}-rich brines. The Ca^{2+}-rich fluid inclusions may reflect inflow of non-marine diagenetic or hydrothermal waters from the margins of the Catalan sub-basin during the Late Eocene (Ayora and others, 1994b, 2001; Cendón and others, 2003). The "upper part of the lower halite" from the Catalan sub-basin (Group III, fig. 2) contains high concentrations of polyhalite and terrigenous clays due to continental recharge (Cendón and others, 2003). The Bresse Basin samples contain no evidence of a seawater parent other than high Br^- concentrations of the halites, and contain Ca^{2+}-rich inclusion brines, in marked contrast to the composition of other Late Eocene inclusion brines. The fluid inclusion compositions from these non-marine or modified marine samples are shown by open symbols on the plots versus Cl^- (fig. 9). All other data are indicated by closed symbols.

TABLE 4

Summary of evidence for origin of the Eocene-Oligocene (36-34 Ma) parent waters. Evidence for non-marine inflow or questionable parent waters is shown in bold

	Basin			Navarra (~36 Ma)	Catalan (~36 Ma)	Bresse (~36 Ma)	Rhine Graben (~34 Ma)
Stratigraphy	Below			Marine	Marine	**Continental**	Marine
	Fossils			Yes	Yes	**No**	Yes
	Above			Continental	Continental	**Continental**	Continental
	Fossils			No	No	No	No
	Late-stage salts			Yes	Yes	No	Yes
	Samples			Biurrun: lower halite unit **Subiza: interbedded with potash**	Groups I and II lower halite unit Group III "upper part of lower halite unit"	Middle of halite section	S1 samples: base to top of unit Mi and Ci: base to potash
Geochemistry	Bromide			Increases upsection (50-300 ppm)	Increases upsection (11-220 ppm)	Increases upsection (100-150 ppm)	Increases upsection (31-300 ppm)
	$\delta^{34}S$			Marine (~+20‰)	Marine (+20.86 to +22.09‰)	NA	Lower S1 (678-670 m) marine (+19.5 - +22.7‰) **Upper S1-Ci (670-643 m) non-marine (+12.4 -+18‰)**
	$\frac{^{87}Sr}{^{86}Sr}$	Carbonate		NA	NA	NA	NA
		Evaporite		NA	NA	NA	**Radiogenic (0.709072 - 0.709550)**
	Fluid Inclusion Analyses		Evaporation Path	Biurrun: yes **Subiza: scattered**	**Groups I and III: scattered** Group II: yes	**Yes, but Ca^{2+}-rich brine.**	Lower S1: yes **Upper S1, Mi and Ci: scattered**
			Overlaps data from other basins?	Biurrun: Yes Subiza: No	Groups I and III: no Group II: yes	No	Lower S1: yes Upper S1, Mi and Ci: no
	Origin			Biurrun: marine Subiza: non-marine inflow/ recycling	Groups I and III: non-marine inflow Group II: marine	Non-marine inflow.	Lower S1: marine Upper S1, Mi and Ci: non-marine inflow/potash recycling.

The sedimentological and geochemical evidence for the Serravallian-Tortonian basins (13.5-11.8 Ma) is summarized in table 5. The low Br^- in the Carpathian Basin halites is interpreted to have been produced by syndepositional recycling of halite by seawater (see below). All the data plotted are interpreted to represent a seawater parent source and are indicated by closed symbols on the plots versus Cl^- (fig. 10).

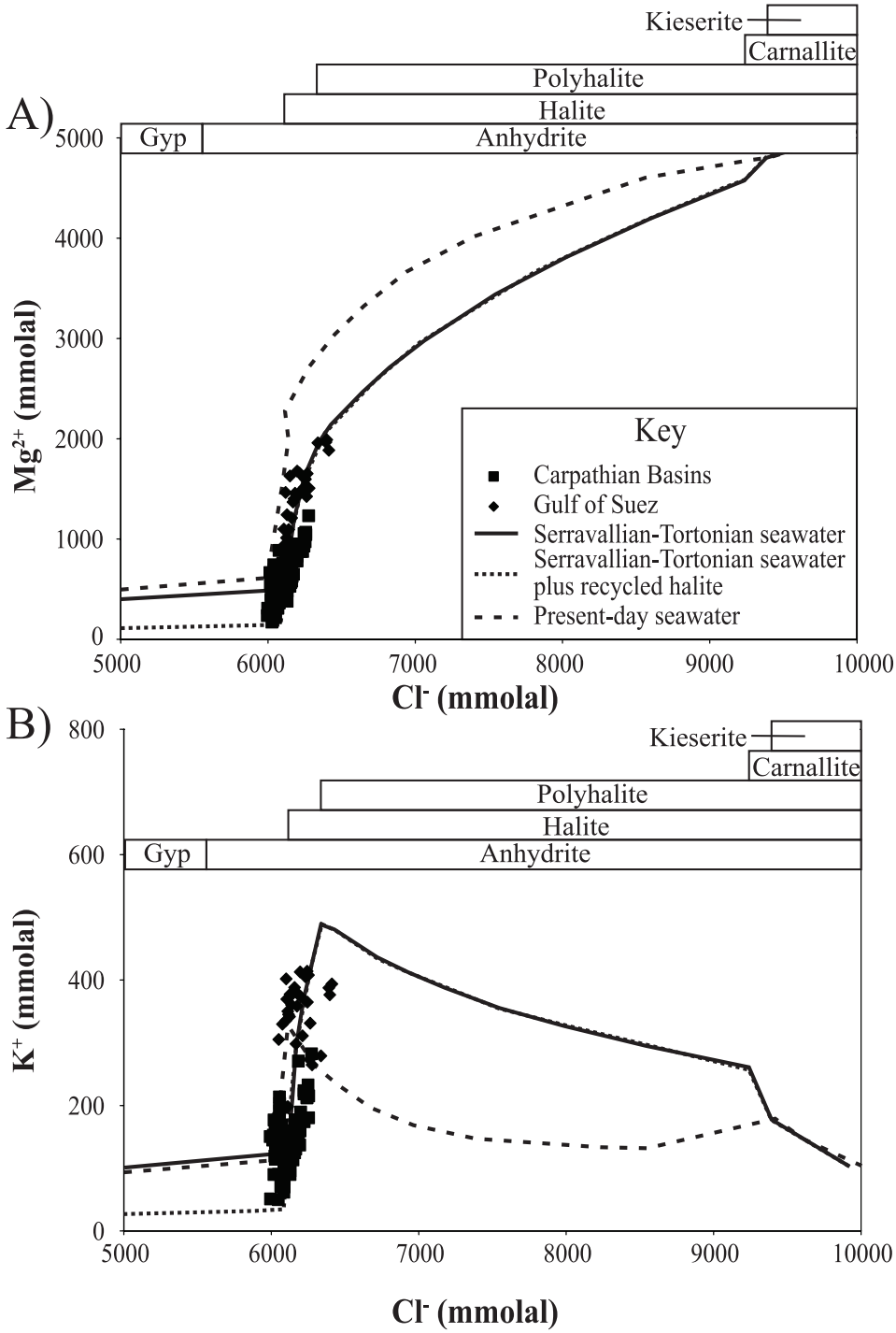

Fig. 10. Plots of the major-ion chemistry of Serravallian-Tortonian (13.5-11.8 Ma) fluid inclusions. Solid lines are the evaporation pathways simulated by the HMW computer program using the calculated composition of Serravallian-Tortonian seawater (table 8). Minerals predicted to precipitate during the evaporation of Serravallian-Tortonian seawater are shown above each plot. Dotted lines represent the evaporation pathways of Serravallian-Tortonian seawater with 1.5 moles of halite recycled per kilogram of H_2O. Dashed lines represent the evaporation pathways of modern seawater (table 8).

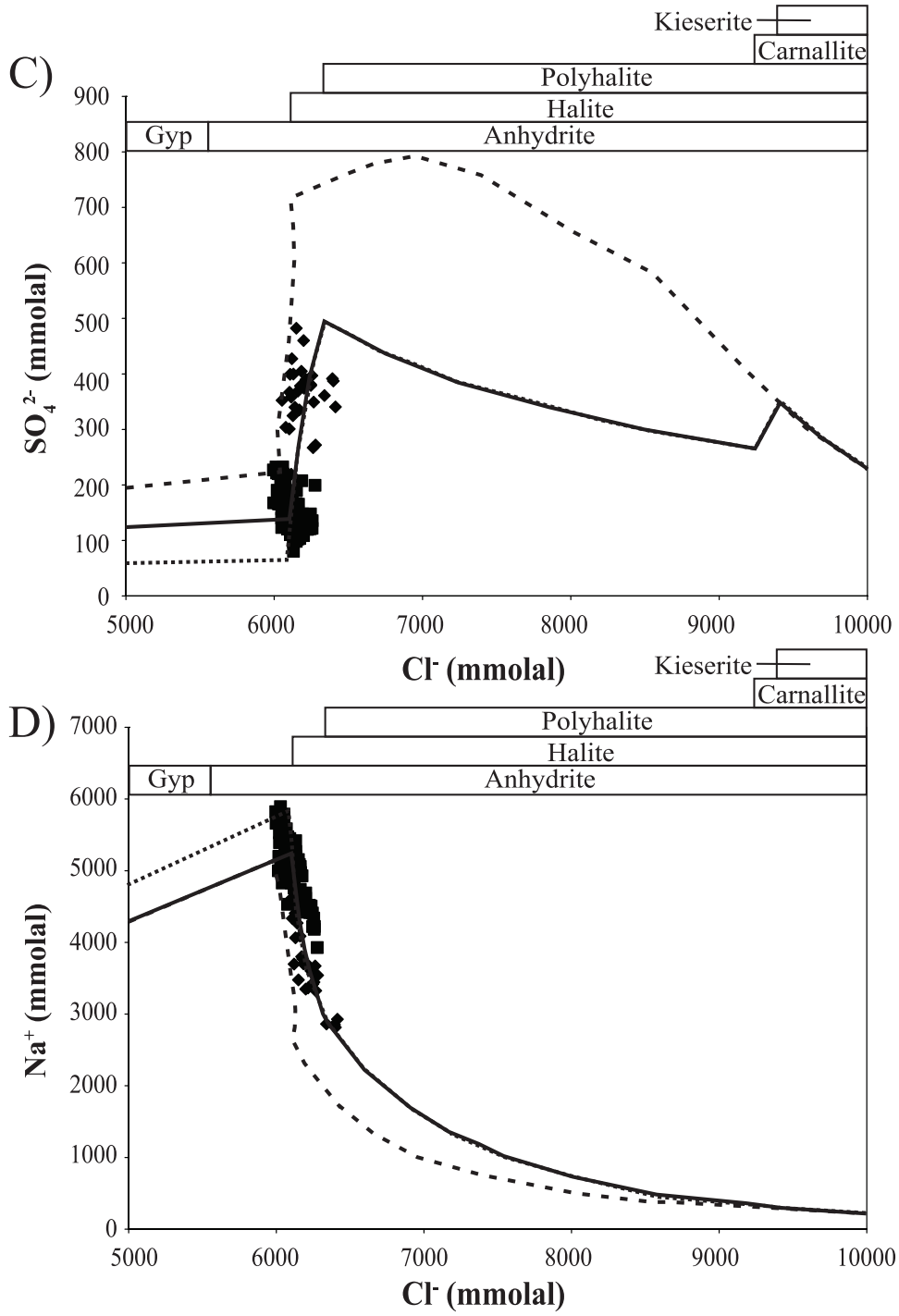

Fig. 10 (continued).

TABLE 5

Summary of evidence for the origin of the Serravallian-Tortonian (~13.5-~11.8 Ma) parent waters. Evidence for non-marine inflow or questionable parent waters is shown in bold

	Basin			Carpathian Basins (~13.5-12.5Ma)	Gulf of Suez (~11.8 Ma)
Stratigraphy	Below			Marine	Marine
	Fossils			Yes	Yes
	Above			Continental	Marine
	Fossils			No	Yes
	Late-stage salts			Not in any of the locations discussed in this paper	Not in the core used in this study
	Samples			Towards base of halite	Towards base of halite
Geochemistry	Bromide			Increases upsection but **low in "first halite" (13 to 89 ppm)**	NA
	$\delta^{34}S$			Marine (+22.7 ± 0.4‰)	Marine (+23.6 to +21.9‰)
	$\frac{^{87}Sr}{^{86}Sr}$	Carbonate		NA	NA
		Evaporite		NA	NA
	Fluid Inclusion Analyses		Evaporation Path	Yes, but Mg^{2+}, K^+, and SO_4^{2-} are low, and Na^+ is high in "first halite"	Yes
			Overlaps data from other basins?	Yes, but ion concentrations are below seawater values: likely that inflowing seawater recycled halite	Yes
	Origin			Marine **(with recycled halite)**	Marine

The sedimentological and geochemical evidence for the Tortonian-Messinian basins (7.6-5 Ma) is summarized in table 6. Some of the fluid inclusions probably did not form strictly from evaporated Miocene seawater, including: (1) The Lorca Basin samples, which are underlain and overlain by non-marine deposits, and have decreasing upward Br^- concentrations. Non-marine inflow waters, including Ca-rich waters for the lower part of the Halite Unit and continental inputs for the upper part of the Halite Unit, have been invoked for the Lorca Basin (Ayora and others, 1994a; García-Veigas and others, 1995; Taberner and others, 2000); and (2) Units A and B of the Halite Member of the Caltanissetta Basin, which contain potash salts that may have influenced brine compositions. The fluid inclusion compositions from these questionable samples are indicated by open symbols on the plots versus Cl^- (fig. 11). One fluid inclusion analysis from the Red Sea is highly concentrated relative to other Red Sea inclusion brines; this anomalous fluid inclusion composition is also indicated by an open symbol (fig. 11). All other data are indicated by closed symbols, including Halite Member C of the Caltanissetta Basin, which has Br^- concentrations below those expected from seawater evaporation, but which is interpreted to have formed from seawater that has recycled halite (see below and García-Veigas and others, 1995).

QUALITATIVE INTERPRETATION OF THE DATA: PLOTS VERSUS CHLORIDE

Cenozoic fluid inclusion compositions and the evaporation path of modern seawater simulated with the HMW computer program are plotted vs. Cl^- (figs. 9-11). These plots are used to determine whether the compositions of Cenozoic fluid inclusions outline evaporation paths and how those paths qualitatively compare to the evaporation paths of modern seawater. Brine evolution, as shown by the evaporation paths, is controlled by evaporative concentration and precipitation of salts. The major

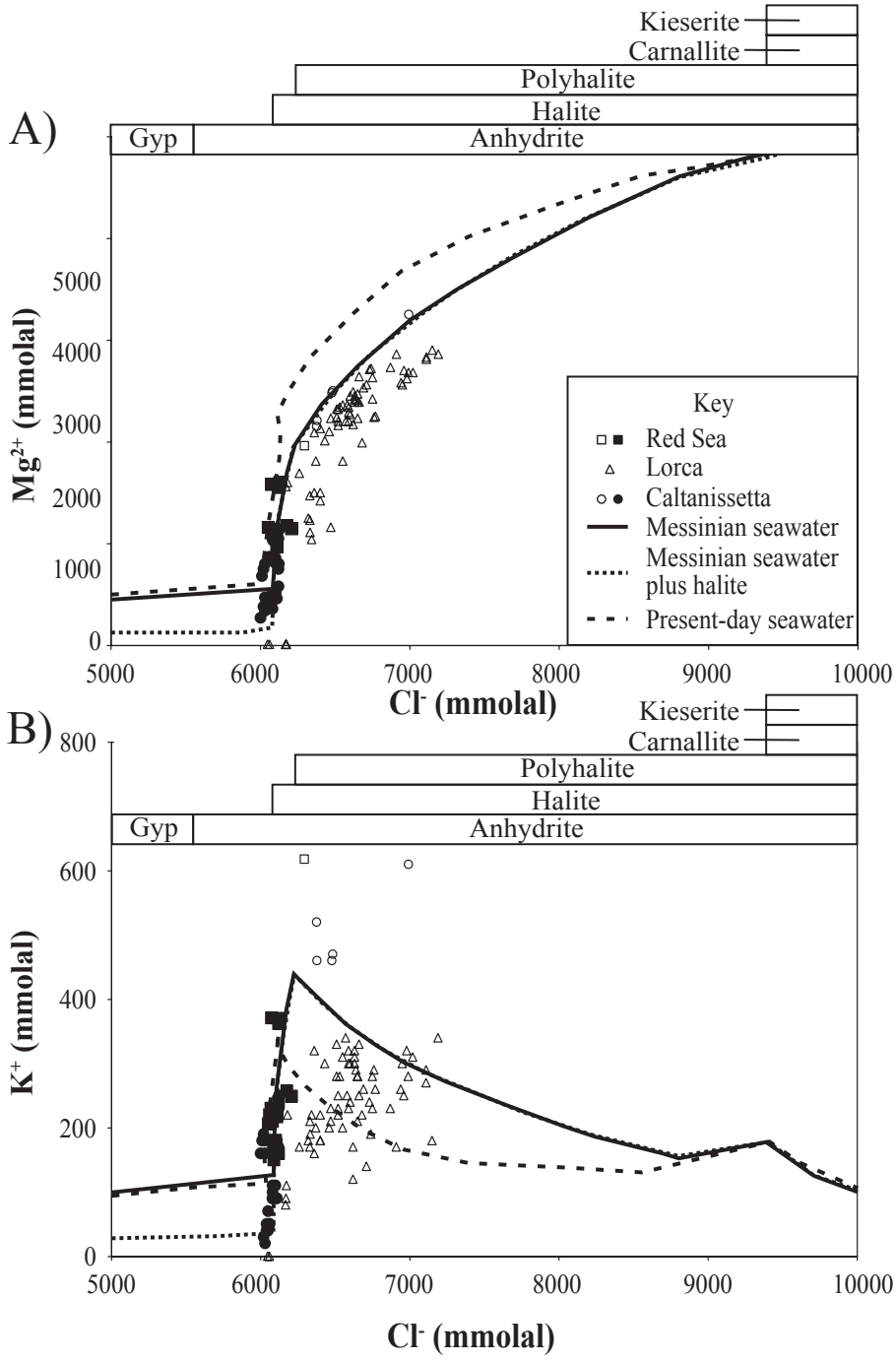

Fig. 11. Plots of the major-ion chemistry of Tortonian-Messinian (~7.6-5 Ma) fluid inclusions. Closed symbols represent fluid inclusions interpreted to contain evaporated seawater. Open symbols represent fluid inclusions from non-marine or questionable samples. Solid lines are evaporation pathways simulated by the

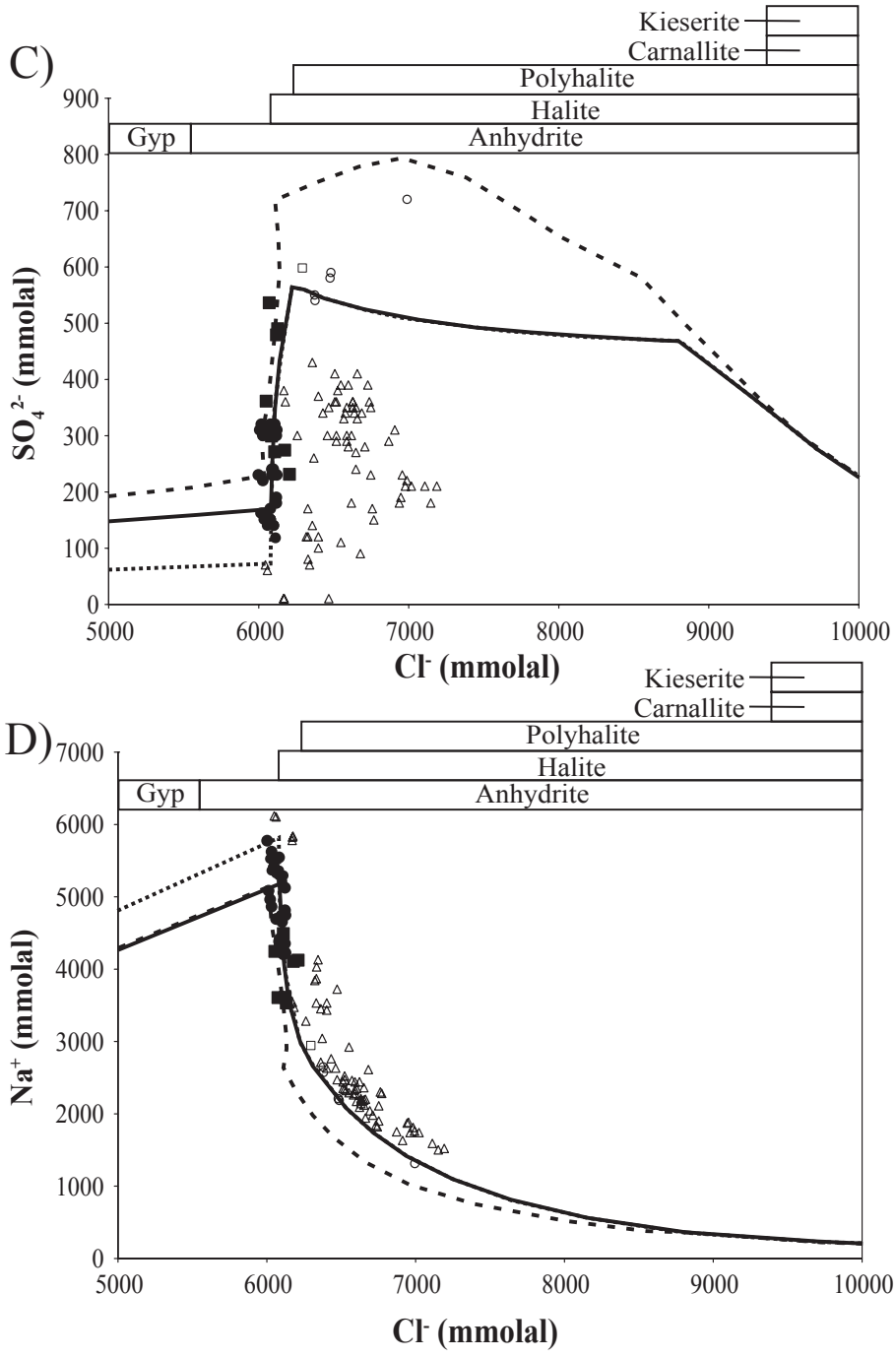

Fig. 11 (continued) HMW computer program using the calculated composition of Messinian seawater (table 8). Minerals predicted to precipitate during the evaporation of Messinian seawater are shown above each plot. Dotted lines show evaporation pathways of Messinian seawater composition but with 1.5 moles of halite recycled per kilogram of H_2O. Dashed lines show the evaporation pathways of modern seawater (table 8).

TABLE 6

Summary of evidence for the origin of the Tortonian-Messinian (7.6-5.0 Ma) parent waters. Evidence for non-marine inflow or questionable parent waters is shown in bold

	Basin			Red Sea (5-6 Ma)	Lorca (7.6 Ma)	Caltanissetta (5.6-6 Ma)
Stratigraphy	Below			NA	Marine?	Marine
	Fossils			NA	**Yes (continental)**	Yes
	Above			Marine	**Continental**	Continental
	Fossils			Yes	**No**	No
	Late-stage salts			No	No	Units A and B, yes Units C and D, no
	Samples			Near base of halite	Base to top of halite	**Units A and B, base to potash** Units C and D, base towards top of halite
Geochemistry	Bromide			Consistent with marine values (48 to 228 ppm)	Lower Member consistent with marine values (45 to 60 ppm) **Upper member less than marine (0 to 40 ppm)**	Marine to low (20-190 ppm). Unit C halites **too low (<20 ppm) for pristine seawater parent**
	$\delta^{34}S$			Marine (+22.8 - 23.3‰).	Marine (+22.86 - +20.83‰)	Marine (+20.3 - +22.9‰)
	$\frac{^{87}Sr}{^{86}Sr}$	Carbonate		NA	NA	NA
		Evaporite		NA	NA	Marine (0.70890 – 0.70888)
	Fluid Inclusion Analyses		Evaporation Path?	Yes	**Scattered**	**Units A and B ?** Units C and D, Yes, but Mg^{2+}, K^{+}, and SO_4^{2-} are low, and Na^{+} is high
			Overlaps data from other basins?	Yes	No	Units A and B: No Units C and D: Yes
	Origin			Marine	Non-marine (Mixed source)	Units A and B, ? Units C and D, marine with recycled halite

change in slope of the modern seawater evaporation paths (figs. 9-11) at Cl^- concentrations of ~6000 millimolal (millimoles per kg of H_2O, hereafter referred to as "mmolal") represents removal of Na^+ and Cl^- in equal molar proportions during halite precipitation.

Late Eocene-Early Oligocene (36-34 Ma)

The Mg^{2+} vs. Cl^- plot (fig. 9A) shows that the closed symbols (fluid inclusions from marine halites) define a brine evolution path that is different from present-day seawater evaporation. The open symbols, with the notable exception of the Bresse Basin data, follow a broadly similar evaporation path. The Mg^{2+} concentrations of the Late Eocene-Early Oligocene fluid-inclusion brines all fall below the modern seawater evaporation path. These low Mg^{2+} values indicate that the Late Eocene-Early Oligo-

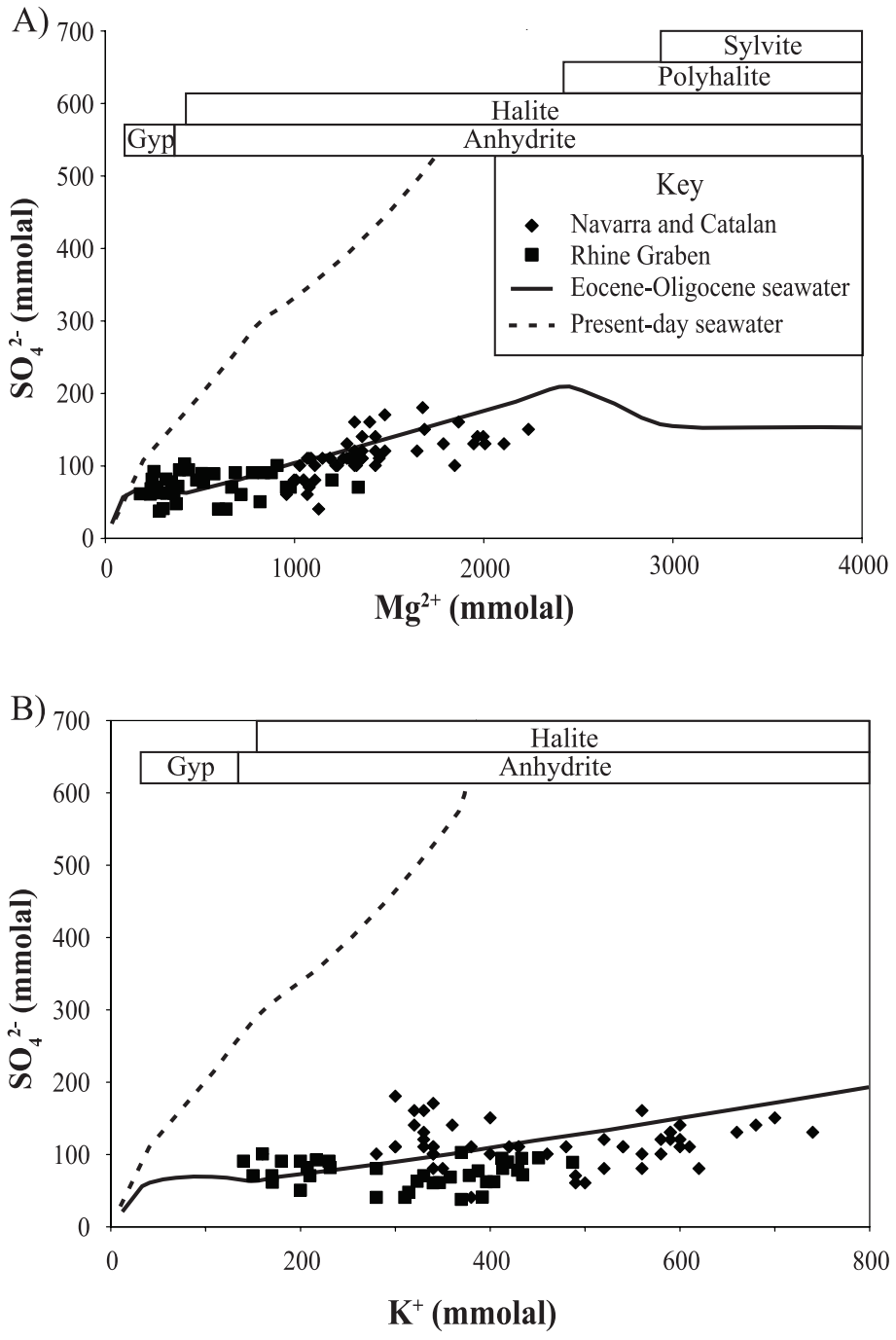

Fig. 12. Plots of the major-ion chemistry of fluid inclusions interpreted to contain evaporated seawater from the Late Eocene-Early Oligocene (A-C), Serravallian-Tortonian (D-F), and Messinian (G-I). Solid lines are evaporation pathways using calculated paleoseawater compositions (table 8). Dashed lines represent evaporation paths of modern seawater (table 8). Minerals predicted to precipitate during evaporative concentration are shown above the plots. Evaporation paths on the plots vs. K^+ (B, E, and H) terminate at polyhalite saturation.

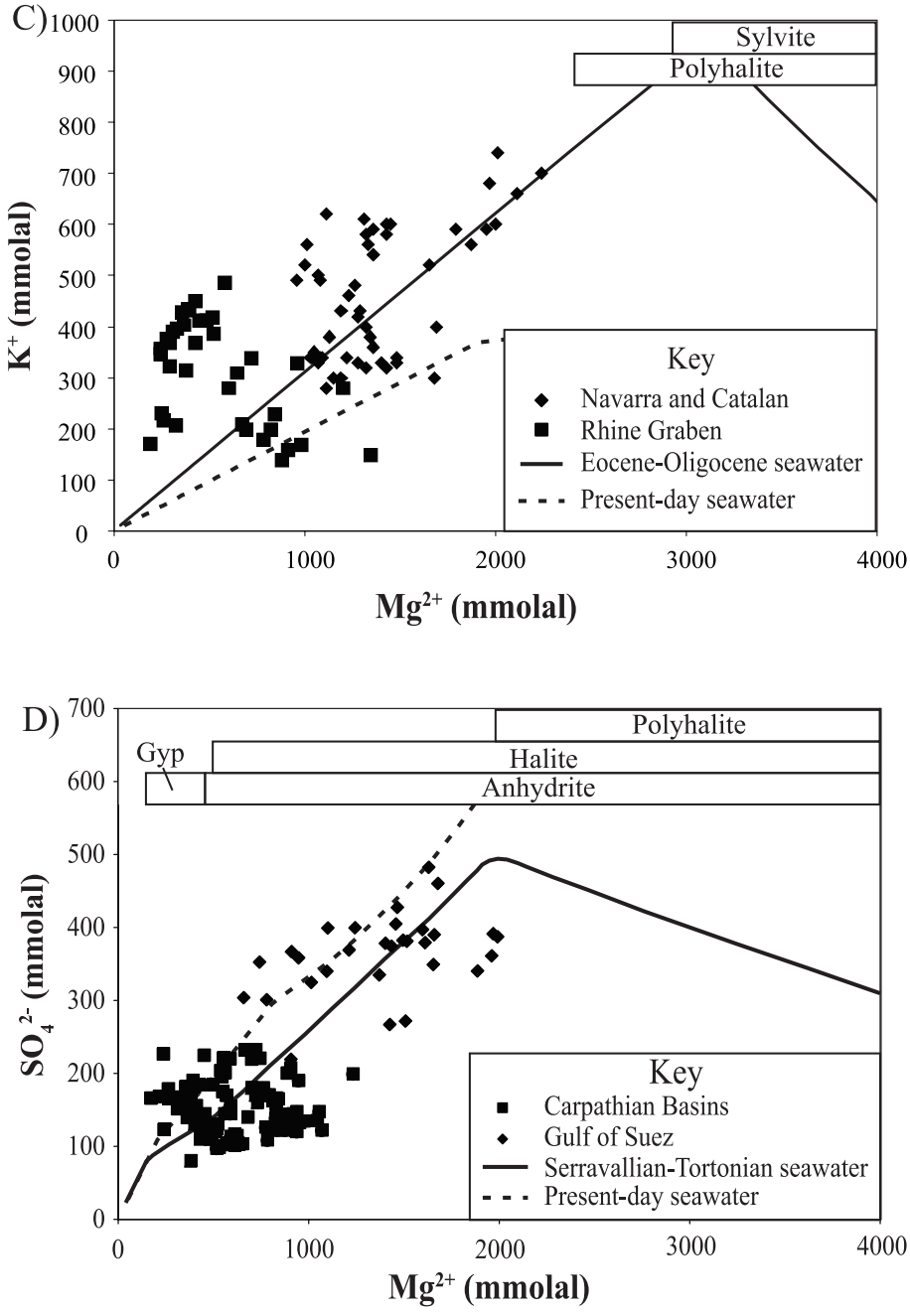

Fig. 12 (continued).

cene parent water was relatively depleted in Mg^{2+} compared to modern seawater. The Mg-bearing salts predicted to form along the evaporation path outlined by the Late Eocene-Early Oligocene fluid inclusion compositions are polyhalite, sylvite, carnallite, and kieserite (fig. 9A), all of which are present in the basins. The mineral assemblage

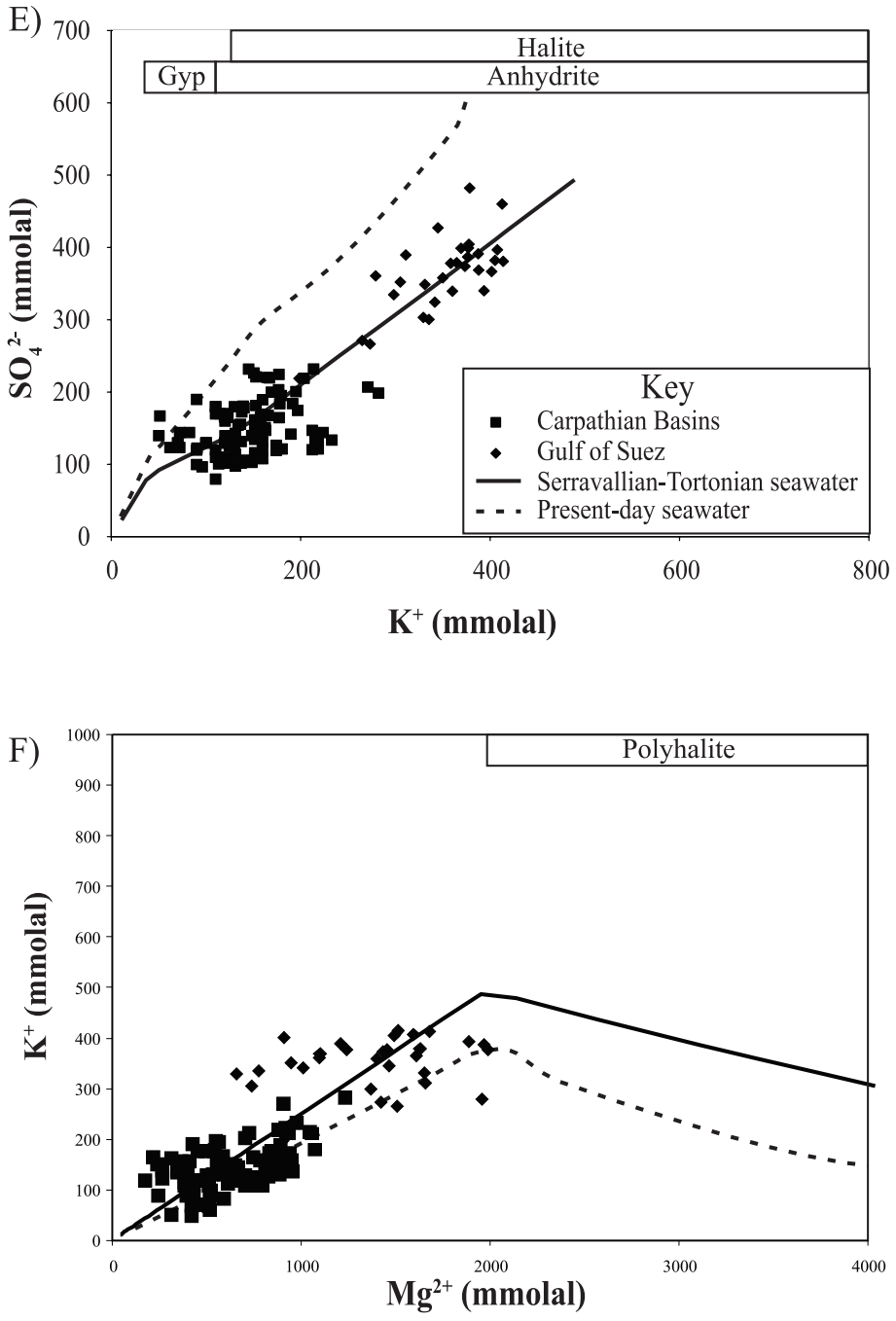

Fig. 12 (continued).

produced from this brine evolution is in marked contrast to modern seawater in which the Mg-bearing sulfate salts epsomite, hexahydrite, and kieserite precipitate after polyhalite and before carnallite (table 2).

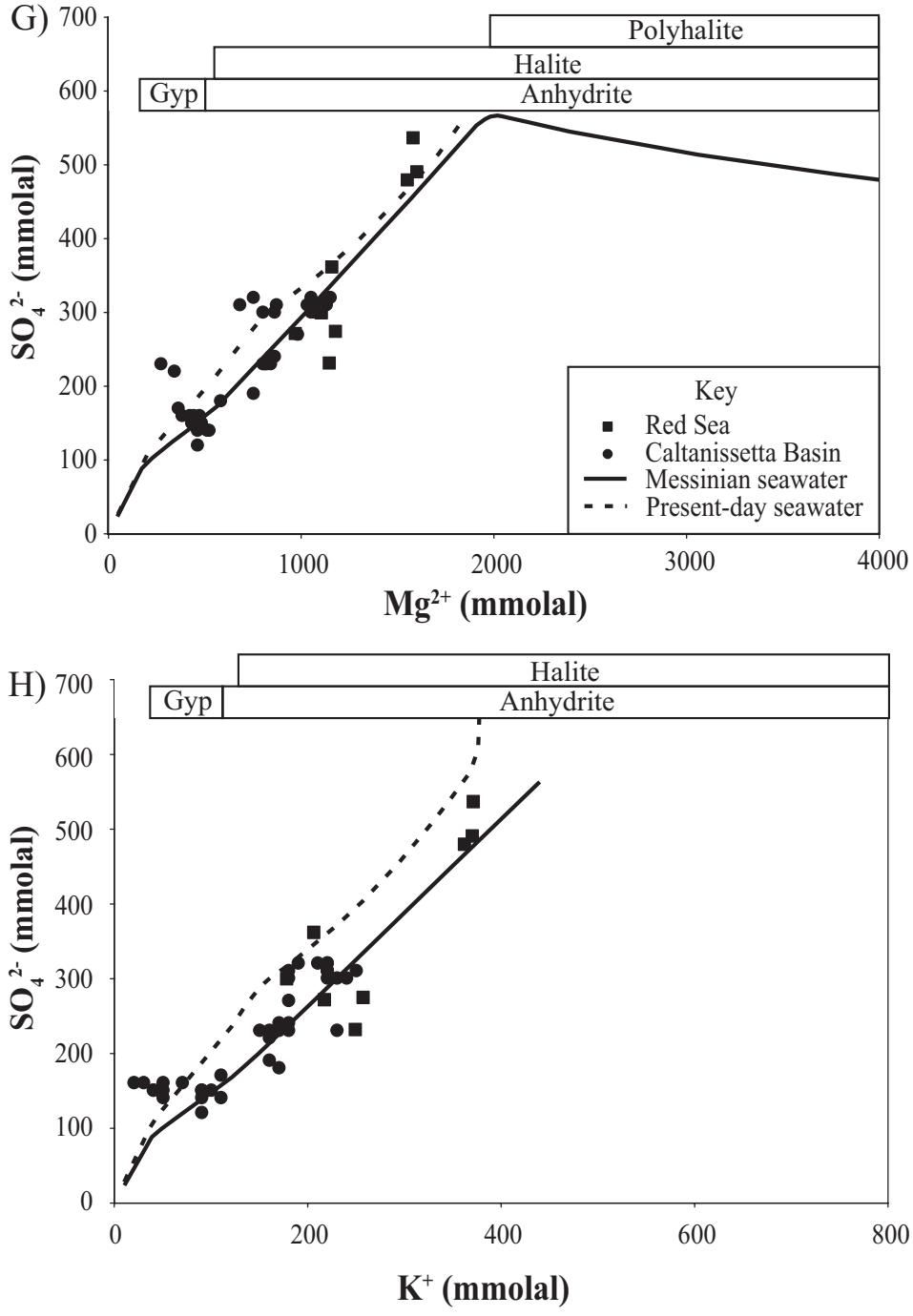

Fig. 12 (continued).

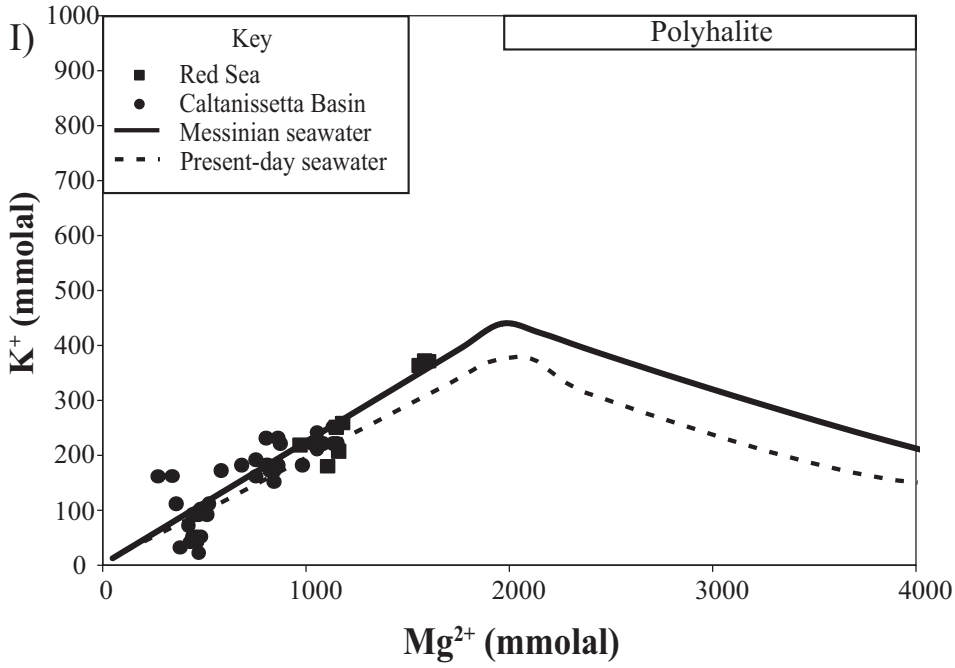

Fig. 12 (continued).

The K^+ vs. Cl^- plot (fig. 9B) also shows that the closed symbols define a brine evolution path that is different from evaporation of present-day seawater. The open symbols show significant scatter on this plot. The K^+ in fluid inclusion brines, with a maximum concentration of 740 mmolal, is higher than predicted from the evaporation of modern seawater (~380 mmolal) (fig. 9B). The K-bearing salts predicted to form based on the evaporation path outlined by the Late Eocene-Early Oligocene fluid inclusion compositions are polyhalite, followed by sylvite (fig. 9B), both of which are present in these basins. The high K^+ concentrations attained by the Late Eocene-Early Oligocene inclusion brines are probably due to the relative depletion of SO_4 in Late Eocene-Early Oligocene seawater, which caused the K-bearing salt polyhalite to form later in the evaporation sequence than during evaporation of modern seawater (see below). This lag in precipitation of polyhalite then allowed K^+ to build up in the evaporating brines.

The most striking aspect of the Late Eocene-Early Oligocene fluid inclusions is shown on the SO_4^{2-} vs. Cl^- plot (fig. 9C). The closed symbols define a brine evolution path that is quite different from modern seawater. The SO_4^{2-} concentrations of the fluid inclusions, with maximum values less than 200 mmolal, fall well below the modern seawater path, which reach SO_4^{2-}-concentrations up to ~800 mmolal. The low SO_4^{2-} concentrations of the Late Eocene-Early Oligocene fluid inclusions in the halite field indicate that SO_4^{2-} was relatively depleted in comparison to modern seawater. Sulfate-bearing minerals predicted to form based on the evaporation pathway of the Late Eocene-Early Oligocene fluid inclusion compositions are gypsum-anhydrite and polyhalite, which are present in the basins.

The Na^+ vs. Cl^- plot (fig. 9D) shows that the closed symbols define an evaporation path. The open symbols also follow the same path. The Cl^- concentrations of the first halites (~6160 mmolal) are slightly higher than those produced during the evapora-

tion of modern seawater (~6030 mmolal). Therefore, the Cl^- concentrations at initial halite saturation were slightly higher in the Late Eocene-Early Oligocene parent water relative to modern seawater.

The Ca^{2+} vs. Cl^- plot (fig. 9E) shows that the Bresse basin data define an evaporation path different from all other fluid inclusion compositions of the same age, which have very low Ca^{2+} concentrations. The Bresse Basin parent waters were compositionally distinct from the parent waters of the other Late Eocene-Early Oligocene basins. Low concentrations of Ca^{2+} were also measured in fluid inclusions from the lower halites of the Lower Halite Unit of the Catalan sub-basin (Group I) which have been interpreted to indicate non-marine diagenetic or hydrothermal inflow waters at that time (Ayora and others, 1994b, 2001; Cendón and others, 2003).

Serravallian-Tortonian (13.5-11.8 Ma)

The Mg^{2+} vs. Cl^- plot (fig. 10A) shows that the closed symbols define a brine evolution path that is slightly different from present-day seawater evaporation. The Mg^{2+} concentrations all fall just below the modern seawater evaporation pathway. Therefore, the Serravallian-Tortonian parent water was relatively depleted with respect to Mg^{2+} compared to modern seawater. The Mg-bearing salts predicted to form based on the evaporation path outlined by the SerravallianTortonian fluid inclusion compositions are polyhalite, followed by carnallite and kieserite. However, there are no late-stage salts in the study areas. The mineral sequence produced during this brine evolution is slightly different than that of modern seawater, in which $MgSO_4$ salts (that is, kieserite) precipitate prior to carnallite.

The K^+ vs. Cl^- plot (fig. 10B) shows that the closed symbols define a brine evolution path very similar to modern seawater. Some of the K^+ concentrations of the Serravallian-Tortonian fluid inclusions are as high as 410 mmolal, which is only slightly higher than evaporated present-day seawater, which reaches maximum K^+ concentrations of ~380 mmolal (fig. 10B). The first K-bearing salt predicted to form based on the evaporation path outlined by the Serravallian-Tortonian fluid inclusion compositions is polyhalite (fig. 10B), which is present in the Serravallian-Tortonian basins. The mineralogy that results from this brine evolution is similar to that formed from evaporation of modern seawater. Therefore, based on the similar evaporation paths, K^+ concentrations, and mineral sequence, the K^+ concentrations of the Serravallian-Tortonian parent water and modern seawater (11 mmolal) are likely the same.

The SO_4^{2-} vs. Cl^- plot (fig. 10C) shows that the closed symbols define a brine evolution path similar to modern seawater, but the maximum SO_4^{2-} concentration of the Serravallian-Tortonian fluid inclusions is 480 mmolal, lower than the maximum concentrations of evaporated present day seawater (~800 mmolal). The low SO_4^{2-} concentrations of Serravallian-Tortonian fluid inclusions in the halite field indicate that SO_4^{2-} was relatively depleted in comparison to modern seawater.

The Na^+ vs. Cl^- plot (fig. 10D) shows that the closed symbols define an evaporation path very similar to the evaporation of modern seawater. The Cl^- concentration of the parent brines from the Serravallian-Tortonian basins at first halite saturation (~6030 mmolal) is the same as in modern seawater.

It should be noted that some of the Serravallian-Tortonian fluid inclusions (Carpathian Basins) have relatively low concentrations of Mg^{2+}, K^+, and SO_4^{2-} (figs. 10A, 10B, and 10C) and relatively high concentrations of Na^+ (fig. 10D). The halites also have relatively low Br^- concentrations (<40 ppm). However, the closed symbols on all the plots follow overlapping evaporation paths. The parent waters of these samples, relatively enriched in Na^+ and Cl^-, likely recycled halite as they entered the basin (see below).

Tortonian-Messinian (7.6-5 Ma)

The Mg^{2+} vs. Cl^- plot (fig. 11A) shows that the closed symbols define a brine evolution path that is slightly different than present-day seawater evaporation. The open symbols are somewhat scattered, but generally appear to follow the same evaporation path. The Mg^{2+}concentrations of the fluid inclusion brines fall slightly below the modern seawater evaporation path. Therefore, the concentration of Mg^{2+} of the Messinian parent seawaters was slightly less than in modern seawater. The Mg-bearing salts predicted to form along the evaporation path outlined by the Messinian fluid inclusion compositions are polyhalite, and then simultaneously, carnallite and kieserite. The Caltanissetta Basin contains kieserite, carnallite, and kainite, which suggests slightly different brine chemistry than evaporated modern seawater. The mineral langbeinite, also found in the Caltanissetta Basin, typically forms during burial diagenesis.

The K^+ vs. Cl^- plot (fig. 11B) shows that the closed symbols define a brine evolution path very similar to modern seawater. The open symbols show significant scatter and do not follow any path. No closed symbol has a K^+ concentration greater than 370 mmolal, which is essentially the same as evaporated present day seawater (~380 mmolal). The first K-bearing salt predicted to form based on the evaporation path outlined by the Late Messinian fluid inclusion compositions is polyhalite (fig. 11B), which is present in the Messinian basins. The similar evaporation paths and maximum K^+ concentrations indicate that the K^+ of the Messinian parent water and modern seawater (11 mmolal) are likely the same.

The SO_4^{2-} vs. Cl^- plot (fig. 11C) shows that the closed symbols define a brine evolution path quite similar to modern seawater. Open symbols show significant scatter and do not follow any path. The maximum SO_4^{2-} concentration of the closed symbols is 540 mmolal, which is less than the maximum SO_4^{2-} of evaporated present day seawater (~800 mmolal). Therefore, the SO_4^{2-} of the Messinian parent water was slightly lower than in present day seawater.

The Na^+ vs. Cl^- plot (fig. 11D) shows that the closed symbols define an evaporation path nearly identical to modern seawater. The open symbols appear to follow the same evaporation path, with some scatter. The Cl^- concentration of the parent brines from the Messinian basins at first halite saturation (~6020 mmolal) was essentially the same as in modern seawater.

It should be noted that some of the Caltanissetta Basin fluid inclusions have relatively low concentrations of Mg^{2+}, K^+, and SO_4^{2-} (figs. 11A, 11B, and 11C) and relatively high concentrations of Na^+ (fig. 11D). However, the closed symbols on all the plots follow overlapping evaporation paths. This basin contains evidence of desiccation and seawater flooding prior to the precipitation of the Unit C halites (Lugli and others, 1999) and thus, the parent waters of these samples likely recycled halite as they entered the basin.

QUANTITATIVE INTERPRETATION OF FLUID INCLUSION DATA: RATIOS OF Mg^{2+}/SO_4^{2-}, K^+/SO_4^{2-} AND Mg^{2+}/K^+

Paleoseawater fluid inclusions ("closed symbols") from the Late Eocene-Early Oligocene (figs. 12A, 12B, and 12C), Serravallian-Tortonian (figs. 12D, 12E, and 12F), and Messinian (figs. 12G, 12H, and 12I) were used to calculate ratios of the concentrations of Mg^{2+}/SO_4^{2-}, K^+/SO_4^{2-} and Mg^{2+}/K^+ in the parent Cenozoic seawaters. The data represented by open symbols were omitted because the sedimentological, geochemical, and fluid inclusion evidence indicates that they do not share parent waters with the same composition as the closed symbol parent waters. The closed symbols form overlapping evaporation paths (figs. 9, 10, and 11), which shows that their parent waters had the same compositions, which was seawater.

Mg^{2+} and K^+ exhibit conservative behavior as no Mg- or K-bearing salts (that is, polyhalite, sylvite) precipitate at the brine concentrations shown on figure 12. Virtually all of the Ca^{2+} is lost from these evaporated seawaters as gypsum/anhydrite prior to halite saturation. Therefore, no SO_4^{2-}-bearing minerals, aside from small amounts of $CaSO_4$, are formed from the brines until the precipitation of polyhalite, which explains the nearly conservative behavior of SO_4^{2-} at the brine concentrations shown on figure 12. The SO_4^{2-} concentrations reported here from fluid inclusion analyses are referred to as SO_4* (Brennan and Lowenstein, 2002; Brennan and others, 2004) because the fluid inclusions contain excess SO_4^{2-} in the halite field after precipitation of calcite and gypsum/anhydrite. Then it follows that $SO_4{*}_i$ (the initial concentration of sulfate in the unevaporated parent seawater is defined as:

$$SO_4{*}_i = {SO_4^{2-}}_i - ({Ca^{2+}}_i - 1/2{HCO_3^-}_i) \quad (1)$$

where ${Ca^{2+}}_i$, ${SO_4^{2-}}_i$, and ${HCO_3^-}_i$ are the initial concentrations of Ca^{2+}, SO_4^{2-}, and HCO_3^- in the unevaporated Cenozoic parent seawater. $SO_4{*}_i$ is the sulfate in the parent seawater left over after appropriate amounts of SO_4^{2-} and virtually all HCO_3^- and Ca^{2+} are removed as calcite and gypsum/anhydrite. In order to determine the actual concentration of SO_4^{2-} in the parent waters (${SO_4^{2-}}_i$), the initial concentrations of Ca^{2+} (${Ca^{2+}}_i$) and HCO_3^- (${HCO_3^-}_i$) must be known (see below).

From the above, it follows that the Mg^{2+}/SO_4^{2-} ratio, shown as the reciprocal of the slope on figures 12A, 12D, and 12G, is actually ${Mg^{2+}}_i/SO_4{*}_i$. This ${Mg^{2+}}_i/SO_4{*}_i$ ratio for each period was calculated from the average ${Mg^{2+}}_i/SO_4{*}_i$ ratio of all the "closed symbol" fluid inclusion analyses plotted. The Late Eocene-Early Oligocene data give an average ${Mg^{2+}}_i/SO_4{*}_i$ ratio of ~13; the Serravallian-Tortonian ${Mg^{2+}}_i/SO_4{*}_i$ ratio is ~4, and the Messinian average ${Mg^{2+}}_i/SO_4{*}_i$ ratio is ~3.5. For comparison, modern seawater has a ${Mg^{2+}}_i/SO_4{*}_i$ ratio of ~3 (55/18). Therefore, the ${Mg^{2+}}_i/SO_4{*}_i$ ratio of Cenozoic seawater was higher than modern seawater.

The ${K^+}_i/SO_4{*}_i$ ratio was calculated in the same manner as the ${Mg^{2+}}_i/SO_4{*}_i$ ratio, using the average of all values plotted on figures 12B, 12E, and 12H. The Late Eocene-Early Oligocene fluid inclusions have an average ${K^+}_i/SO_4{*}_i$ ratio of ~4; Serravallian-Tortonian data have a ${K^+}_i/SO_4{*}_i$ ratio of ~1, and the ratio in Messinian fluid inclusions is ~0.8. Modern seawater, with ${K^+}_i/SO_4{*}_i$ of ~0.6 (11/18), has a lower ${K^+}_i/SO_4{*}_i$ ratio than any Cenozoic seawater examined here.

Finally, the ${Mg^{2+}}_i/{K^+}_i$ ratio in the fluid inclusions was calculated as the average of all values plotted on figures 12C, 12F, and 12I. The Late Eocene-Early Oligocene fluid inclusions have an average ${Mg^{2+}}_i/{K^+}_i$ ratio of ~3.3; Serravallian-Tortonian inclusions have a ${Mg^{2+}}_i/{K^+}_i$ ratio of ~4, and the ratio in Messinian fluid inclusions is ~4.4. Modern seawater, with ${Mg^{2+}}_i/{K^+}_i$ of 5 (55/11), has a higher Mg^{2+}/K^+ ratio than any Cenozoic seawater examined here.

CALCULATION OF THE MAJOR-ION COMPOSITION OF CENOZOIC SEAWATER

The major ion composition (Mg^{2+}, Ca^{2+}, K^+, Na^+, SO_4^{2-}, and Cl^-) of Cenozoic seawater is calculated here from fluid inclusion data for the Eocene-Oligocene (~36-34 Ma), SerravallianTortonian (~13.5-11.8 Ma) and the Messinian (~5 Ma), using the methods and assumptions outlined in table 7. Each of these periods has fluid inclusions from at least two different deposits with chemical compositions that overlap on concentration crossplots, which bolsters the evidence for a global seawater signal.

We assume the chlorinity (565 mmolal) and salinity of Cenozoic seawater was about the same as modern seawater on the basis of evidence from the salinities of fluid inclusions in marine calcite cements, discussed in Lowenstein and others (2005). We ignore the HCO_3^- in seawater in the calculations, because it is a minor constituent (2.5 mmolal in present-day seawater) compared to the major ions. The K^+ concentration is

TABLE 7

Method used to calculate chemical composition of Cenozoic seawaters

(1)	Determine Mg^{2+}/K^{+} directly from fluid inclusion compositions. Assume K^{+} concentration in Cenozoic seawater is 11 mmolal, calculate Mg^{2+} concentration.
(2)	Determine K^{+}/SO_4* ratios from fluid inclusion compositions. Assume K^{+} concentration is 11 mmolal, calculate SO_4* [$SO_4^* = SO_4^{2-}{}_i - (Ca^{2+}{}_i - \frac{1}{2}HCO_3^-{}_i)$].
(3)	Assume $(Ca^{2+}{}_i)(SO_4^{2-}{}_i)$ in seawater varied between 150-450 mmolal^2. Calculate Ca^{2+} and SO_4^{2-} concentrations (lower and upper values, and average) using SO_4*
(4)	Assume HCO_3^- concentration of parent seawater is negligible, Cl^- concentration equal to modern seawater (565 mmolal), and calculate Na^+ from charge balance.
(5)	Generate evaporation paths with HMW computer program using calculated seawater compositions; establish that HMW mineral precipitation sequence matches evaporite record

assumed to be constant (11 mmolal) in the Cenozoic following evidence for relatively constant K^+/Br^- ratios in Phanerozoic seawater (Horita and others, 2002; Lowenstein and others, 2005). The similar K^+/Br^- ratios together with the ~100 million year residence time of Br^- in seawater suggest that K^+ has not varied substantially in the Phanerozoic (Horita and others, 2002; Lowenstein and others, 2005).

Average Mg^{2+}/K^+ ratios from the fluid inclusion analyses (figs. 12C, 12F, and 12I) are used directly for estimating Cenozoic seawater chemical compositions. The inclusion data plotted on figure 12 all come from halites precipitated before any K- and Mg-bearing salts (that is, polyhalite). Thus, the Mg^{2+}/K^+ from these samples should be the same as in Cenozoic seawater: 3.3 for the Late Eocene-Early Oligocene, 4 for the Serravallian-Tortonian and 4.4 in the Messinian (5 in modern seawater). If we assume that the K^+ concentration is 11 mmolal, then the Mg^{2+} concentrations are 36, 44, and 48 mmolal in Late Eocene-Early Oligocene, Serravallian-Tortonian and Messinian seawater, respectively, all below the Mg^{2+} concentration in modern seawater of 55 mmolal (table 8).

The K^+/SO_4^{2-} ratios from fluid inclusions, which are really $K^+{}_i/SO_4{}^*{}_i$, where $SO_4{}^*{}_i$ is "excess" sulfate, as explained above, are used to estimate the SO_4^{2-} concentrations in Cenozoic seawater. Average K^+/SO_4^{2-} values, plotted on figures 12B, 12E, and 12H, together with an assumed K+ concentration of 11 mmolal, give $SO_4{}^*{}_i$ values of 3, 11, and 14 for the Late Eocene-Early Oligocene, Serravallian-Tortonian, and Messinian, respectively. Modern seawater, with Ca^{2+} of ~11 mmolal and SO_4^{2-} of ~29 mmolal, has excess $SO_4{}^*{}_i$ of 18 mmolal, after precipitation of 11 millimoles of $CaSO_4$, which is higher than any Cenozoic seawater examined here. To estimate true SO_4^{2-} concentrations in Cenozoic seawater, we use $SO_4{}^*{}_i$ and make assumptions about the concentrations of $Ca^{2+}{}_i$, because the Cenozoic fluid inclusions interpreted to have formed from the evaporation of seawater had no measurable Ca^{2+}. Ca^{2+} and SO_4^{2-} of paleoseawater was calculated by Horita and others (2002) and Lowenstein and others (2005) using the assumption that the concentration product $(Ca^{2+})(SO_4^{2-})$ was between 150 and 450 mmolal^2, which is between 0.5 and 1.5 times the value of (Ca^{2+} =

TABLE 8

Calculated compositions of Cenozoic seawaters

Major Ion	Eocene-Oligocene seawater (36-34 Ma)	Serravallian-Tortonian seawater (13.5-11.8 Ma)	Messinian seawater (6-5 Ma)	Present-day seawater[a]
Na^+	488	488	486	485
K^+	11	11	11	11
Ca^{2+}	16 (11-20)	13 (8-16)	12 (7-15)	11
Mg^{2+}	36	44	48	55
Cl^-	565	565	565	565
SO_4^{2-}	19 (14-23)	24 (19-27)	26 (21-29)	29
Mg^{2+}/Ca^{2+}	2.3	3.4	4.0	5

All values are millimolal (millimoles per kg of H_2O).
[a] Present day composition of seawater from Holland (1984).

11) (SO_4^{2-} = 29) ~ 319 mmolal^2 in modern seawater. This concentration product is unconstrained, but reasonable, given that there have been no major salinity variations in Phanerozoic seawater. The (Ca^{2+})(SO_4^{2-}) product is well below that at gypsum saturation (>3000 mmolal^2). Here we use the same assumptions to estimate Ca^{2+} and SO_4^{2-} in Cenozoic seawater from excess SO_4^{2-} ($SO_4^*{}_i$) and the (Ca^{2+})(SO_4^{2-}) product of 150 to 450 mmolal^2. Late Eocene-Early Oligocene seawater (36-34 Ma), with $SO_4^*{}_i$ of 3 mmolal, must therefore have Ca^{2+} ~11 mmolal and SO_4^{2-} ~14 mmolal and a (Ca^{2+})(SO_4^{2-}) product of 154 mmolal^2 for a lower limit (table 8). The upper limit for Late Eocene-Early Oligocene seawater is Ca^{2+} ~20 mmolal and SO_4^{2-} ~23 mmolal and a (Ca^{2+})(SO_4^{2-}) product of 460 mmolal^2. If the (Ca^{2+})(SO_4^{2-}) product is assumed to be the same as in modern seawater (~300 mmolal^2), Late Eocene-Early Oligocene seawater had Ca^{2+} ~16 mmolal and SO_4^{2-} ~19 mmolal. The same estimates of Ca^{2+} and SO_4^{2-} are made for Serravallian-Tortonian seawater (13.5-11.8 Ma): Ca^{2+} ~ 13 mmolal and SO_4^{2-} ~24 mmolal if the (Ca^{2+})(SO_4^{2-}) product is equal to that in modern seawater and a range of Ca^{2+} ~ 8 to 16 mmolal and SO_4^{2-} ~ 19 to 27 mmolal. Messinian seawater had Ca^{2+} ~12 mmolal and SO_4^{2-} ~26 mmolal and a possible range of Ca^{2+} ~7 to 15 mmolal and SO_4^{2-} ~21 to 29 mmolal (table 8). Sulfate in Cenozoic seawater, no matter what the estimation procedure, shows progressively increasing concentrations from 36 Ma to the present values, which are the highest of the Cenozoic.

Finally, the Na^+ in Cenozoic seawater is calculated from charge balance, after the concentrations of all other ions (Cl^-, SO_4^{2-}, Ca^{2+}, Mg^{2+}, and K^+) are estimated. Late Eocene-Early Oligocene, Serravallian-Tortonian, and Messinian seawater, contained 488, 488, and 486 mmolal Na^+, respectively, about the same as modern seawater with Na^+ of 485 mmolal (table 8).

Evaporation paths for Late Eocene-Early Oligocene, Serravallian-Tortonian, and Messinian seawater, generated with the HMW computer program using the chemical compositions in table 8, are plotted on the concentration crossplots of figures 9, 10, 11, and 12. These paleoseawater evaporation paths overlap the fluid inclusion brine compositions, which supports the veracity of the calculations. The evaporite mineral sequences predicted by the HMW computer program are the same as those found in the salt deposits, which also adds support to the seawater calculations and assumptions.

The HMW computer program can also be used to simulate syndepositional recycling of halite. Such recycling is suggested by fluid inclusions that outline evapora-

tive concentration paths of Serravallian-Tortonian and Messinian seawater, but the relatively low Mg^{2+}, K^+, and SO_4^{2-} concentrations and high Na^+ concentrations suggest dissolution of halite by undersaturated seawater. Halite recycling can be simulated by adding Na^+ and Cl^- into waters with Serravallian-Tortonian and Messinian seawater compositions. The resulting evaporation paths, shown as dotted lines on figures 10 and 11, incorporated all of the fluid inclusion analyses and followed the calculated evaporation path for Serravallian-Tortonian and Messinian seawater. These computer simulations support the interpretation that for some deposits (Carpathian Basins of Slovakia and Poland and the Caltanisetta Basin of Sicily) inflowing seawater dissolved surface halite deposits.

DISCUSSION AND CONCLUSIONS

Changes in the major ion chemistry of Cenozoic seawater documented here record the final phases of a systematic, long term (>150 My) shift from the Ca^{2+}-rich, Mg^{2+}- and SO_4^{2-}-poor seawater of the Mesozoic ("$CaCl_2$ seas") to the "$MgSO_4$ seas" (with higher Mg^{2+} and SO_4^{2-}>Ca^{2+}) of the Cenozoic (Lowenstein and others, 2001; Horita and others, 2002; Timofeeff and others, 2006). Changes in major ion chemistry over the past 36 My (table 8) are illustrated on composite concentration crossplots of the evaporation paths of Late Eocene-Early Oligocene (36-34 Ma), Serravallian-Tortonian (13.5-11.8 Ma), and Messinian (6-5 Ma) seawaters (fig. 13). The evaporation paths on the Mg^{2+} vs. Cl^- composite plot (fig. 13A) show that the concentration of Mg^{2+} in seawater steadily increased over the past 36 My. The K^+ vs. Cl^- composite plot (fig. 13B) apparently shows a decrease in the K^+ concentration of seawater over the past 36 My. This trend, however, is an artifact due to the lag in the formation of polyhalite, which, when precipitated, removes K^+ from the brine. Assuming that the K^+ concentration in seawater has not varied significantly over the past 36 My, then the lag in polyhalite precipitation is due to the lower concentrations of SO_4^{2-} and Mg^{2+} in seawater earlier in the Cenozoic, which allowed brines to reach higher K^+ before becoming supersaturated with polyhalite. The evaporation paths on the SO_4^{2-} vs. Cl^- composite plot (fig. 13C) illustrate that the concentration of SO_4^{2-} in the halite field (SO_4*) has steadily increased over the past 36 My, which suggests increased SO_4^{2-} concentrations in seawater.

The plots of SO_4^{2-} vs. Mg^{2+} and K^+ (figs. 13D and 13F) and K^+ vs. Mg^{2+} illustrate that the Mg^{2+}/SO_4* and K^+/SO_4* ratios of seawater have steadily decreased and the Mg^{2+}/K^+ ratio has increased over the past 36 My. The changes of these ratios indicate that the concentrations of Mg^{2+} and SO_4^{2-} in seawater have increased over the past 36 My.

The results of this study, shown as calculated concentrations of Mg^{2+}, Ca^{2+}, and SO_4^{2-} plotted against time, closely agree with the estimates of Zimmermann (2000) and Horita and others (2002) (fig. 14), who worked on many of the same deposits analyzed in this study. However, in addition to the new analytical results, a major strength of this study is the careful examination of the marine versus non-marine origin of the halites used for determining the paleo-seawater chemistry, reconciling some of the potential intra-basinal processes observed during halite precipitation (Ayora and others, 2001). Increases in the concentrations of Mg^{2+} and SO_4^{2-} and a decrease in Ca^{2+} in seawater over the past 36 My are predicted by all three studies (fig. 14). The Mg^{2+}/Ca^{2+} ratio of seawater over the past 36 My (fig. 15) shows an increase from a low of ~2.3 at the end of the Eocene, to 3.4 and 4.0, respectively, at 13.5 to 11.8 Ma and 6 to 5 Ma, and 5 in modern seawater. The Mg^{2+}/Ca^{2+} calculated by Horita and others (2002) is essentially the same as that estimated here.

In addition to the fluid inclusion analyses, other methods have been used to estimate the composition and concentration of major ion components of Cenozoic seawater (Ivany and others, 2004; Coggon and others, 2010; and Fantle, 2010). Ivany

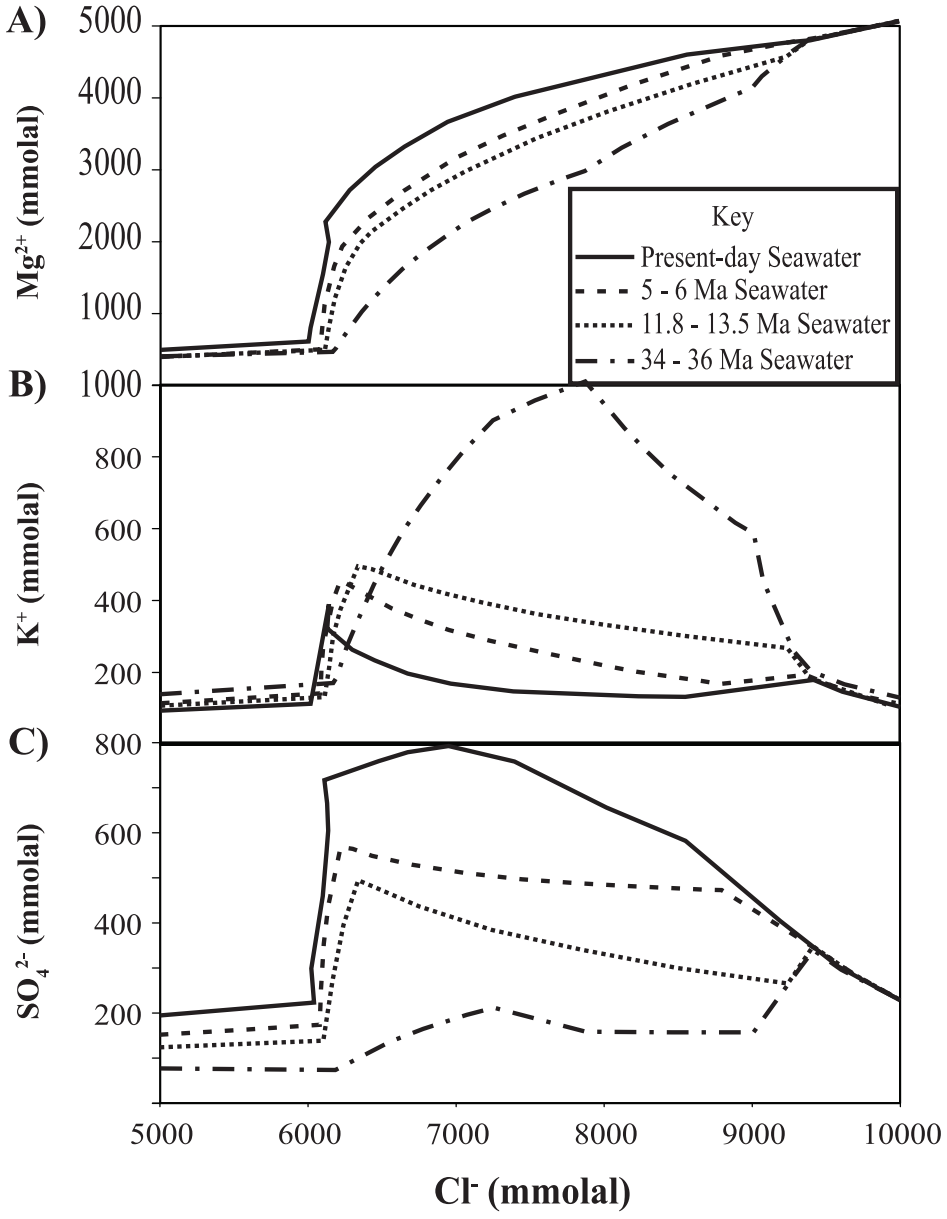

Fig. 13. Composite plots of the paleoseawater evaporation paths shown on figures 9, 10, 11, and 12. These evaporation paths, simulated using major ion chemistries shown in table 8, show that the major-ion chemistry of seawater has changed over the past 36 My.

and others (2004) used analyses of the Mg^{2+}/Ca^{2+} of Oligocene aged corals, and their $\delta^{18}O$ values to correct for partitioning, to estimate a Mg^{2+}/Ca^{2+} ratio of Oligocene seawater of 4.2 (Ivany and others, 2004). This Mg^{2+}/Ca^{2+} of 4.2 is higher than the estimates in this study, yet still less than modern seawater levels. Coggon and others (2010) used analyses of Mg^{2+}/Ca^{2+} ratios of $CaCO_3$ veins in mid-ocean ridge basalts to estimate the Mg^{2+}/Ca^{2+} ratio of seawater from the Jurassic through the present. The

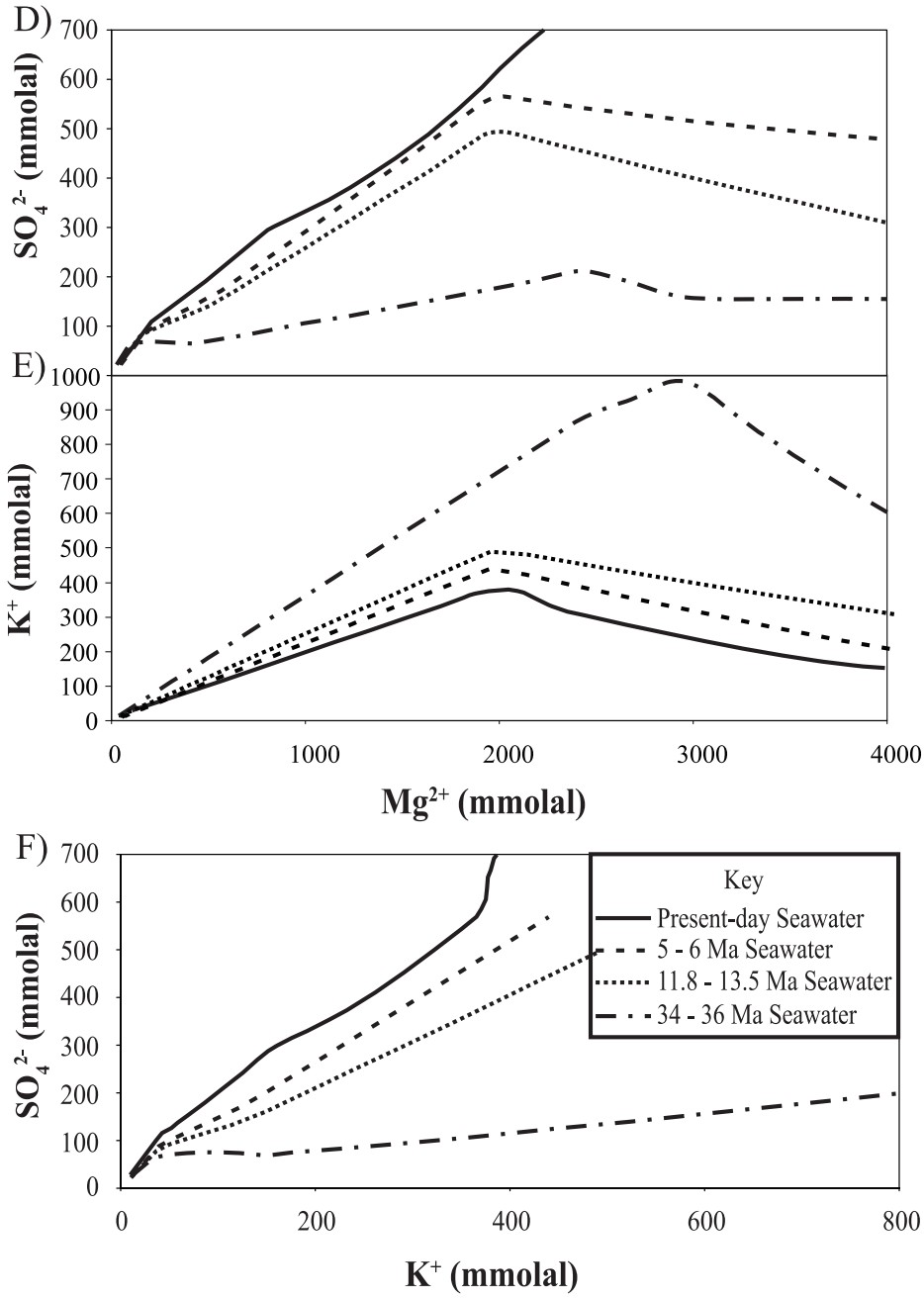

Fig. 13 (continued).

only values from Coggon and others (2010) that were from the same time as this study were analyses from the Eocene through the Oligocene, which estimated Mg^{2+}/Ca^{2+} ratios of between 2 and 2.5, which is the same as those estimated in this study. Finally, Fantle (2010) used analyses of nannofossil ooze $\delta^{44}Ca$ to estimate Ca^{2+} concentration

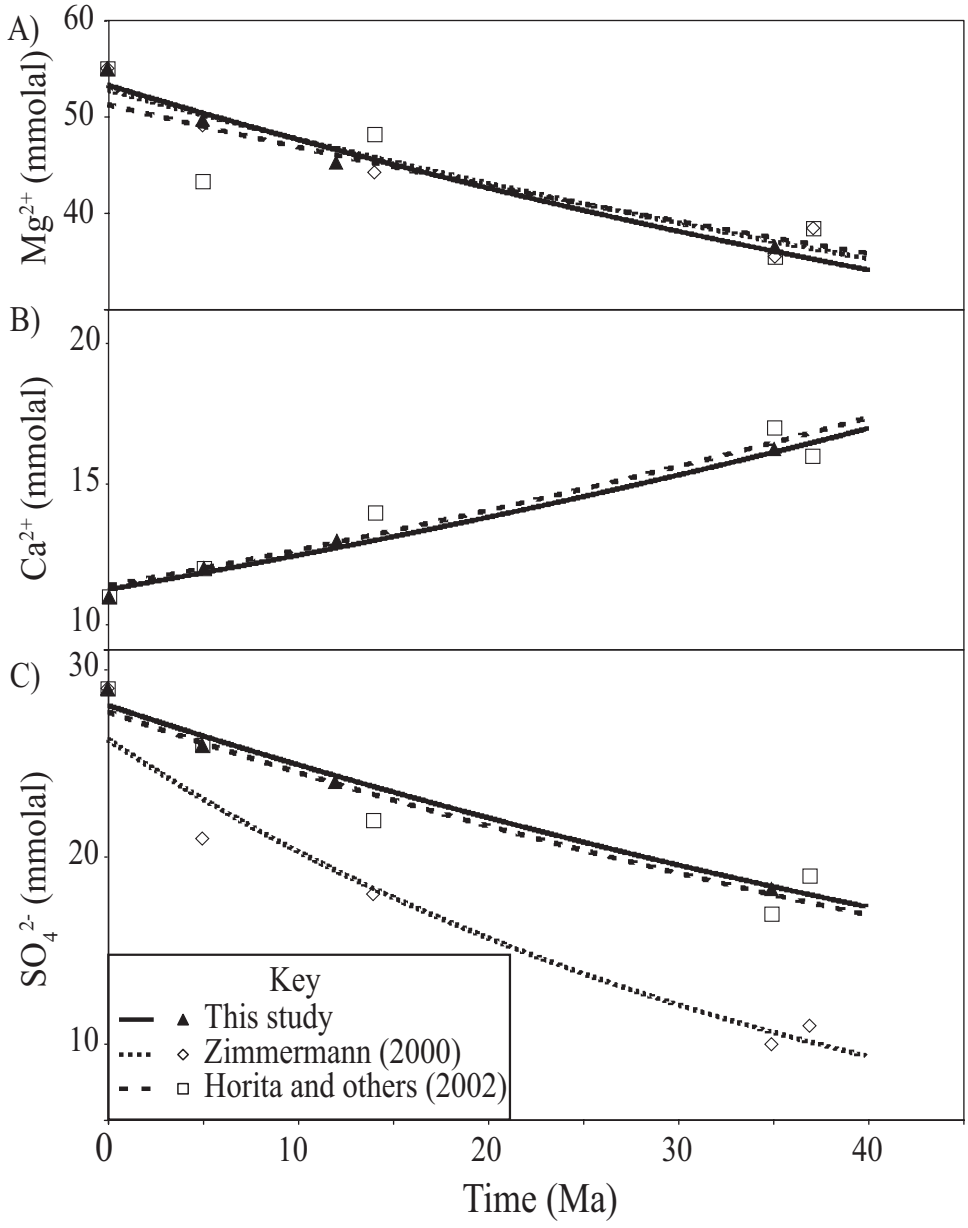

Fig. 14. Major-ion chemistry of seawater over the past 36 My, comparing the results of this study with Zimmermann (2000) and Horita and others (2002). (A) Mg^{2+}. (B) Ca^{2+}. (C) SO_4^{2-}.

changes in seawater during the Cenozoic. Fantle's (2010) work estimates major changes in the concentration of calcium in seawater, with oscillations from 45 Ma to present of Ca^{2+} up to 100 percent higher (in the Oligocene), and up to 50 percent lower (during the mid-Eocene) than modern concentrations. The running average of Ca^{2+} concentrations in seawater over the past 45 My predicted by Fantle (2010) broadly agree with fluid inclusion analyses (Lowenstein and others, 2001; Zimmerman,

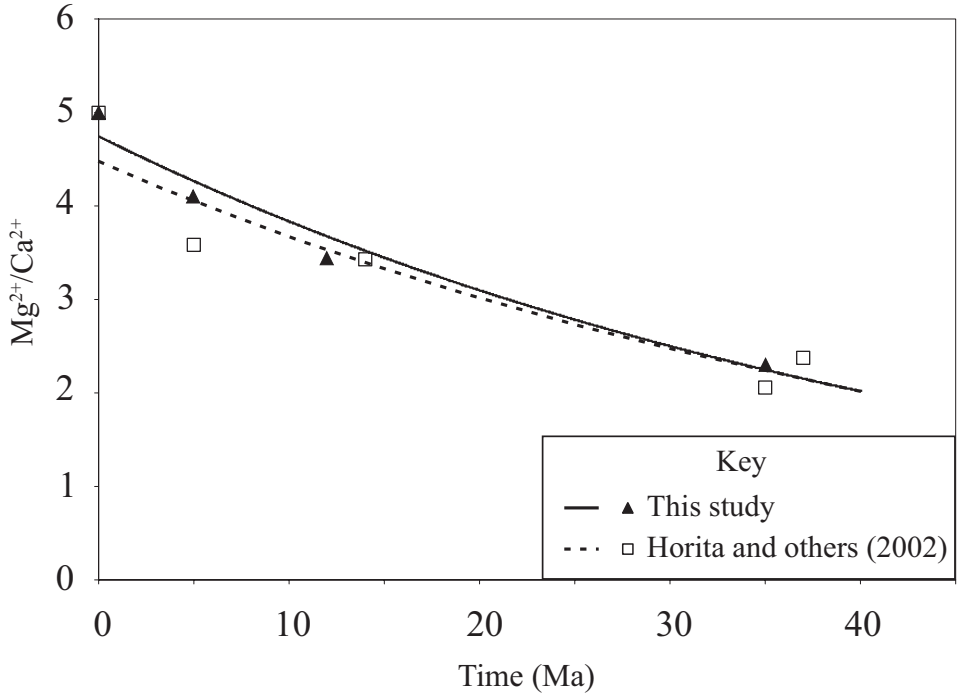

Fig. 15. Changes in the Mg^{2+}/Ca^{2+} ratio over the past 36 My, comparing results from this study with Horita and others (2002).

2001; Horita and others, 2002; and Lowenstein and others, 2003), but predicts high amplitude and short wavelength changes between each of the data points shown in the fluid inclusion studies, including this one.

There is now general agreement that the major ion chemistry of seawater has changed over the past 36 My, but there is less certainty about what controls the compositional changes. Current ideas used to explain major-ion compositional changes in seawater are: (1) global dolomitization rate changes (Holland and Zimmermann, 2000; Holland, 2005); (2) weathering rate changes (Turchyn and Shrag, 2004, 2006); and (3) changes in the rates at which seawater cycles through the mid-ocean ridges (Hardie, 1996; Lowenstein and others, 2001). Ivany and others (2004) and Coggon and others (2010) argue that changes in the Mg^{2+}/Ca^{2+} ratio of seawater were caused by reduced production of mid ocean ridge basalts due to slowing of seafloor spreading rates. Fantle (2010) explains the changes in the concentration of Ca^{2+} in seawater by changes in sedimentation and weathering rates.

Seawater-driven dolomitization involves the reaction of Mg^{2+} (from seawater) and carbonate sediments or limestone to form dolomite with the concomitant release of Ca^{2+}. The Holland and Zimmermann (2000) model predicts that if the global rate of seawater-driven dolomitization slowed down during the Cenozoic as deposition of $CaCO_3$ shifted from the shallow to the deeper oceans, then the concentration of Mg^{2+} in seawater will increase and Ca^{2+} concentration will decrease. Extending further, less Ca^{2+} released during dolomitization will lead to less precipitation of $CaSO_4$ in evaporitic settings and less removal of SO_4^{2-} from the oceans, which will cause seawater SO_4^{2-} concentrations to rise. The dolomitization model thus predicts Ca^{2+} to

decrease and Mg^{2+} and SO_4^{2-} to increase over the past 36 My of the Cenozoic, consistent with the observed trends (fig. 14).

Turchyn and Shrag (2004, 2006) suggest that the sulfate concentration of seawater is controlled by sulfate reduction and sulfide re-oxidation on continental shelves and slopes. Low global sea level over the past 3 My may have caused greater weathering of pyrite over a large area of continental shelf which led to an increase in seawater SO_4^{2-}, as observed. Furthermore, their modeling infers that SO_4^{2-} may have increased by 10 to 15 mmolal throughout the Cenozoic without affecting the isotopic composition of seawater SO_4^{2-}. Regardless, their results and conclusions mirror the results of this study that the SO_4^{2-} concentration increased during the Cenozoic.

The Hardie (1996) model assumes that changes in seawater chemistry are driven by the flux of mid-ocean ridge hydrothermal brines, which is proportional to seafloor spreading rates and ocean crust production. That model assumes constant river water composition and inflow volume. Circulation of seawater through the MOR system produces brines that are highly depleted in Mg^{2+} and SO_4^{2-} and enriched in Ca^{2+} (Von Damm, 1995). They are interpreted to have formed by interaction between seawater and oceanic basalts and gabbros at temperatures of up to ~400 °C (Von Damm, 1995). Geologic periods with high rates of mid-ocean ridge crust production (that is, the Cretaceous) are predicted to have seawater with high Ca^{2+} and low Mg^{2+} and SO_4^{2-}. Thus, the general 150 My trend in seawater chemistry, from the Cretaceous to the modern, could be explained by the slowdown in ocean crust production and MOR hydrothermal circulation.

Demicco and others (2005) extended the Hardie (1996) model to account for (1) variable inflow of river water (at constant composition), and (2) variable rates of seawater alteration on the relatively cool off-axis ridge flanks (Wheat and Mottl, 1994). Demicco and others (2005) found that variable river water inflow during the Phanerozoic Eon results in improved modeling, especially for Mg^{2+}, which suggests that river water flux (and composition) are important controls on the major ion chemistry of seawater. Low-temperature alteration of seawater occurring on mid-ocean ridge flanks can remove large amounts of K^+, little SO_4^{2-}, and no Mg^{2+} during alteration of basalts and deep ocean sediments which nicely accounts for the near constancy of seawater K^+ with contemporaneous increases in SO_4^{2-} and Mg^{2+} over the last 36 My (Demicco and others, 2005).

One problem with models relating mid-ocean ridge hydrothermal circulation and the major ion composition of seawater is that there is little agreement on secular changes in MOR crust production, even for the Cenozoic. Rowley (2002) used the age-area distribution of the modern ocean crust to hypothesize that MOR production rates have not changed over the past 180 My. Conrad and Lithgow-Bertelloni (2007), however, concluded that over the past 140 My the rates of ocean crust production have changed. They calculated that MOR crust production rates dropped by 18 percent over the past 20 My, which could explain the seawater enrichment in Mg^{2+} and SO_4^{2-} and depletion in Ca^{2+} documented here. Furthermore, Miller and others (2005) have argued that the decrease in sea level during this time frame cannot be totally attributed to the growth of ice sheets; therefore, there must be a change in the sea-floor spreading rates.

The most recent models of Müller and others (2008) and Seton and others (2009) show changes in ocean crust production and MOR spreading rates between the Cretaceous and the Cenozoic, which further supports the interpretation that there was "non-steady state" formation of MOR crust in the past. Seton and others (2009) calculate, for example, a general decrease in MOR crust production of 4×10^6 km^2/Ma in the late Cretaceous (80 Ma) to $\sim 3 \times 10^6$ km^2/Ma in the late Cenozoic. Of

great importance is the evidence presented by Seton and others (2009) for the aging of oceanic crust over the past 140 million years. They report, for example, a steady change in mean crustal age of 42 My in the late Cretaceous to 64 My today. Mean ocean crust age increases steadily over the last 40 million years from 55 My to 64 My (Seton and others, 2009). Such "aging" of ocean floor crust could explain the secular changes in seawater chemistry reported here for the Cenozoic because the age and temperature of MOR crust may impact the volume of MOR hydrothermal circulation.

There is general consensus that global sea level dropped over the past 35 My (Kominz, 1984; Haq and others, 1987; Gaffin, 1987; Kominz and others, 1998; Miller and others, 2005). One potential cause for this long-term sea level change could be attributed to the reduction of the volume of hot basalt at the mid ocean ridges, caused by lower seafloor spreading rates (Miller and others, 2005; Conrad and Lithgow-Bertelloni, 2007). With reduced volume of hot basalt, it could be argued that the amount of hydrothermally altered seawater cycling through mid ocean ridges and ridge flanks has also dropped. This reduced rate of MOR brine production could explain all of the major ion compositional changes reported in this and the other fluid inclusion studies. The drop in global sea level over the past 35 My may have also caused changes in global weathering rates and dolomitization, which may have influenced the chemistry of seawater. The results of this study support "non-steady state" formation of MOR crust in the Cenozoic, as well as changes in sea-level, weathering rates, and other geochemical processes that result from variable MOR production rates.

ACKNOWLEDGMENTS

The authors would like to thank Michael Timofeeff for his help with analyses and insightful and helpful discussions throughout the research that led to this manuscript. Reviews by James Coleman and Robert Burruss at the U.S. Geological Survey, as well as those by Michael Bender and Steve Stanley have helped to improve the quality and clarity of this manuscript. Help from the support staff at Binghamton University during the research for this manuscript is greatly appreciated as well. Any use of trade, firm, or product names is for descriptive purposes only and does not imply endorsement by the U.S. Government.

Appendix

Table A1

Major-ion chemistry of fluid inclusions, this study

Sample	Mg	K	Ca	Na	Cl	Sample	Mg	K	SO_4	Na	Cl
Bresse Basin, E4 Salt						**Southern Rhine Graben, S1 Unit**					
ab1 (2/15/01)	620	390	490	3960	6590	arg1 (1/12/01)	420	370	100	5200	6210
ab2 (2/15/01)	740	410	500	3750	6620	arg1 (1/18/01)	520	390	80	5030	6300
ab3 (2/15/01)	470	340	470	4290	6470	arg2 (1/18/01)	380	310	50	5290	6280
ab4 (2/15/01)	590	400	520	3990	6570	arg2 (2/1/01)	350	430	80	5320	6310
ab5 (2/15/01)	500	350	520	4150	6520	arg3 (2/1/01)	290	320	60	5460	6240
ab6 (2/15/01)	490	360	460	4240	6520	brg1 (2/1/01)	260	220	90	5610	6150
ab7 (2/15/01)	370	360	480	4430	6490	brg2 (2/1/01)	250	230	80	5610	6180
bb1 (2/15/01)	1330	380	550	2760	6880	brg3 (2/1/01)	190	170	60	5730	6140
bb2 (2/15/01)	940	380	610	3260	6760	brg4 (2/1/01)	320	210	80	5480	6170
bb3 (2/15/01)	1260	410	620	2760	6930	arg1 (7/21/00)	390	430	90	5260	6290
bb4 (2/15/01)	830	370	550	3530	6660	arg2 (7/21/00)	420	450	100	5200	6330
bb5 (2/15/01)	800	360	540	3610	6630	brg2 (8/3/00)	290	370	40	5420	6290
cb1 (2/15/01)	740	400	520	3720	6640	arg1 (8/24/00)	330	400	60	5370	6270
cb2 (2/15/01)	1330	530	600	2660	7050	arg2 (8/24/00)	360	400	60	5290	6310
cb3 (2/15/01)	740	380	550	3690	6610	arg1 (8/31/00)	580	490	90	4900	6350
cb4 (2/15/01)	1170	500	590	2910	6930	arg2 (8/31/00)	310	390	40	5380	6310
ab1 (2/22/01)	530	410	470	4140	6570	arg2 (9/7/00)	240	360	70	5550	6270
ab2 (2/22/01)	560	400	510	4050	6570	arg3 (9/7/00)	280	380	70	5480	6260
ab3 (2/22/01)	730	440	540	3690	6670	arg4 (9/7/00)	510	420	90	5050	6310
ab4 (2/22/01)	480	400	500	4190	6550	arg5 (9/7/00)	240	350	60	5550	6240
ab5 (2/22/01)	490	400	490	4190	6550	brg1 (9/7/00)	490	410	80	5090	6300
ab6 (2/22/01)	570	430	490	4040	6590	arg1 (9/14/00)	390	430	70	5250	6300
ab7 (2/22/01)	360	360	470	4460	6500	brg5 (9/14/00)	440	410	90	5180	6290
ab8 (2/22/01)	730	430	510	3750	6640						
bb1 (2/22/01)	560	400	480	4080	6580	**Wieliczka Salt Mine, Stratiform Green Salts**					
bb2 (2/22/01)	510	360	450	4220	6540	amp1 (3/22/00)	170	120	170	5900	6040
bb3 (2/22/01)	480	400	480	4230	6530	amp3 (3/22/00)	220	170	170	5790	6040
ab1 (3/3/01)	440	420	500	4270	6530	amp2 (3/24/00)	240	150	230	5830	6000
bb1 (3/3/01)	960	490	590	3230	6820	amp5 (3/17/00)	240	90	120	5730	6040
bb2 (3/3/01)	900	480	600	3310	6790	amp4 (3/22/00)	260	140	180	5720	6040
bb3 (3/3/01)	1070	460	600	3060	6840	amp7 (3/22/00)	270	120	170	5710	6030

Table A1
(continued)

Sample	Mg	K	SO_4	Na	Cl	Sample	Mg	K	SO_4	Na	Cl
Wieliczka Salt Mine, Stratiform Green Salts						**South Gharib Fm, Hurghada D-23R Core**					
amp8 (3/22/00)	310	50	170	5660	6010	ame2 (10/20/00)	1890	390	340	2930	6400
amp4 (3/30/00)	310	160	150	5590	6070	ame1 (10/27/00)	1510	410	380	3570	6260
amp1 (3/30/00)	340	140	160	5540	6060	ame2 (10/27/00)	1490	410	380	3610	6220
bmp1 (3/22/00)	350	150	180	5540	6050	ame3 (10/27/00)	1600	410	400	3450	6240
amp2 (3/16/00)	360	160	140	5470	6090	ame4 (10/27/00)	1610	370	380	3420	6250
amp4 (3/17/00)	370	140	170	5510	6030	ame5 (10/27/00)	1400	360	380	3770	6190
amp9 (3/22/00)	380	110	170	5500	6030	bme1 (10/27/00)	1970	390	390	2850	6380
bmp4 (3/22/00)	400	140	180	5460	6040	bme2 (10/27/00)	1990	380	390	2820	6400
amp4 (3/16/00)	410	160	160	5400	6080	bme3 (10/27/00)	1650	330	350	3330	6280
amp2 (3/22/00)	430	190	180	5390	6040	ame1 (12/13/00)	1010	340	320	4410	6130
bmp2 (3/22/00)	450	180	230	5390	6030	ame2 (12/13/00)	1210	390	370	4090	6160
bmp7 (3/17/00)	500	180	180	5260	6040	ame3 (12/13/00)	1090	360	340	4270	6150
bmp4 (3/17/00)	540	180	200	5200	6020	ame4 (12/13/00)	660	330	300	5040	6070
amp2 (3/17/00)	540	180	200	5180	6060	ame5 (12/13/00)	1460	380	400	3700	6160
amp5 (3/22/00)	550	200	180	5140	6080	ame6 (12/13/00)	910	400	370	4620	6100
amp1 (3/24/00)	550	150	220	5200	6030	ame7 (12/13/00)	780	340	300	4810	6090
amp6 (3/22/00)	560	200	200	5140	6060	bme1 (12/13/00)	1660	310	390	3370	6200
amp3 (3/16/00)	570	160	170	5110	6070	ame4 (12/13/00)	660	330	300	5040	6070
bmp3 (3/22/00)	590	170	220	5130	6020	bme2 (12/13/00)	1430	370	370	3710	6200
amp3 (3/17/00)	670	150	230	5000	5990	ame1 (12/14/00)	1420	270	270	3670	6280
bmp6 (3/17/00)	700	200	220	4900	6060	ame2 (12/14/00)	1510	270	270	3540	6270
bmp5 (3/17/00)	720	210	230	4870	6060	bme1 (12/14/00)	910	200	220	4540	6100
amp1 (3/17/00)	740	160	220	4830	6050	bme2 (12/14/00)	1960	280	360	2860	6340
amp1 (3/16/00)	890	170	200	4530	6080	**Realmonte Mine, Upper Halite Unit, B&C Salts**					
South Gharib Fm, Hurghada D-23R Core											
ame1 (10/19/00)	1460	350	430	3700	6130	AGS1 (1/21/99)	580	170	180	5130	6120
ame2 (10/19/00)	1680	410	460	3350	6200	BGS1 (1/21/99)	340	160	220	5630	6030
ame3 (10/19/00)	1630	380	480	3480	6140	BGS2 (1/21/99)	270	160	230	5780	6000
ame4 (10/19/00)	740	310	350	4970	6040	AGS1 (1/20/99)	740	190	110	4750	6220
ame5 (10/19/00)	1370	300	340	3800	6180	AGS2 (1/20/99)	800	180	300	4870	6030
ame6 (10/19/00)	1100	370	400	4340	6110	AGS3 (1/20/99)	680	180	310	5090	6010
ame7 (10/19/00)	950	350	360	4590	6100	BGS1 (1/20/99)	980	180	270	4510	6110
ame8 (10/19/00)	1240	380	400	4070	6130	BGS2 (1/20/99)	360	110	170	5550	6080

All values are mmolal. Each sample in this table is a unique inclusion, there are no repeat analyses listed. Therefore, sample ab1 (2/15/01) and ab1 (2/22/01) are of two different inclusions. Each new slice of a halite chip was given a letter (a, b, and so on) the second letter referred to the basin that the sample came from (for example: "b" for Bresse basin), and a number for the inclusions analyzed on that slice (1, 2, 3, and so on). The date of the analysis is the remainder of the sample name (for example 2/15/01), Therefore, ab1 (2/15/01) was the first inclusion analyzed on the first halite slice on February 15, 2001.

TABLE A2

Major-ion chemistry of fluid inclusions, from Cendón (1999)

Sample	Data as reported by Cendón (1999)						Equilibrated with HMW computer model					
	Mg	K	SO_4	Na	Cl	Ca	Mg	K	SO_4	Na	Cl	Ca
Catalan Basin, Suria-19 core Group I data												
SU17I1	1360	150	30	3820	5970	80	1360	150	20	3500	6470	70
SU17I2	1480	180	30	3680	5960	60	1480	180	30	3320	6520	60
SU17I3	1570	180	40	3410	6190	50	1570	180	40	3200	6540	50
SU17I5	1500	180	130	3650	6070	20	1500	180	120	3440	6400	10
SU17I6	1520	190	30	3280	6520	50	1520	190	30	3260	6530	50
SU18I1	1680	200	30	2830	6960	50	1680	200	30	3010	6610	50
SU18I2	1580	200	30	2990	6900	50	1580	200	30	3170	6570	50
SU18I3	1330	240	30	3250	7040	40	1330	240	30	3570	6490	40
SU18I4	1740	210	40	2830	6810	40	1740	210	40	2930	6620	40
SU18I5	1760	170	30	2500	7450	40	1760	170	30	2910	6620	40
SU21I1	1700	220	40	3190	6240	50	1700	220	40	2980	6620	50
SU21I2	1780	210	70	3000	6440	20	1780	210	70	2920	6590	20
SU21I3	1790	280	80	3280	5930	30	1790	280	70	2880	6640	20
SU21I4	1690	220	30	3070	6490	50	1690	220	30	2980	6620	50
SU23I1	1720	210	50	2700	7180	20	1720	210	50	3000	6590	20
SU23I10	1910	240	40	3180	6800	60	1910	240	30	2640	6740	50
SU23I3	1610	200	40	3170	6500	40	1610	200	40	3140	6560	40
SU23I4	1530	160	60	3510	6160	30	1530	160	60	3320	6480	30
SU23I5	1530	180	120	3700	5920	20	1530	180	120	3380	6420	20
SU23I6	1770	170	70	3030	6420	20	1770	170	70	2950	6560	20
SU23I7	1550	200	60	3440	6220	30	1550	200	60	3270	6510	30
SU23I8	1180	130	110	4010	6260	20	1180	130	110	3980	6290	20
SU23I9	1300	150	50	3900	6080	40	1300	150	50	3680	6410	40
SU26I1	1410	280	40	3250	6860	40	1410	280	40	3430	6530	40
SU26I2	1400	280	40	3240	6900	40	1400	280	40	3450	6530	40
SU26I3	1430	290	40	3120	6820	170	1430	290	10	3220	6630	140
SU26I4	1420	320	40	3230	6860	40	1420	320	40	3400	6560	40
SU26I5	1380	280	40	3300	6840	40	1380	280	40	3480	6520	40
SU26I1	1750	190	20	3050	6270	100	1750	190	20	2830	6680	100
SU26I2	1760	190	20	2870	6570	110	1760	190	20	2800	6690	110
SU27I1	1380	210	40	3300	6830	40	1380	210	40	3510	6480	40
SU27I2	1340	220	40	3350	6840	40	1340	220	40	3570	6470	40
SU27I3	1410	230	40	3180	6900	110	1410	230	20	3360	6550	90
SU27I4	1380	210	40	3210	6850	120	1380	210	20	3400	6530	100
SU27I5	1390	200	40	3310	6800	40	1390	200	40	3500	6480	40
SU27I6	1400	190	40	3310	6770	40	1400	190	40	3480	6470	40
Catalan Basin, Suria-19 core Group II data												
SUA28I1	1280	330	130	3880	6210	20	1280	330	130	3740	6410	20
SUA28I2	1480	330	130	3790	5900	20	1480	330	120	3410	6480	10
SUA28I3	1680	300	180	3330	6760	10	1680	300	180	3150	6470	10
SUA28I4	1400	330	160	3510	6840	10	1400	330	160	3580	6410	10
SUA28I5	1480	340	170	3980	5850	10	1480	340	170	3450	6430	10
SUA28I7	1320	320	160	4070	5880	10	1320	320	160	3720	6380	10
SUA28I8	1430	320	140	3230	6910	10	1430	320	140	3520	6440	10
SUC32I1	1190	300	110	4110	6210	10	1190	300	110	3900	6380	10
SUC32I2	1110	280	100	4250	6490	10	1110	280	100	4040	6360	10
SUC32I3	1150	300	110	4270	6390	10	1150	300	110	3970	6370	10
SUA35I1	1070	330	110	4030	6450	20	1070	330	110	4080	6370	20
SUA35I2	1090	340	110	4030	6700	10	1090	340	110	4060	6380	10
SUA35I3	1030	340	100	3780	6900	10	1030	340	100	4150	6370	10
SUA35I4	1080	340	110	3940	6560	20	1080	340	110	4060	6380	20
SUA35I5	1050	340	80	4570	7210	10	1050	340	80	4100	6400	10
SUA35I6	1050	350	80	4570	6580	10	1050	350	80	4090	6400	10
SUA101I1	1260	480	110	4030	6400	10	1260	480	110	3710	6510	10
SUA101I2	1190	430	110	4020	6210	20	1190	430	110	3840	6470	20

TABLE A2
(continued)

Sample	Data as reported by Cendón (1999)						Equilibrated with HMW computer model					
	Mg	K	SO_4	Na	Cl	Ca	Mg	K	SO_4	Na	Cl	Ca
Catalan Basin, Suria-19 core Group II data												
SUA101I3	1220	340	100	4090	6140	10	1220	340	100	3830	6430	10
SUA101I4	1280	420	110	3890	6190	20	1280	420	110	3690	6490	20
SUA101I5	1340	380	110	4140	6150	10	1340	380	110	3620	6480	10
SUA101I6	1320	400	100	3910	6920	10	1320	400	100	3630	6490	10
SUA101I7	1230	460	100	3860	6360	20	1230	460	100	3750	6510	20
SUA101I9	1290	430	110	3810	6290	20	1290	430	110	3670	6500	20
SU102I1	1430	600	120	3640	6240	20	1430	600	120	3380	6640	20
SU102I2	1450	600	110	3270	6960	10	1450	600	110	3350	6650	10
SU102I3	1430	580	100	3160	7020	20	1430	580	100	3370	6650	20
SU102I5	1360	590	120	3130	7230	10	1360	590	120	3510	6600	10
SU102I6	1310	610	110	3940	6050	20	1310	610	110	3560	6610	20
SU102I7	1320	580	120	3170	7290	10	1320	580	120	3580	6580	10
SU102I9	1330	560	100	3340	6930	20	1330	560	100	3540	6600	20
SU102I10	1360	540	110	3830	6100	20	1360	540	110	3510	6590	20
SU102111	1360	540	110	3300	6950	10	1360	540	110	3520	6580	10
SU103I1	1070	500	60	3850	6690	30	1070	500	60	3950	6530	30
SU103I2	960	490	60	3970	6760	30	960	490	60	4140	6490	30
SU103I3	1130	380	40	3880	6460	40	1130	380	40	3860	6500	40
SU103I4	1110	620	80	3990	6370	30	1110	620	80	3850	6590	30
SU103I5	1080	490	70	3840	6680	30	1080	490	70	3950	6520	30
SU103I6	1010	560	80	4200	6320	30	1010	560	80	4050	6530	30
SU103I7	1000	520	80	3890	6790	20	1000	520	80	4090	6490	20
SU103I9	1850	160	100	3000	6320	20	1850	160	100	2860	6560	20
Catalan Basin, Suria-19 core Group III data												
SU104I1	2230	680	90	2260	6860	20	2230	680	90	2140	7140	20
SU104I2	2190	690	90	2290	6910	20	2190	690	90	2190	7120	20
SU104I3	2210	690	100	2300	6830	20	2210	690	100	2170	7120	20
SU104I4	2250	660	90	2260	6820	20	2250	660	90	2120	7140	20
SU104I5	2250	980	100	2210	6940	20	2250	980	100	2040	7360	20
SU104I6	2140	660	90	2400	6770	20	2140	660	90	2270	7070	20
SU105I1	3870	500	200	730	7940	0	3870	500	200	640	8480	0
SU105I2	3960	250	40	660	8010	20	3960	250	30	570	8700	10
SU105I3	2550	840	50	1560	7930	20	2550	840	50	1680	7560	20
SU105I4	3460	380	210	860	8320	0	3460	380	210	950	7830	0
SU105I5	3910	470	230	680	8110	0	3910	470	230	630	8460	0
SU105I6	3290	310	210	1080	8240	10	3290	310	210	1100	7590	10
SU105I7	3770	340	220	800	7760	0	3770	340	220	730	8170	0
SU105I8	3840	440	240	740	7930	0	3840	440	240	680	8320	0
SU105I9	3740	350	250	760	8050	0	3740	350	250	760	8090	0
SU105I10	3690	320	190	830	7800	0	3690	320	190	780	8100	0
SU107I1	3040	390	180	1550	6650	10	3040	390	180	1320	7450	10
SU107I2	2990	390	170	1610	6610	10	2990	390	170	1360	7410	10
SU107I3	3030	410	170	1550	6700	10	3030	410	170	1320	7470	10
SU107I4	3050	390	180	1540	6670	10	3050	390	180	1310	7460	10
SU107I5	3090	410	190	1520	6640	10	3090	410	190	1270	7500	10
SU112I2	3470	150	30	1120	8540	10	3470	150	30	910	7960	10
SU112I3	3420	140	30	780	9270	10	3420	140	30	950	7890	10
Navarra Basin, Biurrun Core												
BI425I1	2110	660	130	2550	6550	10	2110	660	130	2350	6990	10
BI425I2	2240	700	150	2400	6550	10	2240	700	150	2170	7070	10
BI425I3	1790	590	130	2680	7080	10	1790	590	130	2840	6770	10
BI425I4	2010	740	130	2410	7120	10	2010	740	130	2470	6990	10
BI425I5	2000	600	140	2780	6390	10	2000	600	140	2530	6870	10
BI425I6	1950	590	130	2760	6530	10	1950	590	130	2600	6850	10
BI425I7	1970	680	140	2440	7150	10	1970	680	140	2550	6910	10

TABLE A2
(continued)

Sample	Data as reported by Cendón (1999)						Equilibrated with HMW computer model					
	Mg	K	SO_4	Na	Cl	Ca	Mg	K	SO_4	Na	Cl	Ca
Navarra Basin, Subiza Mine												
E1032I2	3470	910	160	810	8720	0	3470	790	160	870	8280	0
E1032I3	3310	890	180	1120	7520	10	3310	860	180	990	8090	10
El032I4	3340	910	150	1100	7530	10	3340	840	150	960	8160	10
E1032I5	3390	880	180	900	8390	0	3390	830	180	930	8180	0
E1032I6	3280	870	180	1160	7420	10	3280	870	180	1010	8060	10
El032I7	3260	930	170	1290	7010	10	3260	870	170	1030	8060	10
E1032I8	3450	850	160	1060	7390	10	3450	800	160	880	8240	10
E1032I9	3120	890	160	1280	7380	10	3120	890	160	1140	7930	10
ES1031I1	3220	500	170	930	8710	0	3220	500	170	1120	7720	0
ES1031I2	3270	570	170	910	8670	0	3270	570	170	1070	7840	0
ES1031I3	3500	660	200	770	8760	0	3500	660	200	880	8140	0
ES1031I4	3850	760	200	620	8730	0	3850	660	200	640	8600	0
ES1031I5	3750	360	200	670	8650	0	3750	360	200	740	8200	0
E2011I1	3410	550	110	900	8270	10	3410	550	110	930	8060	10
E2011I2	3470	510	150	940	7870	10	3470	510	150	900	8030	10
E2011I3	3350	610	100	820	8950	10	3350	610	100	970	8060	10
E2011I4	3030	440	170	1100	8410	0	3030	440	170	1320	7480	0
E2011I5	3390	540	190	1030	7690	0	3390	540	190	980	7920	0
E2011I6	3180	390	190	1080	8060	0	3180	390	190	1190	7560	0
E2011I7	3770	570	120	680	8590	0	3770	570	120	680	8550	0
E2011I8	3460	370	150	730	9140	0	3460	370	150	930	7920	0
E2011I9	3480	520	180	830	8470	0	3480	520	180	900	8020	0
E2011I10	3650	570	80	700	8790	10	3650	570	80	740	8430	10
EN203I1	2350	840	150	1850	7620	10	2350	840	150	2000	7220	10
EN203I2	2190	470	160	1890	7970	10	2190	470	160	2330	6840	10
EN203I3	2580	820	150	1720	7390	10	2580	820	150	1720	7380	10
EN203I4	2730	810	160	1610	7350	10	2730	810	160	1560	7490	10
EN203I5	2310	400	170	1750	8050	10	2310	400	170	2190	6850	10
EN203I6	2770	410	200	1550	7410	10	2770	410	200	1620	7150	10
EN203I7	2990	820	170	1410	7280	10	2990	820	170	1290	7730	10
EN203I8	1980	630	170	2290	7480	10	1980	630	170	2590	6820	10
E303I1	3640	440	90	680	8910	10	3640	440	90	770	8290	10
E303I2	3400	720	130	960	7970	10	3400	720	130	920	8160	10
E303I3	3070	750	130	1180	7920	10	3070	750	130	1200	7810	10
E303I4	3020	710	130	1290	7600	10	3020	710	130	1260	7730	10
E303I5	2840	730	130	1360	7890	10	2840	730	130	1440	7570	10
E303I6	3330	740	130	1040	7820	10	3330	740	130	980	8100	10
E303I7	3120	760	120	1120	8050	10	3120	760	120	1150	7890	10
E303I8	3170	720	130	1160	7720	10	3170	720	130	1120	7900	10
E303I9	3300	720	120	1010	7990	10	3300	720	120	1000	8060	10
ER400I8	3020	610	210	1120	8320	0	3020	610	210	1310	7540	0
ER400I9	2670	840	190	1240	8850	0	2670	840	190	1630	7430	0
ER400I10	2850	810	180	1170	8630	0	2850	810	180	1440	7590	0
ER400I11	2670	790	160	1260	8770	0	2670	790	160	1630	7440	0
ER400I12	3220	750	140	930	8690	0	3220	750	140	1070	7980	0
E401I1	2740	380	150	1410	7980	10	2740	380	150	1640	7180	10
E401I2	2710	310	170	1580	7470	10	2710	310	170	1700	7070	10
E401I4	2290	290	170	1590	8560	0	2290	290	170	2250	6780	0
E401I5	2530	350	170	1870	7090	10	2530	350	170	1910	6960	10
E401I6	2160	450	140	1960	7800	10	2160	450	140	2360	6830	10

TABLE A2
(continued)

Sample	Data as reported by Cendón (1999)						Equilibrated with HMW computer model					
	Mg	K	SO_4	Na	Cl	Ca	Mg	K	SO_4	Na	Cl	Ca
Southern Rhine Graben, MAX Core, Unit S1												
M3I1	1850	670	40	2730	6750	40	1850	670	40	2610	6980	40
M3I2	1620	600	30	2890	6980	50	1620	600	30	2960	6840	50
M3I3	1600	580	90	3080	6750	20	1600	580	90	3090	6730	20
M3I4	1710	330	50	2720	7140	30	1710	330	50	2960	6670	30
M3I5	1720	480	30	2920	6690	50	1720	480	30	2850	6810	50
M3I6	1690	330	40	2790	7030	30	1690	330	40	2980	6670	30
M3I7	1650	250	60	3010	6740	30	1650	250	60	3090	6580	30
M3I8	1550	530	30	2730	7490	40	1550	530	30	3110	6760	40
M3I9	1770	750	30	2700	7200	10	1770	750	30	2740	6990	10
M3I10	1690	730	40	2950	6720	40	1690	730	40	2830	6940	40
M5I2	1680	760	80	2750	7480	10	1680	760	80	2910	6890	10
M5I3	1680	750	70	3030	6630	30	1680	750	70	2880	6910	30
M5I4	1720	790	70	3040	6490	30	1720	790	70	2810	6960	30
M5I5	1560	760	70	2850	7280	20	1560	760	70	3070	6850	20
M5I7	1540	720	70	2980	7060	20	1540	720	70	3120	6820	20
M5I8	1460	510	60	3040	7140	30	1460	510	60	3300	6670	30
M5I9	820	930	40	4340	6460	60	820	930	40	4130	6740	60
M6I1	1870	10	60	2850	6510	30	1870	10	60	2830	6520	30
M6I2	1980	0	60	2970	6020	30	1980	0	60	2670	6570	30
M6I5	1430	90	60	3280	6780	20	1430	90	60	3520	6390	20
M6I7	1690	160	90	3080	7030	10	1690	160	90	3110	6490	10
M6I8	1510	120	50	3210	6700	30	1510	120	50	3350	6450	30
M6I9	1710	170	70	3110	6930	10	1710	170	70	3060	6530	10
M6I10	1690	180	60	3090	6500	30	1690	180	60	3050	6550	30
M6I11	1570	190	70	3280	6450	20	1570	190	70	3260	6490	20
M12XI1	640	310	50	5330	5630	50	640	310	40	4740	6330	40
Ml2XI2	720	340	60	5210	5640	40	720	340	60	4610	6350	40
M12XI5	600	280	50	5220	5840	50	600	280	40	4830	6310	40
Ml2X16	1340	150	80	4050	5800	30	1340	150	70	3650	6380	20
Ml2X17	980	170	70	4600	5840	30	980	170	70	4250	6300	30
M12ZI2	1200	280	80	4550	6750	10	1200	280	80	3870	6410	10
M12ZI5	960	330	70	4650	7110	10	960	330	70	4250	6380	10
M17ZI6	820	200	50	4820	6890	10	820	200	50	4530	6290	10
Ml7X12	690	200	90	5330	5590	10	690	200	90	4810	6230	10
Ml7X13	880	140	90	4820	5790	10	880	140	90	4490	6230	10
Ml7X14	910	160	100	4780	5780	10	910	160	100	4440	6240	10
M17X15	780	180	90	5380	5350	10	780	180	90	4650	6230	10
Ml7X16	670	210	70	5580	5430	10	670	210	70	4820	6250	10
Ml7X17	840	230	90	5240	5390	10	840	230	90	4520	6270	10
Southern Rhine Graben, MAX Core, Mi unit												
F130I1	2440	980	40	2070	6720	40	2440	980	40	1750	7610	40
F130I2	2730	830	50	1510	7590	20	2730	830	50	1480	7710	20
F130I3	2680	760	50	1680	7190	30	2680	760	50	1540	7620	30
F130I4	2090	1400	40	2300	7050	50	2090	1320	30	2080	7600	40
F130I5	2530	950	40	1610	7840	20	2530	950	40	1670	7640	20
F25312	1430	1020	60	2850	7590	20	1430	1020	60	3170	6970	20
F253I4	1820	980	70	2720	6900	30	1820	980	70	2600	7140	30
F253I5	1920	1120	70	2250	7680	20	1920	1120	70	2420	7280	20
F253I6	1740	960	70	2530	7510	20	1740	960	70	2730	7070	20
F253I8	2050	730	80	2610	6530	20	2050	730	80	2360	7070	20
TB52I1	1630	710	80	3190	6490	30	1630	710	80	2980	6850	30
TB52I2	1700	560	40	2520	7590	30	1700	560	40	2890	6830	30
TB52I4	1660	560	60	2810	7090	20	1660	560	60	2980	6780	20
TB52I6	1810	650	70	2790	6800	20	1810	650	70	2730	6900	20
TB52I7	1910	450	80	2700	6720	20	1910	450	80	2650	6800	20

TABLE A2
(continued)

Sample	Data as reported by Cendón (1999)						Equilibrated with HMW computer model					
	Mg	K	SO_4	Na	Cl	Ca	Mg	K	SO_4	Na	Cl	Ca
Southern Rhine Graben, MAX Core, Mi unit												
TB52I8	1690	560	60	3040	6590	30	1690	560	60	2920	6800	30
TB52I9	1830	420	80	2590	7120	20	1830	420	80	2780	6740	20
F154I1	1840	840	70	2580	7140	20	1840	840	70	2620	7040	20
F154I2	1860	850	70	2630	6970	20	1860	850	70	2590	7060	20
F154I3	1800	850	80	2710	6960	20	1800	850	80	2680	7010	20
F154I5	1860	590	70	3010	6240	30	1860	590	70	2660	6890	30
F154I6	1750	670	70	2760	7000	20	1750	670	70	2810	6880	20
F154I7	1760	850	80	2680	7150	20	1760	850	80	2740	6990	20
F154I8	1870	520	70	2940	6350	30	1870	520	60	2670	6850	20
F154I9	1800	660	70	2650	7070	20	1800	660	70	2740	6900	20
F155I1	1620	790	60	3240	6380	30	1620	790	60	2950	6920	30
F155I2	1570	790	80	3380	6290	30	1570	790	80	3040	6870	30
F155I3	1570	770	80	3360	6310	30	1570	770	80	3050	6860	30
F155I4	1600	820	80	3360	6270	30	1600	820	80	2990	6910	30
F155I5	1620	790	70	3400	6140	30	1620	790	70	2960	6910	30
F155I6	1570	760	60	3420	6190	40	1570	760	60	3020	6880	40
F155I7	1610	720	60	2970	6890	30	1610	720	60	2990	6870	30
F155I8	1500	750	60	3060	7010	30	1500	750	60	3150	6840	30
F155I9	1580	720	50	3460	6110	40	1580	720	50	3010	6870	40
F155I10	1430	790	100	3050	7210	20	1430	790	100	3290	6780	20
TB51I1	1500	590	40	3190	7830	10	1500	590	40	3220	6750	10
TB51I2	1590	580	50	2800	7280	30	1590	580	50	3060	6780	30
TB51I3	1590	500	30	2930	7000	40	1590	500	30	3060	6760	40
TB51I4	1470	490	70	3280	7030	10	1470	490	70	3330	6640	10
TB51I5	1240	560	50	4090	6870	10	1240	560	50	3660	6620	10
F156I3	1270	770	70	3780	6980	10	1270	770	70	3550	6740	10
F156i2	1300	710	80	4540	6840	10	1300	710	80	3530	6700	10
Southern Rhine Graben, MAX Core, Ci unit												
244I1	2600	600	60	1710	7340	20	2600	600	60	1680	7400	20
244I2	2500	540	70	2170	6370	20	2500	540	70	1820	7260	20
244I3	2620	640	50	1860	6820	30	2620	640	50	1630	7470	30
244I4	2540	600	70	1690	7560	20	2540	600	70	1760	7340	20
244I5	2400	610	60	1960	7120	20	2400	610	60	1920	7250	20
244I6	2440	590	60	1900	7220	20	2440	590	60	1870	7260	20
244I7	2750	860	50	1420	7940	10	2750	860	50	1460	7740	10
244I8	2570	790	70	1700	7440	20	2570	790	70	1680	7510	20
VT141I1	2540	980	50	1720	7430	30	2540	980	50	1650	7670	30
VT141I2	2480	1010	50	1720	7610	20	2480	1010	50	1720	7630	20
VT141I3	2360	1020	40	1780	7710	30	2360	1020	40	1840	7560	30
VT141I4	2540	1030	40	1670	7550	40	2540	1030	40	1620	7730	40
VT141I5	2500	1010	50	1660	7740	30	2500	1010	50	1680	7650	30
F131I1	2440	1290	40	2080	7710	10	2440	1180	40	1730	7730	10
F131I2	2150	700	50	2230	7100	30	2150	700	50	2200	7160	30
F131I3	2030	800	40	2390	7030	40	2030	800	40	2320	7180	40
F131I5	2000	450	50	2320	7290	30	2000	450	50	2490	6900	30
F131I7	2030	410	140	2600	6650	10	2030	410	140	2550	6760	10
Carpathian Foredeep Basin, Wojnicz IG-4 Core												
WJ3I1	680	120	140	4940	6100	10	680	120	140	4930	6130	10
WJ3I2	790	110	170	5060	5750	10	790	110	170	4770	6120	10
WJ3I3	790	120	170	4950	5880	10	790	120	170	4760	6120	10
WJ3I4	760	110	180	4620	6530	10	760	110	180	4830	6100	10
WJ3I5	700	130	180	4840	6180	10	700	130	180	4930	6100	10
WJ3I6	720	120	170	4660	6370	10	720	120	170	4890	6110	10
WJ3I7	770	120	170	4580	6430	10	770	120	170	4800	6120	10
WJ3I8	730	120	160	4530	6510	10	730	120	160	4860	6120	10

TABLE A2
(continued)

Sample	Data as reported by Cendón (1999)						Equilibrated with HMW computer model					
	Mg	K	SO_4	Na	Cl	Ca	Mg	K	SO_4	Na	Cl	Ca
Carpathian Foredeep Basin, Wojnicz IG-4 Core												
WJ3I10	700	110	180	4650	6420	10	700	110	180	4940	6090	10
WJ13I2	520	100	130	5280	6010	20	520	100	130	5220	6100	20
WJ13I3	510	110	120	5470	5820	20	510	110	120	5230	6120	20
WJ13I5	510	70	130	5580	5710	20	510	70	130	5260	6090	20
WJ13I6	420	50	140	5950	5500	20	420	50	140	5440	6050	20
WJ13I7	420	100	130	5830	5610	20	420	100	130	5410	6090	20
WJ13I8	450	120	130	5510	5890	20	450	120	130	5340	6100	20
WJ18I2	400	100	130	5760	5720	20	400	100	130	5450	6090	20
WJ18I3	450	120	130	5490	5910	20	450	120	130	5340	6100	20
WJ18I4	420	120	130	5520	5950	20	420	120	130	5400	6100	20
WJ18I5	500	130	130	5600	5690	20	500	130	130	5250	6120	20
WJ18I6	480	120	110	5650	5680	20	480	120	110	5270	6130	20
WJ18I8	490	120	110	5780	5520	20	490	120	110	5250	6130	20
WJ22I2	760	0	180	5380	6410	10	760	0	180	4880	6040	10
WJ22I3	820	0	180	5070	6500	10	820	0	180	4770	6050	10
WJ26I2	430	90	120	5300	6740	10	430	90	120	5380	6090	10
WJ26I3	420	70	130	5960	6260	10	420	70	130	5420	6070	10
WJ26I5	390	90	190	5220	6680	10	390	90	190	5530	6020	10
WJB31I1	380	110	80	5650	5840	30	380	110	80	5420	6130	30
WJB31I2	430	110	110	5850	5560	20	430	110	110	5360	6110	20
WJB31I4	520	90	100	5730	5510	30	520	90	100	5200	6130	30
WJB31I7	470	20	80	5530	5800	30	470	20	80	5300	6100	30
WJ36I1	580	40	150	5210	6000	10	580	40	150	5160	6060	10
WJ36I2	490	50	150	5250	6090	10	490	50	150	5320	6050	10
WJ36I3	450	60	130	5220	6220	10	450	60	130	5370	6070	10
WJ36I4	550	50	140	5150	6400	10	550	50	140	5200	6070	10
WJ36I5	510	0	150	5270	6060	10	510	0	150	5310	6030	10
WJ36I6	580	40	150	5270	5920	10	580	40	150	5160	6060	10
WJ36I7	550	10	150	5210	6050	10	550	10	150	5230	6040	10
WJ41I3	580	90	120	5600	5530	20	580	90	120	5110	6120	20
WJ41I6	530	70	100	5260	6020	10	530	70	100	5190	6120	10
WJ41I1	640	20	130	5340	5710	20	640	20	130	5040	6080	20
WJ41I3	650	40	130	5740	6030	10	650	40	130	5010	6090	10
WJ41I4	650	40	130	5850	5910	10	650	40	130	5010	6090	10
Lorca Basin, Lorca-4 Core (originally from García-Veigas 1993, except for L147I1 to I7 and L212AI1 to I7)												
L76	10	0	60	5750	6570	25	10	0	60	6110	6050	30
	10	0	70	5720	6470	22	10	0	70	6120	6060	20
L77	10	110	10	5570	6870	109	10	110	10	5850	6160	110
	10	90	10	5520	6580	125	10	90	10	5830	6160	130
	10	80	10	5740	6400	151	10	80	10	5790	6170	150
L111	1040	220	70	3840	6780	23	1040	220	70	4140	6340	20
	1110	190	80	3940	6470	22	1110	190	80	4040	6330	20
	1230	210	120	3680	6620	13	1230	210	120	3880	6330	10
	1160	210	10	3340	7210	115	1160	210	10	3730	6460	120
L112	1250	180	120	3800	6400	15	1250	180	120	3850	6310	20
	1470	170	170	3770	5980	13	1470	170	170	3540	6330	10
	1420	180	100	3530	6520	17	1420	180	100	3540	6400	20
	1500	180	120	3560	6770	12	1500	180	120	3440	6400	10
	1500	160	140	3660	6630	12	1500	160	140	3460	6360	10
L139	1810	200	110	2740	6900	13	1810	200	110	2930	6550	10
	2250	260	150	2510	6300	12	2250	260	150	2290	6770	10
	1990	220	90	2460	7040	15	1990	220	90	2620	6680	20
L147i1	2830	270	210	1700	6760	10	2830	270	210	1580	7110	10

TABLE A2
(continued)

Sample	Data as reported by Cendón (1999)						Equilibrated with HMW computer model					
	Mg	K	SO_4	Na	Cl	Ca	Mg	K	SO_4	Na	Cl	Ca
Lorca Basin, Lorca-4 Core (originally from García-Veigas 1993, except for L147I1 to I7 and L212AI1 to I7)												
L147i2	2900	180	180	1630	6770	10	2900	180	180	1510	7150	10
L147i3	2700	250	230	1690	7190	10	2700	250	230	1750	6960	10
L147I1	2680	310	210	1860	7010	10	2680	310	210	1750	7020	10
L147I2	2860	340	210	1780	6460	10	2860	340	210	1530	7190	10
L147I3	2680	280	220	2000	6360	10	2680	280	220	1770	6990	10
L147I4	2620	320	210	1700	7320	10	2620	320	210	1820	6980	10
L147I5	2810	290	210	1900	6280	10	2810	290	210	1600	7110	10
L147I6	2560	300	190	1710	7450	10	2560	300	190	1890	6950	10
L147I7	2240	290	170	1930	7710	10	2240	290	170	2310	6760	10
L173I1	2580	260	180	1570	7830	0	2580	260	180	1880	6940	0
L173I2	2390	210	270	1930	7350	0	2390	210	270	2200	6650	0
L173I3	2230	280	240	2240	6970	10	2230	280	240	2370	6650	10
L193i1	2420	230	230	2340	6260	10	2420	230	230	2120	6750	10
L193i2	2860	170	310	1730	6660	0	2860	170	310	1640	6910	0
L193i3	2560	140	280	2150	6350	10	2560	140	280	1990	6710	10
L193i4	2720	190	360	1930	6460	0	2720	190	360	1830	6740	0
L193i5	2490	120	300	2210	6370	10	2490	120	300	2100	6620	10
L193i6	2530	260	340	2110	6530	0	2530	260	340	2050	6690	0
L193i7	2390	330	330	2220	6610	0	2390	330	330	2210	6660	0
L212i1	2160	230	290	2840	5930	10	2160	230	290	2530	6520	10
L212i2	2200	220	300	2540	6400	10	2200	220	300	2480	6520	10
L212i3	1810	200	260	2830	6780	10	1810	200	260	3050	6370	10
L212AI1	2170	170	180	2740	6030	10	2170	170	180	2450	6620	10
L212AI2	2240	280	360	2620	6180	10	2240	280	360	2450	6510	10
L212AI3	2390	310	350	2400	6240	10	2390	310	350	2220	6630	10
L212AI5	2340	300	350	2450	6270	10	2340	300	350	2290	6590	10
L212AI6	2360	310	390	2390	6350	0	2360	310	390	2300	6550	0
L212AI7	2420	320	360	2340	6300	0	2420	320	360	2190	6630	0
L222il	2200	320	300	2670	6280	10	2200	320	300	2450	6590	10
L222i2	2320	330	420	2650	5960	10	2320	330	410	2360	6510	0
L226il	2130	220	370	2910	5910	10	2130	220	370	2640	6400	10
L226i2	2730	230	300	2120	6020	10	2730	230	290	1760	6870	0
L226i3	1600	220	360	3030	7170	0	1600	220	360	3480	6180	0
L226i4	1690	170	300	3220	6380	10	1690	170	300	3290	6260	10
L226i5	2230	230	350	2500	6430	0	2230	230	350	2480	6470	0
L226i6	1560	260	380	3360	6470	0	1560	260	380	3550	6170	0
L228i1	2710	240	390	2010	6550	0	2710	240	390	1850	6730	0
L228i2	2630	280	360	2170	6170	10	2630	280	350	1910	6750	0
L228i3	2470	280	360	2360	6140	10	2470	280	350	2130	6650	0
L228i4	2450	300	390	2360	6200	0	2450	300	390	2180	6600	0
L228i5	2290	230	290	2520	6220	10	2290	230	290	2340	6590	10
L228i6	2340	280	380	2300	6610	0	2340	280	380	2330	6530	0
L228i7	2100	200	300	2610	6540	10	2100	200	300	2640	6460	10
L228i8	2410	290	340	2500	5990	10	2410	290	340	2190	6640	10
L228i9	2270	240	280	2330	6670	10	2270	240	280	2360	6600	10
L229il	2010	300	340	3050	5920	10	2010	300	340	2770	6430	10
L229i2	2320	250	370	2560	6100	10	2320	250	360	2350	6520	0
L229i3	2450	300	370	2580	5750	10	2450	300	360	2150	6630	0
L229i4	2360	250	340	2540	6020	10	2360	250	340	2270	6580	10
L229i5	2090	320	430	2830	6180	0	2090	320	430	2720	6360	0
L229i6	2200	340	330	2750	6020	10	2200	340	330	2470	6570	10
L229i7	2640	250	420	2320	5830	10	2640	250	410	1950	6660	0

TABLE A2
(continued)

Sample	Data as reported by Cendón (1999)						Equilibrated with HMW computer model					
	Mg	K	SO_4	Na	Cl	Ca	Mg	K	SO_4	Na	Cl	Ca
Caltanissetta Basin, Realmonte Mine												
KR146I1	1070	220	300	4720	5620	10	1070	220	300	4330	6110	10
KR146I2	1080	220	310	4560	5790	10	1080	220	310	4320	6100	10
KR146I3	1130	220	320	4440	5840	10	1130	220	320	4240	6100	10
KR146I4	1050	240	300	4610	5780	10	1050	240	300	4360	6120	10
KR146I5	860	230	300	5230	5460	10	860	230	300	4700	6070	10
KR146I6	1050	210	320	4480	5950	10	1050	210	320	4390	6080	10
KR146I7	870	220	310	4850	5880	10	870	220	310	4700	6060	10
KR146I9	1150	220	320	4600	5620	10	1150	220	320	4210	6110	10
KR 144I1	860	180	240	4930	5790	10	860	180	240	4660	6100	10
KR144I4	810	180	230	4880	5920	10	810	180	230	4740	6100	10
KR144I5	840	150	230	4610	6210	10	840	150	230	4700	6090	10
KR144I6	840	170	240	4670	6120	10	840	170	240	4700	6090	10
KR144I7	750	160	190	4750	6210	10	750	160	190	4820	6120	10
KR85I1	460	50	140	5810	6270	10	460	50	140	5350	6060	10
KR85I2	440	50	160	5680	6370	10	440	50	160	5410	6040	10
KR85I4	430	40	150	5190	6380	10	430	40	150	5420	6040	10
KR85I5	380	30	160	5820	5700	10	380	30	160	5530	6020	10
KR85I6	470	20	160	5570	5890	10	470	20	160	5370	6030	10
KR85I7	460	40	150	5660	5770	10	460	40	150	5370	6050	10
KR85I8	480	50	150	5900	6210	10	480	50	150	5330	6060	10
83i1	520	110	150	5600	5670	20	520	110	140	5210	6100	10
83i2	460	90	120	5560	5820	20	460	90	120	5300	6110	20
83i3	480	100	160	5650	5690	20	480	100	150	5300	6080	10
83i4	420	70	160	5520	5960	10	420	70	160	5440	6050	10
83i5	470	90	150	5590	5790	20	470	90	150	5310	6080	20
83i6	440	90	150	5620	5810	20	440	90	150	5370	6080	20
83i7	510	90	140	5660	5630	20	510	90	140	5230	6100	20

Original data as reported in Cendón (1999) are shown on left. Most values from Lorca were recalculated from García-Veigas (1993). All data were modified with the HMW computer program to ensure that brine analyses were in equilibrium with halite, modified values are shown on the right. All values are mmolal.

TABLE A3

Major-ion chemistry of fluid inclusions, compiled by Zimmermann (2000)

Sample	Data as compiled by Zimmermann (2000)						Equilibrated with HMW computer model					
	Mg	K	SO_4	Na	Cl	Ca	Mg	K	SO_4	Na	Cl	Ca
Navarra Basin, Biurrun Core (Ayora and others, 1994b)												
BI-425	1870	560	160	2640	6570	0	1870	560	160	2760	6740	0
BI-430	1650	520	120	2580	6640	0	1650	520	120	3090	6670	0
BI-436	1690	400	150	2730	6590	0	1690	400	150	3090	6570	0
BI-437	1360	360	140	3680	6910	0	1360	360	140	3630	6430	0
Carpathian Foredeep Basin (Kovalevich and Petrichenko, 1997; Galamay and others, 1997)												
breccia	818	144	136	NA	NA	NA	820	140	140	4670	6170	0
spiza salt	918	155	184	NA	NA	NA	920	160	180	4530	6130	0
spiza salt	1195	274	193	NA	NA	NA	1200	270	190	4000	6270	0
shaft salt	945	226	130	NA	NA	NA	950	230	130	4400	6230	0
green salt	877	263	201	NA	NA	NA	880	260	200	4570	6190	0
105	813	172	160	NA	NA	NA	810	170	160	4690	6160	0
106	804	169	123	NA	NA	NA	800	170	120	4670	6200	0
107	809	155	118	NA	NA	NA	810	160	120	4660	6200	0
16	863	184	138	NA	NA	NA	860	180	140	4570	6210	0
120	909	169	116	NA	NA	NA	910	170	120	4470	6240	0
118	890	217	140	NA	NA	NA	890	220	140	4510	6210	0
117	904	206	117	NA	NA	NA	900	210	120	4460	6250	0
98	850	212	118	NA	NA	NA	850	210	120	4560	6250	0
100	850	212	129	NA	NA	NA	850	210	130	4570	6220	0
99	827	155	128	NA	NA	NA	830	160	130	4640	6180	0
97	750	121	122	NA	NA	NA	750	120	120	4780	6160	0
6	804	147	147	NA	NA	NA	800	150	150	4700	6170	0
87	854	147	131	NA	NA	NA	850	150	130	4590	6200	0
91	1013	209	131	NA	NA	NA	1010	210	130	4280	6270	0
89	1022	206	143	NA	NA	NA	1020	210	140	4280	6250	0
12	854	147	133	NA	NA	NA	850	150	130	4600	6190	0
10	909	158	143	NA	NA	NA	910	160	140	4500	6180	0
9	922	133	128	NA	NA	NA	920	130	130	4480	6210	0
8	859	127	139	NA	NA	NA	860	130	140	4600	6170	0
East Slovakian Basin (Kovalevich and Petrichenko, 1997; Galamay and Karoli, 1997)												
Ep-2. 238.4	804	153	161	NA	NA	NA	800	150	160	4710	6160	0
Ep-2. 239.2	786	147	157	NA	NA	NA	790	150	160	4740	6150	0
Ep-2. 71	631	144	100	NA	NA	NA	630	140	100	4970	6170	0
Ep-2, 70	609	136	101	NA	NA	NA	610	140	100	5010	6150	0
Ep-2. 68	591	110	98	NA	NA	NA	590	110	100	5050	6160	0
Ep-2. 65	759	155	105	NA	NA	NA	760	160	110	4740	6200	0
Ep-2. 63	586	147	108	NA	NA	NA	590	150	110	5060	6150	0
Ep-2. 61	513	127	95	NA	NA	NA	510	130	100	5190	6160	0
Ep-2. 59	613	121	99	NA	NA	NA	610	120	100	5010	6170	0
Ep-2. 57	581	136	103	NA	NA	NA	580	140	100	5070	6150	0
Ep-2. 56	563	144	101	NA	NA	NA	560	140	100	5090	6170	0
Ep-2. 55	591	147	113	NA	NA	NA	590	150	110	5050	6160	0
Ep-2. 54	550	133	99	NA	NA	NA	550	130	100	5120	6170	0
Ep-2. 53	604	127	111	NA	NA	NA	600	130	110	5040	6150	0
Ep-2. 52	572	127	110	NA	NA	NA	570	130	110	5090	6160	0
Ep-2. 50	500	93	94	NA	NA	NA	500	90	90	5230	6120	0
Red Sea, DSDP Sites 225 and 227 (Kovalevich and others, 1997; Lazar and Holland, 1999)												
30-2/2	1550	362	479	3520	6170	0	1550	360	480	3520	6020	0
32-4/2	1960	618	598	2910	6050	0	1960	620	600	2910	6250	0
35-5/1	1600	370	490	3500	6170	0	1600	370	490	3500	6090	0
35-5/3	1580	371	536	3630	6400	0	1580	370	540	3630	6100	0
35-1/110-112	1104	178	299	NA	NA	NA	1100	180	300	4300	6100	0
43-4/015-017	1158	206	361	NA	NA	NA	1160	210	360	4250	6040	0

TABLE A3
(continued)

Sample	Data as compiled by Zimmermann (2000)						Equilibrated with HMW computer model					
	Mg	K	SO_4	Na	Cl	Ca	Mg	K	SO_4	Na	Cl	Ca
Red Sea, DSDP Sites 225 and 227 (Kovalevich and others, 1997; Lazar and Holland, 1999)												
BI-425	1870	560	160	2640	6570	0	1870	560	160	2760	6740	0
27-2/110-112	1145	249	231	NA	NA	NA	1150	250	230	4130	6200	0
27-2/137-140	968	217	271	NA	NA	NA	970	220	270	4500	6100	0
28-1/062-066	1177	257	274	NA	NA	NA	1180	260	270	4110	6170	0
Caltanissetta Basin, Central Sicily (Garcia-Veigas and others, 1995; Zimmermann, 2000)												
647	2150	520	550	2470	6190	0	2150	520	550	2660	6380	0
745	2480	460	580	2620	6880	0	2480	460	580	2220	6480	0
675	2500	470	590	2200	6490	0	2500	470	590	2190	6480	0
647	3250	610	720	1360	7030	0	3250	610	720	1320	6990	0
3'	2210	460	540	2430	6230	0	2210	460	540	2580	6380	0
340	800	230	230	4420	5790	0	800	230	230	4750	6120	0
13	1130	250	310	4210	6100	0	1130	250	310	4230	6120	0
SRe95-14/04	820	170	230	4770	6050	0	820	170	230	4750	6100	0
SRe95-14/06	1030	220	310	4690	5740	0	1030	220	310	4420	6080	0

Major-ion chemistry of fluid inclusions, compiled by Zimmermann (2000), shown on left. Data screened by Zimmermann that are used in this paper are from: Ayora and others (1994b), Galamay and Karoli (1997), Galamay and others (1997), García-Veigas and others (1995), Kovalevich and Petrichenko (1997), Kovalevich and others (1997), Lazar and Holland (1999), and Zimmermann (2000). Fluid inclusion chemistries equilibrated with the HMW computer program to ensure equilibrium with halite, are shown on right. All values are mmolal.

REFERENCES

Attia, O. A., Lowenstein, T. K., and Wali, A. M. A., 1995, Middle Miocene Gypsum, Gulf of Suez: marine or nonmarine?: Journal of Sedimentary Research, v. A65, p. 614–626, http://dx.doi.org/10.1306/D4268176-2B26-11D7-8648000102C1865D

Ayora, C., and Fontarnau, R., 1990, X-Ray microanalysis of frozen fluid inclusions: Chemical Geology, v. 89, n. 1–2, p. 135–148, http://dx.doi.org/10.1016/0009-2541(90)90063-D

Ayora, C., García-Veigas, J., and Pueyo, J.-J., 1994a, X-ray microanalysis of fluid inclusions and its application to the geochemical modeling of evaporitic basins: Geochimica et Cosmochimica Acta, v. 58, n. 1, p. 43–55, http://dx.doi.org/10.1016/0016-7037(94)90444-8

——— 1994b, The chemical and hydrological evolution of an ancient potash-forming evaporitic basin as constrained by mineral sequence, fluid inclusion composition, and numerical simulation: Geochimica et Cosmochimica Acta, v. 58, p. 3379–3394, http://dx.doi.org/10.1016/0016-7037(94)90093-0

Ayora, C., Taberner, C., Pierre, C., and Pueyo, J.-J., 1995, Modeling the sulfur and oxygen isotopic composition of sulfates through a halite-potash sequence: Implications for the hydrological evolution of the Upper Eocene South Pyrenean Basin: Geochimica et Cosmochimica Acta, v. 59, n. 9, p. 1799–1808, http://dx.doi.org/10.1016/0016-7037(95)00083-C

Ayora, C., Cendón, D. I., Taberner, C., and Pueyo, J. J., 2001, Brine-mineral reactions in evaporite basins: Implications for the composition of ancient oceans: Geology, v. 29, n. 3, p. 251–254, http://dx.doi.org/10.1130/0091-7613(2001)029⟨0251:BMRIEB⟩2.0.CO;2

Benali, S., Schreiber, B. C., Helman, M. L., and Philip, R. P., 1995, Characterization of organic matter from a restricted/evaporative sedimentary environment: Late Miocene of Lorca basin, southeastern Spain: AAPG Bulletin, v. 79, n. 6, p. 816–830.

Bertini, A., Londeix, L., Maniscalco, R., DiStefano, A., Suc, J.-P., Clauzon, G., Gautier, F., and Grasso, M., 1998, Paleobiological evidence of depositional conditions in the Salt Member, Gessoso-Solfifera Formation (Messinian, Upper Miocene) of Sicily: Micropaleontology, v. 44, n. 4, p. 413–433, http://dx.doi.org/10.2307/1486042

Blanc-Valleron, M.-M., and Schuler, M., 1997, The salt basins of Alsace (Southern Rhine Graben), *in* Busson, G., and Schreiber, C. B., editors, Sedimentary deposition in rift and foreland basins in France and Spain (Paleogene and Neogene): New York, Columbia University Press, p. 95–135.

Bloch, M. R., and Scherb, J., 1953, On the Cl^-/Br^--ratio and the distribution of Br-ions in liquids and solids during the evaporation of bromide-containing chloride solutions: Bulletin of the Research Council of Israel, v. 3, p. 151–158.

Braitsch, O., and Herrmann, A. G., 1963, Zur geochemie des broms in salinaren sedimenten; Teil I, experimentelle bestimmung der Br-verteilung in verschiedenen natuerlichen salzsystemen: Geochimica et Cosmochimica Acta, v. 27, n. 4, p. 361–391, http://dx.doi.org/10.1016/0016-7037(63)90077-2

Brennan, S. T., and Lowenstein, T. K., 2002, The major-ion composition of Silurian seawater: Geochimica et Cosmochimica Acta, v. 66, n. 15, p. 2683–2700, http://dx.doi.org/10.1016/S0016-7037(02)00870-0
Brennan, S. T., Lowenstein, T. K., and Horita, J., 2004, Seawater chemistry and the advent of biocalcification: Geology, v. 32, n. 6, p. 473–476, http://dx.doi.org/10.1130/G20251.1
Bukowski, K., 1997, Sedimentation of clastic strata associated with Miocene salts in Wieliczka (Southern Poland): Slovak Geological Magazine, v. 3, p. 157–163.
Butler, R. W. H., and Lickorish, W. H., 1997, Using high resolution stratigraphy to date fold and thrust activity: examples from the Neogene of south-central Sicily: Journal of the Geological Society, London, v. 154, n. 4, p. 633–643, http://dx.doi.org/10.1144/gsjgs.154.4.0633
Canals, A., Carpentier, B., Huc, A. Y., Guilhaumou, N., and Ramsey, M. H., 1993, Microanalysis of primary fluid inclusions in halite; constraints for an evaporitic sedimentation modeling; application to the Mulhouse Basin, France: Organic Geochemistry, v. 20, n. 8, p. 1139–1151, http://dx.doi.org/10.1016/0146-6380(93)90005-V
Cendón, D. I., ms, 1999, Evolución geoquímica de cuencas evaporíticas Terciarias: Implicaciones en la composición isotópica del sulfato disuelto en el océano durante el Terciario: Barcelona, Spain, Universitat de Barcelona, Ph. D. Dissertation, 270 p., http://www.tdx.cat/handle/10803/81705
Cendón, D. I., Ayora, C., and Pueyo, J. J., 1998, The origin of barren bodies in the Subiza potash deposit, Navarra, Spain: Implications for sylvite formation: Journal of Sedimentary Research, v. 68, n. 1, p. 43–52, http://dx.doi.org/10.2110/jsr.68.43
Cendón, D. I., Ayora, C., Pueyo, J. J., and Taberner, C., 2003, The geochemical evolution of the Catalan potash subbasin, South Pyrenean foreland basin (Spain): Chemical Geology, v. 200, p. 339–357, http://dx.doi.org/10.1016/S0009-2541(03)00195-5
Cendón, D. I., Peryt, T. M., Ayora, C., Pueyo, J. J., and Taberner, C., 2004, The importance of recycling processes in the Middle Miocene Badenian evaporite basin (Carpathian foredeep): palaeoenviornmental implications: Palaeogeography, Palaeoclimatology, Palaeoecology, v. 212, p. 141–158, http://dx.doi.org/10.1016/j.palaeo.2004.05.021
Cendón, D. I., Ayora, C., Pueyo, J. J., Taberner, C., and Blanc-Valleron, M.-M., 2008, The chemical and hydrological evolution of the Mulhouse potash basin (France): Are "marine" ancient evaporites always representative of synchronous seawater chemistry?: Chemical Geology, v. 252, p. 109–124, http://dx.doi.org/10.1016/j.chemgeo.2008.01.019
Claypool, G. E., Holser, W. T., Kaplan, I. R., Sakai, H., and Zak, I., 1980, The age curves of sulfur and oxygen isotopes in marine sulfate and their mutual interpretation: Chemical Geology, v. 28, p. 199–260, http://dx.doi.org/10.1016/0009-2541(80)90047-9
Coggon, R. M., Teagle, D. A., Smith-Duque, C. E., Alt, J. C., and Cooper, M. J., 2010, Reconstructing past seawater Mg/Ca and Sr/Ca from mid-ocean ridge flank calcium carbonate veins: Science, v. 327, p. 1114–1117, http://dx.doi.org/10.1126/science.1182252
Conrad, C. P., and Lithgow-Bertelloni, C., 2007, Faster seafloor spreading and lithosphere production during the mid-Cenozoic: Geology, v. 35, n. 1, p. 29–32, http://dx.doi.org/doi:10.1130/G22759A.1
Curial, A., and Moretto, R., 1997, The salt basin of Bresse: southern Saône Graben, *in* Busson, G., and Schreiber, B. C., editors, Sedimentary deposition in rift and foreland basins in France and Spain (Paleogene and Neogene): New York, Columbia University Press, p. 136–194.
Decima, A., 1978, Initial data on bromine distribution in the Miocene salt formation of southern Sicily: Memorie della Società Geologica Italiana, v. 16, p. 39–43.
Decima, A., and Wezel, F. C., 1971, Osservazioni sulle evaporiti Messiniane della Sicilia centromeridionale: Revista Mineraria Siciliana, v. 16, p. 172–187.
Decima, A., McKenzie, J. A., and Schreiber, B. C., 1988, The origin of "evaporative" limestone: an example from the Messinian of Sicily (Italy): Journal of Sedimentary Petrology, v. 58, n. 2, p. 256–272, http://dx.doi.org/10.1306/212F8D6E-2B24-11D7-8648000102C1865D
Demicco, R. V., Lowenstein, T. K., Hardie, L. A., and Spencer, R. J., 2005, Model of seawater composition for the Phanerozoic: Geology, v. 33, n. 11, p. 877–880, http://dx.doi.org/10.1130/G21945.1
Denison, R. D., Kirkland, D. W., and Evans, R., 1998, Using strontium isotopes to determine the age and origin of gypsum and anhydrite beds: The Journal of Geology, v. 106, n. 1, p. 1–17, http://dx.doi.org/10.1086/515996
DePaolo, D. J., and Ingram, B. L., 1985, High-resolution stratigraphy with strontium isotopes: Science, v. 227, n. 4689, p. 938–941, http://dx.doi.org/10.1126/science.227.4689.938
Dyni, J. R., Hite, R. J., and Raup, O. B., 1970, Lacustrine deposits of bromide-bearing halite, Green River Formation, northwestern Colorado, *in* Third Symposium on Salt, v. 1: Cleveland, Ohio, Northern Ohio Geological Society, p. 166–180.
Elderfield, H., 1986, Strontium isotope stratigraphy: Palaeogeography Palaeoclimatology Palaeoecology, v. 57, n. 1, p. 71–90, http://dx.doi.org/10.1016/0031-0182(86)90007-6
Fantle, M. S., 2010, Evaluating the Ca isotope proxy: American Journal of Science, v. 310, n. 3, p. 194–230, http://dx.doi.org/10.2475/03.2010.03
Gaffin, S., 1987, Ridge volume dependence on sea-floor generation rate and inversion using long-term sea-level change: American Journal of Science, v. 287, n. 6, p. 596–611, http://dx.doi.org/10.2475/ajs.287.6.596
Galamay, A. R., and Karoli, S., 1997, Geochemistry of the Badenian salts from the East Slovakian Basin, Slovakia: Slovak Geological Magazine, v. 3, p. 187–192.
Galamay, A. R., Bukowski, K., and Przybylo, J., 1997, Chemical composition of origin of brines in the Badenian evaporite basin of the Carpathian Foredeep: fluid inclusion data from Wieliczka (Poland): Slovak Geological Magazine, v. 3, p. 165–171.
García-Veigas, J., ms, 1993, Geoquímica de inclusiones fluidas en formaciones salinas, Microanálisis Cryo-SEM-EDS: Barcelona, Spain, Universitat de Barcelona, Ph. D. Dissertation, 260 p.

García-Veigas, J., Ortí, F., Rosell, L., and Inglès, M., 1994, Caracterización petrológica y geoquímica de la Unidad Salina Messiniense de la cuenca de Lorca (sondeos S4 y S5): Geogaceta, v. 15, p. 78–81.
García-Veigas, J., Ortí, F., Rosell, L., Ayora, C., Rouchy, J.-M., and Lugli, S., 1995, The Messinian salt of the Mediterranean: geochemical study of the salt from the Central Sicily Basin and comparison with the Lorca Basin (Spain): Bulletin de la Société Géologique de France, v. 166, n. 6, p. 699–710.
Garlicki, A., and Wali, A. M. A., 1981, Geochemical characteristics of the Bochnia Evaporites Member, with new aspects in Br/Cl ratio determinations: Mineralogia Polonica, v. 12, n. 2, p. 25–47.
Garlicki, A., and Wiewiórka, J., 1981, The distribution of bromine in some halite rocks of the Wieliczka salt deposit (Poland): Annales de la Société Géologique de Pologne, v. 51, p. 353–359.
Geel, T., 1976, Messinian gypsiferous deposits of the Lorca Basin (Province of Murcia, SE Spain): Memorie della Società Geologica Italiana, v. 16, p. 369–385.
Griffin, D. L., 1999, The late Miocene climate of northeastern Africa: unraveling the signals in the sedimentary succession: Journal of the Geological Society, London, v. 156, n. 4, p. 817–826, http://dx.doi.org/10.1144/gsjgs.156.4.0817
Haq, B. U., Hardenbol, J., and Vail, P. R., 1987, Chronology of fluctuating sea levels since the Triassic (250 million years ago to present): Science, v. 235, n. 4793, p. 1156–1167, http://dx.doi.org/10.1126/science.235.4793.1156
Hardie, L. A., 1984, Evaporites: marine or non-marine: American Journal of Science, v. 284, n. 3, p. 193–240, http://dx.doi.org/10.2475/ajs.284.3.193
——— 1996, Secular variation in seawater chemistry: An explanation for the coupled secular variation in the mineralogies of marine limestones and potash evaporites over the past 600 my: Geology, v. 24, n. 3, p. 279–283, http://dx.doi.org/10.1130/0091-7613(1996)024⟨0279:SVISCA⟩2.3.CO;2
Hardie, L. A., and Eugster, H. P., 1970, The evolution of closed basin-brines: Mineralogical Society of America, Special Paper 3, p. 273–290.
Harvie, C. E., Møller, N., and Weare, J. H., 1984, The prediction of mineral solubilities in natural waters: the Na-K-Mg-Ca-H-Cl-SO_4-OH-HCO_3-CO_3-CO_2-H_2O system to high ionic strengths at 25°C: Geochimica et Cosmochimica Acta, v. 48, n. 4, p. 723–751, http://dx.doi.org/10.1016/0016-7037(84)90098-X
Holland, H. D., 1984, The Chemical Evolution of the Atmosphere and Oceans: Princeton, Princeton University Press, 582 p.
——— 2005, Sea level, sediments, and the composition of seawater: American Journal of Science, v. 305, n. 3, p. 220–239, http://dx.doi.org/10.2475/ajs.305.3.220
Holland, H. D., and Zimmermann, H., 2000, The dolomite problem revisited: International Geology Review, v. 42, n. 6, p. 481–490, http://dx.doi.org/10.1080/00206810009465093
Holser, W. T., 1966, Bromide geochemistry of salt rocks, *in* Rau, J. L., editor, Proceedings of the second symposium on salt: Cleveland, Northern Ohio Geological Society, p. 248–275.
Horita, J., Zimmermann, H., and Holland, H. D., 2002, The chemical evolution of seawater during the Phanerozoic: Implications from the record of marine evaporites: Geochimica et Cosmochimica Acta, v. 66, n. 21, p. 3733–3756, http://dx.doi.org/10.1016/S0016-7037(01)00884-5
Ivany, L. C., Peters, S. C., Wilkinson, B. H., Lohmann, K. C., and Reimer, B. A., 2004, Seawater Sr/Ca and Mg/Ca records from an Oligocene coral: Geobiology, v. 2, n. 2, p. 97–106, http://dx.doi.org/10.1111/j.1472-4677.2004.00025.x
Karoli, S., Janocko, J., Kotul'ák, P., and Verdon, P., 1997, Sedimentology of Karpathian evaporites in the East-Slovakian Neogene basin (Slovakia): Slovak Geological Magazine, v. 3, p. 201–211.
Kominz, M. A., 1984, Oceanic ridge volume and sea-level change—An error analysis, *in* Schlee, J. S., editor, Interregional unconformities and hydrocarbon accumulation: AAPG Memoir 36, p. 109–127.
——— 2001, Sea Level Variations Over Geologic Time, *in* Steele, J. H., Thorpe, S. A., and Turekian, K. K., editors, Encyclopedia of Ocean Sciences: Oxford, Academic Press, p. 2605–2613.
Kominz, M. A., Miller, K. G., and Browning, J. V., 1998, Long-term and short-term global Cenozoic sea-level estimates: Geology, v. 26, n. 4, p. 311–314, http://dx.doi.org/10.1130/0091-7613(1998)026⟨0311:LTASTG⟩2.3.CO;2
Kovalevich, V. M., and Petrichenko, O. I., 1997, Chemical composition of brines in Miocene evaporite basins of the Carpathian region: Slovak Geological Magazine, v. 3, p. 173–180.
Kovalevich, V. M., Jarmolowicz-Szulc, K., Peryt, T. M., and Poberegski, A. V., 1997, Messinian chevron halite from the Red Sea (DSDP Sites 225 and 227): fluid inclusion study: Neues Jahrbuch Mineralogie, Monatshefte, v. 10, p. 433–450.
Kovalevich, V. M., Peryt, T. M., and Petrichenko, O. I., 1998, Secular variation in seawater chemistry during the Phanerozoic as indicated by brine inclusions in halite: Journal of Geology, v. 106, n. 6, p. 695–712, http://dx.doi.org/10.1086/516054
Kovalevych, V. M., Peryt, T. M., Beer, W., Geluk, M., and Halas, S., 2002, Geochemistry of Early Triassic seawater as indicated by study of the Röt halite in the Netherlands, Germany, and Poland: Chemical Geology, v. 182, n. 2–4, p. 549–563, http://dx.doi.org/10.1016/S0009-2541(01)00343-6
Kovalevych, V. M., Marshall, T., Peryt, T. M., Petrychenko, O. Y., and Zhukova, S. A., 2006, Chemical composition of seawater in Neoproterozoic: results of fluid inclusion study of halite from Salt Range (Pakistan) and Amadeus Basin (Australia): Precambrian Research, v. 144, n. 1–2, p. 39–51, http://dx.doi.org/10.1016/j.precamres.2005.10.004
Krijgsman, W., Garcés, M., Agustí, J., Raffi, I., Taberner, C., and Zachariasse, W. J., 2000, The "Tortonian salinity crisis" of the eastern Betics (Spain): Earth and Planetary Science Letters, v. 181, n. 4, p. 497–511, http://dx.doi.org/10.1016/S0012-821X(00)00224-7
Krzywiec, P., 2001, Contrasting tectonic and sedimentary history of the central and eastern parts of the Polish Carpathian foredeep basin—results of seismic data interpretation: Marine and Petroleum Geology, v. 18, n. 1, p. 13–38, http://dx.doi.org/10.1016/S0264-8172(00)00037-4

Lazar, B., and Holland, H. D., ms, 1999, Fluid inclusion analyses of Messinian chevron halite in the Red Sea (DSDP Site 227).
Lowenstein, T. K., and Hardie, L. A., 1985, Criteria for the recognition of salt-pan evaporites: Sedimentology, v. 32, n. 5, p. 627–644, http://dx.doi.org/10.1111/j.1365-3091.1985.tb00478.x
Lowenstein, T. K., and Spencer, R. J., 1990, Syndepositional origin of potash evaporites: petrographic and fluid inclusions evidence: American Journal of Science, v. 290, n. 1, p. 1–42, http://dx.doi.org/10.2475/ajs.290.1.1
Lowenstein, T. K., Timofeeff, M. N., Brennan, S. T., Hardie, L. A., and Demicco, R. V., 2001, Oscillations in Phanerozoic seawater chemistry: Evidence from fluid inclusions in salt deposits: Science, v. 294, n. 5544, p. 1086–1088, http://dx.doi.org/10.1126/science.1064280
Lowenstein, T. K., Hardie, L. A., Timofeeff, M. N., and Demicco, R. V., 2003, Secular variation in seawater chemistry and the origin of calcium chloride basinal brines: Geology, v. 31, n. 10, p. 857–860, http://dx.doi.org/10.1130/G19728R.1
Lowenstein, T. K., Timofeeff, M. N., Kovalevych, V. M., and Horita, J., 2005, The major-ion composition of Permian seawater: Geochimica et Cosmoschimica Acta, v. 69, n. 7, p. 1701–1719, http://dx.doi.org/10.1016/j.gca.2004.09.015
Lugli, S., Schreiber, B. C., and Triberti, B., 1999, Giant polygons in the Realmonte Mine (Agrigento, Sicily): Evidence for the desiccation of a Messinian halite basin: Journal of Sedimentary Research, v. 69, n. 3, p. 764–771, http://dx.doi.org/10.2110/jsr.69.764
Lutz, F., ms, 1975, Die verteilung von bromid in Gezüchteten und natürlichen chloridischen salzmineralen: Tübingen, Germany, Eberhard-Karls Univeristy, Ph. D. dissertation, Eberhard-Karls University, 85 p.
McArthur, J. M., Howarth, R. J., and Bailey, T. R., 2001, Strontium isotope stratigraphy: LOWESS version 3: best fit to the marine Sr-isotope curve for 0–509 Ma and accompanying look-up table for deriving numerical age: Journal of Geology, v. 109, n. 2, p. 155–170, http://dx.doi.org/10.1086/319243
Miller, K. G., Kominz, M. A., Browning, J. V., Wright, J. D., Mountain, G. S., Katz, M. E., Sugarman, P. J., Cramer, B. S., Christie-Blick, N., and Pekar, S. F., 2005, The Phanerozoic record of global sea-level change: Science, v. 310, n. 5752, p. 1293–1298, http://dx.doi.org/10.1126/science.1116412
Moretto, R., 1985, Sédimentologie de la série salifère du Paléogène de la Bresse (France): Bulletin de la Societe Géologique de France, v. 8, p. 849–855.
——— 1987, Étude sédimentologique et géochimique des despots de la série salifère paléogène du basin de Bourg-en-Bresse (France): Mémoir Science de la Terre, v. 50, 252 p.
Müller, D. W., and Mueller, P. A., 1991, Origin and age of the Mediterranean Messinian evaporites; implications from Sr isotopes: Earth and Planetary Science Letters, v. 107, n. 1, p. 1–12, http://dx.doi.org/10.1016/0012-821X(91)90039-K
Müller, R. D., Sdrolias, M., Gaina, C., Steinberger, B., and Heine, C., 2008, Long-term sea-level fluctuations driven by ocean basin dynamics: Science, v. 319, n. 5868, p. 1357–1362, http://dx.doi.org/10.1126/science.1151540
Ouda, K., Massoud, M., and Tammam, N., 2000, Stratigraphy of the Miocene sequence of the northern Red Sea: Neues Jahrbuch fuer Geologie und Palaeontologie, Abhandlungen, v. 215, p. 125–176.
Patton, T. L., Moustafa, A. R., Nelson, R. A., and Abdine, S. A., 1994, Tectonic Evolution and Structural Setting of the Suez Rift, *in* Landon, S. M., editor, Interior Rift Basins: AAPG Memoir 59, p. 9–55.
Paytan, A., Kastner, M., Campbell, D., and Thiemens, M. H., 1998, Sulfur isotopic composition of Cenozoic seawater sulfate: Science, v. 282, n. 5393, p. 1459–1462, http://dx.doi.org/10.1126/science.282.5393.1459
Peryt, T. M. Karoli, S., Peryt, D., Petrichenko, O. I., Gedl, P., Narkiewicz, W., Durkovicova, J., and Dobieszynska, Z., 1997, Westernmost occurrence of the Middle Miocene Badenian gypsum in central Paratethys (Koberice, Moravia, Czech Republic): Slovak Geological Magazine, v. 3, p. 105–120.
Petrichenko, O. I., 1973, Methods of study of inclusions in minerals of saline deposits, Naukova Dumka, Kiev, 90 p. (in Ukrainian), translated in (1979) Fluid Inclusions Research, v. 12, p. 214–274.
Petrychenko, O. Y., and Peryt, T. M., 2004, Geochemical conditions of deposition in the Upper Devonian Prypiac' and Dnipro-Donets evaporite basins (Belarus and Ukraine): The Journal of Geology, v. 112, n. 5, p. 577–592, http://dx.doi.org/10.1086/422667
Petrychenko, O. Y., Peryt, T. M., and Chechel, E. I., 2005, Early Cambrian seawater chemistry from fluid inclusions in halite from Siberian evaporites: Chemical Geology, v. 219, n. 1–4, p. 149–161, http://dx.doi.org/10.1016/j.chemgeo.2005.02.003
Puigdefàbregas, C., and Souquet, P., 1986. Tectono-sedimentary cycles and depositional sequences of the Mesozoic and Tertiary from the Pyrenees: Tectonophysics, v. 129, n. 1–4, p. 173–203, http://dx.doi.org/10.1016/0040-1951(86)90251-9
Rauscher, R., and Schuler, M., 1988, Les dinokystes, des témoins d'influences marines dans le Paléogène d/Alsace: Bulletin des Centres de Recherches Exploration-Production Elf-Aquitaine, v. 12, n. 1, p. 405–425.
Rosell, L., and Pueyo, J. J., 1997, Second marine evaporitic phase in the South Pyrenean foredeep: The Priabonian potash basin (Late Eocene: Autochthonous-Allochthonous Zone), *in* Busson, G., and Schreiber, B. C., editors, Sedimentary deposition in rift and foreland basins in France and Spain (Paleogene and Neogene): New York, Columbia University Press, p. 358–387.
Rouchy, J. M., 1997, Paleogene continental rift system of western Europe: Introduction and stratigraphy, *in* Busson, G., and Schreiber, B. C., editors, Sedimentary deposition in rift and foreland basins in France and Spain (Paleogene and Neogene): New York, Columbia University Press, p. 45–94.
Rouchy, J. M., Taberner, C., Blanc-Valleron, M.-M., Sprovieri, R., Russell, M., Pierre, C., Di Stefano, E., Pueyo, J. J., Caruso, A., Dinarés-Turell, J., Gomis-Coll, E., Wolff, G. A., Cespuglio, G., Ditchfield, P., Pestrea, S., Combourieu-Nebout, N., Santisteban, C., and Grimalt, J. O., 1998, Sedimentary and diagenetic markers of the restriction in a marine basin: the Lorca Basin (SE Spain) during the

Messinian: Sedimentary Geology, v. 121, n. 1–2, p. 23–55, http://dx.doi.org/10.1016/S0037-0738(98)00071-2
Rowley, D. B., 2002, Rate of plate creation and destruction: 180 Ma to present: Geological Society of America Bulletin, v. 114, n. 8, p. 927–933, http://dx.doi.org/10.1130/0016-7606(2002)114⟨0927:ROPCAD⟩2.0.CO;2
Santanach, P., 1997, The Ebro Basin in the structural framework of the Iberian Plate, *in* Busson, G., and Schreiber, B. C., editors, Sedimentary deposition in rift and foreland basins in France and Spain (Paleogene and Neogene): New York, Columbia University Press, p. 303–318.
Satterfield, C. L., Lowenstein, T. K., Vreeland, R. H., Rosenzweig, W. D., and Powers, D. W., 2005a, New evidence for 250 Ma age of halotolerant bacterium from a Permian salt crystal: Geology, v. 33, p. 265–268, http://dx.doi.org/10.1130/G21106.1
Satterfield, C. L., Lowenstein, T. K., Vreeland, R. H., and Rosenzweig, W. D., 2005b, Paleobrine temperatures, chemistries, and paleoenvironments of Silurian Salina Formation F-1 Salt, Michigan Basin, U.S.A., from petrography and fluid inclusions in halite: Journal of Sedimentary Research, v. 75, p. 534–544, http://dx.doi.org/10.2110/jsr.2005.044
Schütz, K. I., 1994, Structure and stratigraphy of the Gulf of Suez, Egypt, *in* Landon, S. M., editor, Interior Rift Basins: AAPG Memoir 59, p. 57–96.
Servant-Vildary, S., Rouchy, J. M., Pierre, C., and Foucault, A., 1990, Marine and continental water contributions to a hypersaline basin using diatom ecology, sedimentology, and stable isotopes: an example in the late Miocene of the Mediterranean (Hellin basin, southern Spain): Palaeogeography Palaeoclimatology Palaeoecology, v. 79, n. 3–4, p. 189–204, http://dx.doi.org/10.1016/0031-0182(90)90017-2
Seton, M., Gaina, C., Müller, R. D., and Heine, C., 2009, Mid-Cretaceous seafloor spreading pulse: Fact or fiction?: Geology, v. 37, n. 8, p. 687–690, http://dx.doi.org/10.1130/G25624A.1
Shanks, W. C., Bischoff, J. L., and Kaplan, I. R., 1974, Sulfur isotope studies of evaporites and shales from Sites 225, 227, and 228 in the Red Sea: Initial Reports of the Deep Sea Drilling Project, v. 23, p. 947–950, http://dx.doi.org/10.2973/dsdp.proc.23.132.1974
Stoffers, P., and Kühn, R., 1974, Red Sea evaporites: a petrographic and geochemical study: Initial Reports of the Deep Sea Drilling Project, v. 23, p. 821–847, http://dx.doi.org/10.2973/dsdp.proc.23.122.1974
Stoffers, P., and Ross, D. A., 1974, Sedimentary history of the Red Sea: Initial Reports of the Deep Sea Drilling Project, v. 23, p. 849–865, http://dx.doi.org/10.2973/dsdp.proc.23.123.1974
Strauss, H., 1999, Geological evolution from isotope proxy signals—sulfur: Chemical Geology, v. 161, n. 1–3, p. 89–101, http://dx.doi.org/10.1016/S0009-2541(99)00082-0
Taberner, C., Cendón, D. I., Pueyo, J. J., and Ayora, C., 2000, The use of environmental markers to distinguish marine vs. continental deposition and to quantify the significance of recycling in evaporite basins: Sedimentary Geology, v. 137, n. 3–4, p. 213–240, http://dx.doi.org/10.1016/S0037-0738(00)00105-6
Timofeeff, M. N., Lowenstein, T. K., and Blackburn, W. H., 2000, ESEM-EDS: An improved technique for major element chemical analysis of fluid inclusions: Chemical Geology, v. 164, n. 3–4, p. 171–182, http://dx.doi.org/10.1016/S0009-2541(99)00153-9
Timofeeff, M. N., Lowenstein, T. K., Brennan, S. T., Demicco, R. V., Zimmermann, H., Horita, J., and von Borstel, L. E., 2001, Evaluating seawater chemistry from fluid inclusions in halite: Examples from modern marine and nonmarine environments: Geochimica et Cosmochimica Acta, v. 65, n. 14, p. 2293–2300, http://dx.doi.org/10.1016/S0016-7037(01)00591-9
Timofeeff, M. N., Lowenstein, T. K., da Silva, M. A. M., and Harris, N. B., 2006, Secular variation in the major-ion chemistry of seawater: Evidence from fluid inclusions in Cretaceous halites: Geochimica et Cosmochimica Acta, v. 70, n. 8, p. 1977–1994, http://dx.doi.org/10.1016/j.gca.2006.01.020
Turchyn, A. V., and Schrag, D. P., 2004, Oxygen isotope constraints on the sulfur cycle over the past 10 million years: Science, v. 303, n. 5666, p. 2004–2007, http://dx.doi.org/10.1126/science.1092296
——— 2006, Cenozoic evolution of the sulfur cycle: Insight from oxygen isotopes in marine sulfate: Earth and Planetary Science Letters, v. 241, n. 3–4, p. 763–779, http://dx.doi.org/10.1016/j.epsl.2005.11.007
Von Damm, K. L., 1995, Controls on the chemistry and temporal variability of seafloor hydrothermal fluids, *in* Humphris, S. E., Zierenberg, R. A., Mullineaux, L. S., and Thompson, R. E., editors, Seafloor Hydrothermal Systems: Physical, Chemical, Biologic and Geologic Interactions: Washington D.C., American Geophysical Union, Geophysical Monograph Series, v. 91, p. 222–247, http://dx.doi.org/10.1029/GM091p0222
Wheat, C. G., and Mottl, M. J., 2000, Composition of pore and spring waters from Baby Bare: Global implications of geochemical fluxes from a ridge flank hydrothermal system: Geochimica et Cosmochimica Acta, v. 64, n. 4, p. 629–642, http://dx.doi.org/10.1016/S0016-7037(99)00347-6
Witmarsh, R. B., Ross, D. A., Ali, S., Boudreaux, J. E., Coleman, R., Fleisher, R. L., Girdler, R. W., Manheim, F. T., Matter, A., Nigrini, C., Stoffers, P., and Supko, P. R., 1974a, Site 225: Initial Reports of the Deep Sea Drilling Project, v. 23, p. 539–594, http://dx.doi.org/10.2973/dsdp.proc.23.115.1974
——— , 1974b, Site 227: Initial Reports of the Deep Sea Drilling Project, v. 23, p. 601–676, http://dx.doi.org/10.2973/dsdp.proc.23.117.1974
Zimmermann, H., 2000, Tertiary seawater chemistry—implications from primary fluid inclusions in marine halite: American Journal of Science, v. 300, n. 10, p. 723–767, http://dx.doi.org/10.2475/ajs.300.10.723
——— 2001, On the origin of fluids included in Phanerozoic marine halite—basic interpretation strategies: Geochimica et Cosmochimica Acta, v. 65, n. 1, p. 35–45, http://dx.doi.org/10.1016/S0016-7037(00)00508-1
Zoetemeijer, R., Desegaulx, P., Cloetingh, S., Roure, F., and Moretti, I., 1990, Lithospheric dynamics and tectonic-stratigraphic evolution of the Ebro Basin: Journal of Geophysical Research—Solid Earth, v. 95, n. B3, p. 2701–2711, http://dx.doi.org/10.1029/JB095iB03p02701